The stability and instabilities of stationary solutions to the nonlinear Schrödinger equation and the sine-Gordon equation

Benjamin L. Segal

A dissertation
submitted in partial fulfillment of the
requirements for the degree of

Doctor of Philosophy

University of Washington

2017

Reading Committee:

Bernard Deconinck, Chair

Anne Greenbaum

Randy LeVeque

Hong Qian

Program Authorized to Offer Degree:
Department of Applied Mathematics

University of Washington

Abstract

The stability and instabilities of stationary solutions
to the nonlinear Schrödinger equation
and the sine-Gordon equation

Benjamin L. Segal

Chair of the Supervisory Committee:
Professor Bernard Deconinck
Department of Applied Mathematics

I present an analysis of the stability spectrum of all stationary elliptic-type solutions to the focusing Nonlinear Schrödinger equation and the sine-Gordon equation. An analytical expression for the spectrum is given. From this expression, various quantitative and qualitative results about the spectrum are derived. Specifically, the solution parameter space is shown to be split into regions of distinct qualitative behavior of the spectrum. Additional results on the stability of solutions with respect to perturbations of an integer multiple of the period are given, as well as a procedure for approximating the greatest real part of the spectrum.

TABLE OF CONTENTS

LIST OF FIGURES

ACKNOWLEDGMENTS

I would like to first thank Bernard Deconinck, my advisor and mentor. His unwavering support and belief in me has allowed me to get to this point. The five years of research retreats, game lunches, dessert parties, and many many group readings that he organized have made our research group incredibly close, and for that I am very grateful. Along with Bernard, I thank the rest of my supervisory committee Anne Greenbaum, Randy LeVeque, Hong Qian, and Jim Riley – for their time and effort. Thanks also to Katie Oliveras, John Carter and all of their students at Seattle University for your support and discussions during our Math Methods reading group.

Although the work we completed together is not in this thesis, the privilege of collaborating with Nghiem Nguyen, Henrik Kalisch, and Daulet Moldabayev was invaluable to my progression as a graduate student. Thank you to Peter McGill for your collaboration on the sine-Gordon equation; working with you last year was a joy. Thank you to Jeremy Upsal for all of your editing. Your eyes have seen most of the work in this thesis. Thank you to the rest of Bernard's group who I have overlapped with throughout the years: Vishal Vasan, Tom Trogdon, Olga Trichtchenko, Chris Swierczewski, Natalie Sheils, Xin Chen, and Ryan Creedon.

I also need to mention my classmates who began the program with me and helped me through the first year: Rosie Leung, Xin Chen and Ken Roche. Thanks to Kameron Harris and Yian Ma for the climbing, skiing, and conversations. To Don Rim for all of our lunches together before Soylent. To my officemates Lowell Thompson and Jake Price, our conversations and office competitions have kept school fun and competitive. And to Trevor Caldwell, a friend since we roomed together over prospective student weekend back in 2012.

I should also thank everyone from my various activities outside of the department over the years, like the Husky Masters swim team, the Rubik's cube club, and especially to all of those I played ultimate frisbee with. Having breaks from work has kept me sane.

From Northwestern, thank you to my old roommates: Geoff Hill, who has been my family in Seattle, and Kevin Shepherd, who never complains when I ask for last-minute copy editing. And finally, thank you to my undergraduate academic advisors Alvin Bayliss and Vladimir Volpert who inspired me to pursue this path and put me on the right track to success.

DEDICATION

To my family: mom, dad, and Leah.

NOTATION AND ABBREVIATIONS

$\mathbb{C}$	:	The complex plane
C_b^0	:	Continuous bounded functions
cn	:	Jacobi elliptic cn function
dn	:	Jacobi elliptic dn function
$\mathcal{E}(k)$	:	The complete elliptic integral of the second kind
$I(\zeta)$	:	The integral condition
k	:	The ellptic modulus
KdV	:	Korteweg–de Vries equation
$\mathcal{K}(k)$	:	The complete ellptic integral of the first kind
mKdV	:	The modified Korteweg-de Vries equation
μ	:	The Floquet exponent
NLS	:	Nonlinear Schrödinger equation
$\wp$	:	Weierstrass $\wp$ function
SG	:	The sine-Gordon eqution
sn	:	Jacobi elliptic sn function
σ_L	:	The Lax spectrum
$\sigma_{\mathcal{L}}$	:	The linear stability spectrum
$\sigma_{\mathcal{L}} \cap i\mathbb{R}$	:	The $\sigma_{\mathcal{L}}$ on the imaginary axis
$\overline{\sigma_{\mathcal{L}} \setminus i\mathbb{R}}$	:	The closure of $\sigma_{\mathcal{L}}$ not on the imaginary axis.
σ_w	:	Weierstrass σ function
$T(k)$	:	The period of the solution
ζ_w	:	Weierstrass ζ function

Chapter 1

INTRODUCTION

The study of the stability of nonlinear waves is a rich field which is constantly developing. The particular area of research that this work focuses on is the study of integrable Hamiltonian systems. These equations occur in many mathematical and physical areas, including water waves, nonlinear optics, plasma physics, astronomy, quantum mechanics, and more. They are recognized and studied for their soliton solutions (spatially localized waves which do not dissipate in time) and for their exact solvability of initial data by use of the Inverse Scattering Transformation. In this thesis, I focus my attention specifically on the class of stationary periodic traveling wave solutions, those which limit to the solitons for large period.

Most generically, stability theory addresses the question of whether or not solutions persist when affected by small perturbations. A solution is considered stable if solutions with nearby initial conditions remain nearby as time evolves. The study of stability is important for applications in science and engineering as unstable solutions are not likely to be physically realizable. Understanding how and why solutions go unstable is of great importance. Studying the stability and instabilities of traveling waves helps us understand the universe at all scales, ranging from deformations along DNA double helix to the emergence of galaxies and cosmological phenomena [53, 72].

In the literature a few different definitions are used to describe stability. Most general of them is *nonlinear stability*. We call a solution $u_e(x, t)$ nonlinearly stable if for every neighborhood U of $u_e(x, t)$ there exists a neighborhood V of $u_e(x, t)$ such that all trajectories $u(x, t)$ which start in V never leave U. Assuming we have a norm, this condition can be written as

$$\forall \epsilon > 0, \ \exists \delta > 0 : ||u(x, 0) - u_e(x, 0)|| < \delta \Rightarrow ||u(x, t) - u_e(x, t)|| < \epsilon, \forall t > 0. \qquad (1.1)$$

It turns out this definition is too restrictive for Hamiltonian PDEs. This was discussed first in detail in Benjamin's 1972 paper on the stability of solitary waves in the KdV equation [9]. For Hamiltonian PDEs any small difference in initial velocity between two solutions can manifest itself into a arbitrarily large phase shift in finite time.

A more apt definition for stability of traveling waves was introduced by Benjamin and allows for a phase shift. This definition is an example of *orbital stability* and can be written as

$$\forall \epsilon > 0, \ \exists \delta > 0 : ||u(x,0) - u_e(x,0)|| < \delta \Rightarrow \inf_{x_0 \in \mathbb{R}} ||u(x,t) - u_e(x + x_0, t)|| < \epsilon, \forall t > 0. \quad (1.2)$$

Prior to this work, using methods relying on integrability, orbital stability was shown for stationary periodic solutions of the KdV equation [23], the defocusing NLS equation [12], and the defocusing mKdV equation [26] with respect to subharmonic perturbations. Subharmonic perturbations are periodic perturbations that have period equal to an integer multiple of the base period of the solution.

A weaker form of stability is *linear stability*. We call a solution $u_e(x,t)$ linearly stable if there exists small enough perturbations $\delta u(x,t)$ to $u_e(x,t)$ such that these perturbations stay arbitrarily small for all time. Assuming we have a norm defined, this condition can be written as

$$\forall \epsilon > 0, \ \exists \delta > 0 : ||\delta u(x,0)|| < \delta \Rightarrow ||\delta u(x,t)|| < \epsilon, \forall t > 0. \quad (1.3)$$

For Hamiltonian problems, a sufficient condition for linear stability is that the linear stability spectrum consists of eigenvalues on the imaginary axis with a complete set of eigenfunctions. If the eigenfunctions are not complete, instabilities can occur with polynomial growth rates.

The final definition of stability that we mention is *spectral stability*. This is the weakest of the definitions of stability we mention. It only requires that the spectrum for the linear operator has no positive real part. In the case of Hamiltonian systems, the spectrum is symmetric with respect to the real and imaginary axes [71]. Thus the spectrum must be purely imaginary for spectral stability. We note that spectral stability is a necessary condition for linear stability and nonlinear stability.

In this thesis, most of our attention is focused on spectral stability and instabilities. This is because most of the solutions studied here are spectrally unstable and hence linearly and orbitally unstable. For the focusing NLS equation, as we demonstrate below, all stationary elliptic solutions are spectrally unstable. For the sine-Gordon equation, except for in the subluminal rotational case, all stationary elliptic solutions are spectrally unstable. The bulk of this thesis focuses on classifying, these instabilities as much as possible. Fortunately, not all hope for stability is lost. In Sections 2.9 and 3.9 we discuss the spectral stability of particular solutions with respect to subharmonic perturbations. In a forthcoming paper we prove the orbital stability of these solutions [28], with respect to these perturbations.

The outline of the thesis is as follows. In Chapter 2 we extend the methods of [11, 12, 26] to the focusing NLS equation. We present an explicit method for determining an analytical expression for the spectrum and detail various quantitative and qualitative results about the spectrum. Additionally, we present results on the spectral stability of solutions with respect to perturbations of an integer multiple of their period, as well as giving a procedure for approximating the greatest real part of the spectrum. Following this, in Chapter 3 we present similar results for the sine-Gordon equation. The work for the NLS equation was done first, but Chapters 2 and 3 are self-contained and one can read Chapter 3 without reading Chapter 2 if so desired. In Chapter 4, we conclude by highlighting where this work fits in to a broader research project of studying the stability of periodic solutions to integrable equations and we give some directions for further work.

Chapter 2

THE STABILITY SPECTRUM FOR ELLIPTIC SOLUTIONS TO THE FOCUSING NLS EQUATION

In this chapter, I present an analysis of the stability spectrum of all stationary elliptic-type solutions to the focusing Nonlinear Schrödinger equation. An analytical expression for the spectrum is given. From this expression, various quantitative and qualitative results about the spectrum are derived. Specifically, the solution parameter space is shown to be split into regions of distinct qualitative behavior of the spectrum. Additional results on the stability of solutions with respect to perturbations of an integer multiple of the period are given, as well as a procedure for approximating the greatest real part of the spectrum. The methods used in this chapter are not new, but expand on the techniques of [11, 12, 26] to accommodate a problem where the linear operator associated with the stability problem is not self adjoint. This chapter is published work [27].

2.1   Introduction

The focusing, one-dimensional, cubic Schrödinger equation (NLS) is given by

$$i\Psi_t + \frac{1}{2}\Psi_{xx} + \Psi|\Psi|^2 = 0. \tag{2.1}$$

In the context of water waves, nonlinear optics, and plasma physics, $\Psi(x,t)$ represents a complex-valued function describing the envelope of a slowly modulated carrier wave in a dispersive medium [19, 51, 65, 73]. The equation also arises in the description of Bose-Einstein condensates [38, 58], where Ψ represents a mean-field wave function.

We begin by looking at stationary solutions to (2.1) in the form

$$\Psi = e^{-i\omega t}\phi(x). \tag{2.2}$$

Then $\phi(x)$ satisfies

$$\omega\phi = -\frac{1}{2}\phi_{xx} - \phi|\phi|^2. \tag{2.3}$$

The stationary solutions we study in this chapter are the elliptic solutions to this equation and their limits. These solutions are periodic or quasi-periodic in x and limit to the well-known soliton solution as their period goes to infinity. More details on the periodic and quasi-periodic solutions relevant to our investigation are presented in Section 2.2.

Rowlands [60] was the first to study the stability of elliptic solutions. Using regular perturbation theory, treating the Floquet parameter as a small parameter, he conjectured that the stationary periodic solutions to focusing NLS are unstable. Since he expanded in a neighborhood of the origin of the spectral plane, his calculations suggest modulational instability for elliptic solutions of focusing NLS. More recently, Gallay and Hărăguş [34] examined the stability of small-amplitude elliptic solutions, with respect to arbitrary periodic and quasiperiodic perturbations. In a second paper [33], using the methods of [36, 37], they proved that periodic and quasiperiodic solutions are orbitally stable with respect to disturbances having the same period. Also, they showed that the cnoidal wave solutions (see below) are stable with respect to perturbations of twice the period. Hărăguş and Kapitula [41] put some of these results in the more general framework of determining the spectrum for the linearization of an infinite-dimensional Hamiltonian system about a spatially periodic traveling wave. For the quasi-periodic solutions of sufficiently small amplitude, they establish spectral instability. Following this, Ivey and Lafortune [42] examine the spectral stability of cnoidal wave solutions to focusing NLS with respect to periodic perturbations, using the algebro-geometric framework of hyperelliptic Riemann surfaces and Riemann theta functions [8]. Their calculations make use of the squared eigenfunction connection as do ours below. Additionally, they use a periodic generalization of the Evans function. This gives an analytical description of the spectrum for the cnoidal wave solutions, which we replicate in this chapter using elliptic functions. Lastly, we mention a recent paper by Gustafson, Coz, and Tsai [39]. In this paper, the authors give a rigorous version of the formal asymptotic calculation of Rowlands to establish the linear instability of a class of real-valued periodic

waves against perturbations with period a large multiple of their fundamental period. They achieve this by directly constructing the branch of eigenvalues using a formal expansion and the contraction mapping theorem. In terms of elliptic function solutions, their results are limited to the cnoidal and dnoidal solutions. Using entirely different methods, we confirm their results and extend their findings to nontrivial-phase solutions, in effect making the results of Rowlands rigorous for all elliptic solutions of NLS.

In Sections 2.3, 2.4 and 2.5, using the same methods as [11,12,26], we exploit the integrability of (2.1) to associate the spectrum of the linear stability problem with the Lax spectrum using the squared eigenfunction connection [1]. This allows us to obtain an analytical expression for the spectrum of the operator associated with the linearization of (2.1) in the form of a condition on the real part of an integral over one period of some integrand. However, unlike in [11,12,26] the linear operator associated with the focusing NLS equation is not self adjoint. The self adjointness of the linear operator was directly exploited in these papers and that is not available here. Instead, we proceed by integrating the integrand explicitly. This is done in Section 2.6. Next, using the expressions obtained, we prove results concerning the location of the stability spectrum on the imaginary axis in Section 2.7. In Section 2.8, we present analytical results about the spectrum, and we make use of the integral condition to split parameter space into different regions where the spectrum shows qualitatively different behavior. In Section 2.9 we examine the spectral stability of solutions against perturbations of an integer multiple of their fundamental period confirming and extending results of [33,34,39]. Finally, in Section 2.10 we discuss approximations to the spectral curves in $\mathbb{C}$ found by expanding around known spectral elements. We use those approximations to give estimates for the maximal real part of the spectrum.

2.2 Elliptic solutions to focusing NLS

The results of this section are presented in more detail in [18]. We limit our analysis to just what is necessary for the following sections. We split ϕ into its amplitude and phase

$$\phi(x) = R(x)e^{i\theta(x)}, \tag{2.4}$$

where $R(x)$ and $\theta(x)$ are real-valued, bounded functions of $x \in \mathbb{R}$. Substituting (2.4) into (2.3), we find the standard Jacobi elliptic function solutions given by

$$R^2(x) = b - k^2 \text{sn}^2(x, k), \tag{2.5}$$

$$\omega = \frac{1}{2}(1 + k^2) - \frac{3}{2}b, \tag{2.6}$$

$$\theta(x) = \int_0^x \frac{c}{R^2(y)} dy, \tag{2.7}$$

$$c^2 = b(1 - b)(b - k^2). \tag{2.8}$$

Here $\text{sn}(x, k)$ is the Jacobi elliptic sn function with elliptic modulus k [17,52,55,70]. Besides k, the only other parameter present is b, which is an offset parameter for the solutions. We are not specifying the full class of parameters allowed by the four Lie point symmetries of (2.1) [56]. Specifically, we are neglecting to include a scaling and a horizontal shift in x. The use of a Galilean shift allows for the application of our results to traveling wave solutions as well stationary solutions. The different symmetries are not included here as they do not produce qualitatively different results to what is covered here, but the methods presented apply equally well.

In order for our solutions to be valid, we require that both $R^2(x)$ and c^2 are real, positive, and bounded. These conditions result in constraints on our parameters:

$$0 \leq k < 1, \tag{2.9}$$

$$k^2 \leq b \leq 1. \tag{2.10}$$

Of special importance is the boundary of this region, as many of the well-studied solutions to (2.1) lie on the boundary. Specifically, when $b = k^2$ or when $b = 1$ we have that $c = 0$ and

$\phi(x) = \text{cn}(x, k)$ or $\phi(x) = \text{dn}(x, k)$ respectively. Here $\text{cn}(x, k)$ and $\text{dn}(x, k)$ are the Jacobi elliptic cn and dn functions respectively. These solutions are called trivial-phase solutions, as there is no phase in $\phi(x)$, *i.e.*, $c = 0$. These solutions are periodic in x, of period $4\mathcal{K}(k)$ and $2\mathcal{K}(k)$ respectively. Here

$$\mathcal{K}(k) = \int_0^{\pi/2} \frac{1}{\sqrt{1 - k^2 \sin^2 y}} dy, \tag{2.11}$$

is the complete elliptic integral of the first kind. As $k \to 1$ these solutions approach the well-studied stationary soliton solution of (2.1): $\phi(x) = \text{sech}(x)$.

The other part of the boundary of parameter space occurs when $k = 0$. Here the amplitude of $\phi(x)$ is constant and thus the analysis of the solutions simplifies greatly. These solutions are called Stokes wave solutions. They have the form $\phi(x) = \sqrt{b} \exp\left(ix\sqrt{1 - b}\right)$. The stability of all these boundary cases has been examined to some extent in the literature. See [34, 42, 48], among others. Figure 2.1 depicts a plot of parameter space with labels for the boundary cases.

We reformulate our elliptic solutions to (2.1) using Weierstrass elliptic functions [55] rather than Jacobi elliptic functions. This will simplify working with the integral condition (2.58) in Section 2.4, as formulas for integrating Weierstrass elliptic functions are well documented [17, 35]. It is important to note that nothing is lost by switching to Weierstrass elliptic functions, as we can map any Weierstrass elliptic function to a Jacobi elliptic function, and vice versa [55]. Let

$$\wp(z + \omega_3, g_2, g_3) - e_3 = \left(\frac{\mathcal{K}(k)k}{\omega_1}\right)^2 \text{sn}^2\left(\frac{\mathcal{K}(k)z}{\omega_1}, k\right), \tag{2.12}$$

with g_2 and g_3 the lattice invariants of the Weierstrass $\wp$ function, e_1, e_2, and e_3 the zeros of the polynomial $4t^3 - g_2 t - g_3$, and ω_1 and ω_3 the half-periods of the Weierstrass lattice given by

$$\omega_1 = \int_{e_1}^{\infty} \frac{dz}{\sqrt{4z^3 - g_2 z - g_3}}, \tag{2.13}$$

$$\omega_3 = i \int_{-e_3}^{\infty} \frac{dz}{\sqrt{4z^3 - g_2 z + g_3}}. \tag{2.14}$$
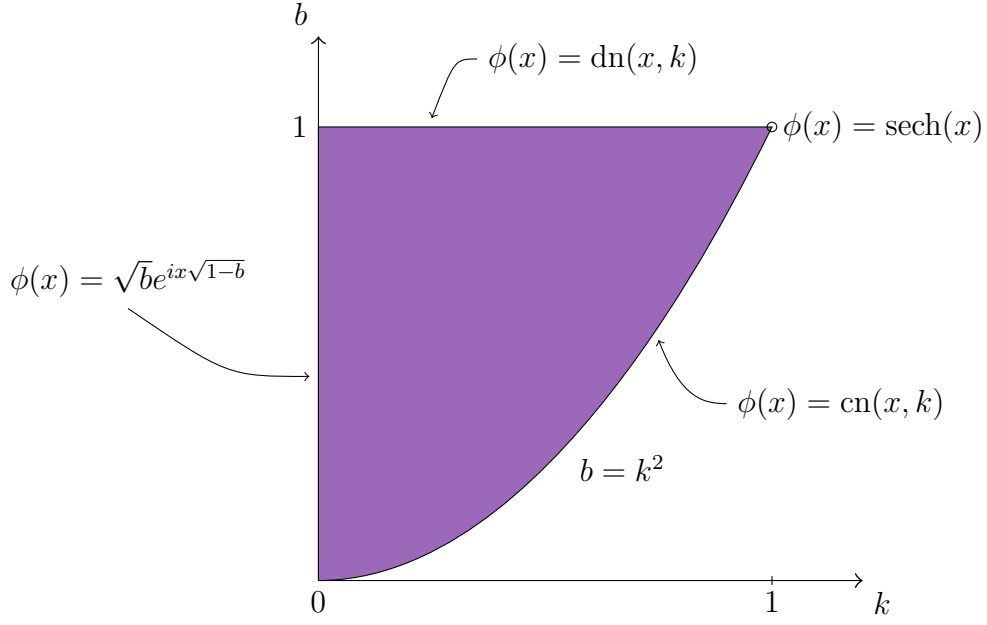
Figure 2.1: Visualization of parameter space in terms of b and k with special solutions on the boundaries labeled.

We look for stationary solutions to (2.1) of the form (2.2). We split ϕ into its amplitude and phase, letting

$$\phi_w(x) = R_w(x)e^{i\theta_w(x)}, \tag{2.15}$$

where R_w and θ_w are expressed in terms of Weierstrass elliptic functions. Substituting this ansatz into (2.3) gives solutions in Weierstrass form [21]:

$$\theta_w(x) = \pm\frac{i}{2}\left(\log\left(\frac{\sigma_w(x + x_w + a_w, g_2, g_3)}{\sigma_w(x + x_w - a_w, g_2, g_3)}\right) + 2(x + x_w)\zeta_w(a)\right), \tag{2.16}$$

$$R_w^2(x) = e_0 - \wp(x + x_w, g_2, g_3), \tag{2.17}$$

$$g_2 = 12e_0^2 + K_2, \tag{2.18}$$

$$g_3 = 4K_1 - 8e_0^3 - e_0 K_2, \tag{2.19}$$

$$e_0 = -\frac{2\omega}{3} = \wp(a_w, g_2, g_3). \tag{2.20}$$

Here σ_w and ζ_w are the Weierstrass σ and Weierstrass ζ functions respectively [55], and ω, K_1, K_2, and x_w are free parameters. The constant a_w from (2.20) is given explicitly as

$$a_w = \wp^{-1}(e_0, g_2, g_3). \tag{2.21}$$

We can recover the Jacobi elliptic solutions from these solutions by fixing the free parameters

$$\omega = \frac{1}{2}\left(1 + k^2 - 3b\right), \tag{2.22}$$

$$K_1^2 = c^2 = b(1-b)(b-k^2), \tag{2.23}$$

$$K_2 = -4\left(k^2 - 2bk^2 + 3b^2 - 2b\right), \tag{2.24}$$

$$x_w = i\mathcal{K}'(k), \tag{2.25}$$

where $\mathcal{K}'(k)$ is the complement to $\mathcal{K}(k)$ given by $\mathcal{K}'(k) = K\left(1 - k^2\right)$. Under this mapping we have

$$g_2 = \frac{4}{3}\left(1 - k^2 + k^4\right), \tag{2.26}$$

$$g_3 = \frac{4}{27}\left(2 - 3k^2 - 3k^4 + 2k^6\right), \tag{2.27}$$

$$e_1 = \frac{1}{3}\left(2 - k^2\right), \quad e_2 = \frac{1}{3}\left(-1 + 2k^2\right), \quad e_3 = \frac{1}{3}(-1 - k^2), \tag{2.28}$$

$$\omega_1 = \mathcal{K}(k), \quad \omega_3 = i\mathcal{K}'(k). \tag{2.29}$$

The homogeneity property of the Weierstrass $\wp$ function [55],

$$\wp(x, g_2, g_3) = g_2^{\frac{1}{2}} \wp\left(g_2^{\frac{1}{4}} x, 1, g_3 g_2^{-\frac{3}{2}}\right). \tag{2.30}$$

allows us to rewrite (2.17) as

$$R_w^2(x) = -\left(g_2^{\frac{1}{2}} \wp\left(g_2^{\frac{1}{4}}(x + x_w), 1, g_3 g_2^{-\frac{3}{2}}\right) - e_0\right), \tag{2.31}$$

which has only one varying lattice invariant $g_3 g_2^{-\frac{3}{2}}$. This comes at the cost of rescaling x and the magnitude of the Weierstrass $\wp$ function. The formulation (2.31) allows for a display of parameter space as in Figure 2.1, but using the Weierstrass parameters, see Figure 2.2. In this figure, we see where the cn, dn, and Stokes wave solutions map to in the Weierstrass domain.
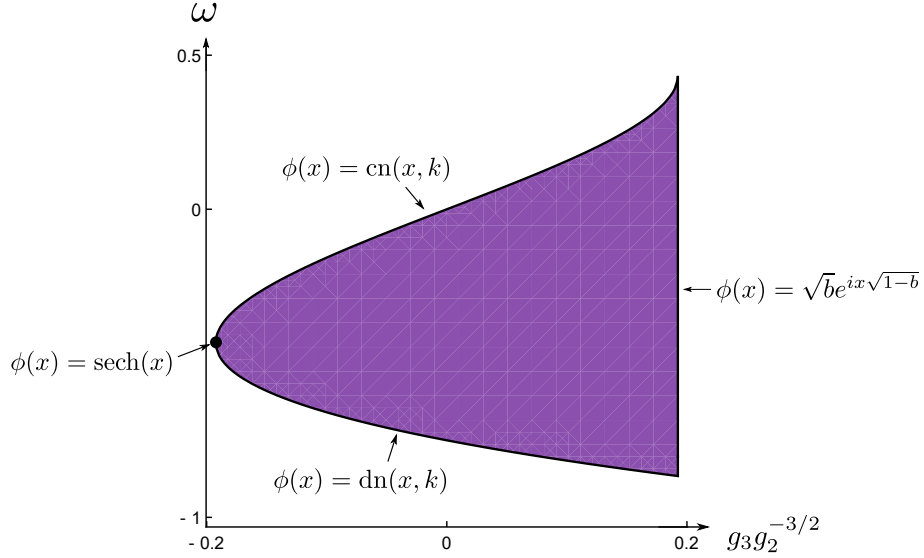
Figure 2.2: The parameter space for elliptic solutions in Weierstrass form (2.31). The cn, dn and Stokes wave solutions are found on the boundaries of this space, with the soliton solution occurring at the limiting point where the dn and cn curves meet.

2.3   The linear stability problem

To examine the linear stability of our solutions we consider

$$\Psi(x,t) = e^{-i\omega t} e^{i\theta(x)} \left(R(x) + \epsilon u(x,t) + \epsilon i v(x,t) + \mathcal{O}(\epsilon^2) \right), \tag{2.32}$$

where ϵ is a small parameter and $u(x,t)$ and $v(x,t)$ are the real and imaginary parts of our perturbation, which depends on both x and t. Substituting (2.32) into (2.1), isolating $O(\epsilon)$ terms, and splitting into real and imaginary parts, we obtain a system of equations

$$\frac{\partial}{\partial t} \begin{pmatrix} u \\ v \end{pmatrix} = \mathcal{L} \begin{pmatrix} u \\ v \end{pmatrix} = \begin{pmatrix} -S & \mathcal{L}_- \\ -\mathcal{L}_+ & -S \end{pmatrix} \begin{pmatrix} u \\ v \end{pmatrix} = J \begin{pmatrix} \mathcal{L}_+ & S \\ -S & \mathcal{L}_- \end{pmatrix} \begin{pmatrix} u \\ v \end{pmatrix}, \tag{2.33}$$

with

$$J = \begin{pmatrix} 0 & 1 \\ -1 & 0 \end{pmatrix}. \tag{2.34}$$

The linear operators $\mathcal{L}_+$, $\mathcal{L}_-$, and S are given by

$$\mathcal{L}_- = -\frac{1}{2}\partial_x^2 - R^2(x) - \omega + \frac{c^2}{2R^4(x)}, \tag{2.35}$$

$$\mathcal{L}_+ = -\frac{1}{2}\partial_x^2 - 3R^2(x) - \omega + \frac{c^2}{2R^4(x)}, \tag{2.36}$$

$$S = \frac{c}{R^2(x)}\partial_x - \frac{cR'(x)}{R^3(x)} = \frac{c}{R(x)}\partial_x\frac{1}{R(x)}. \tag{2.37}$$

An elliptic solution $\phi(x) = R(x)e^{i\theta(x)}$ is by definition linearly stable if for all $\epsilon > 0$ there exists a $\delta > 0$ such that if $||u(x,0) + iv(x,0)|| < \delta$ then $||u(x,t) + iv(x,t)|| < \epsilon$ for all $t > 0$. This definition depends on the choice of norm $||\cdot||$ which is specified in the definition of the spectrum in (2.40) below.

Since (2.33) is autonomous in t, we separate variables to look at solutions of the form

$$\begin{pmatrix} u(x,t) \\ v(x,t) \end{pmatrix} = e^{\lambda t}\begin{pmatrix} U(x) \\ V(x) \end{pmatrix}, \tag{2.38}$$

resulting in the spectral problem

$$\lambda\begin{pmatrix} U \\ V \end{pmatrix} = \mathcal{L}\begin{pmatrix} U \\ V \end{pmatrix} = \begin{pmatrix} -S & \mathcal{L}_- \\ -\mathcal{L}_+ & -S \end{pmatrix}\begin{pmatrix} U \\ V \end{pmatrix} = J\begin{pmatrix} \mathcal{L}_+ & S \\ -S & \mathcal{L}_- \end{pmatrix}\begin{pmatrix} U \\ V \end{pmatrix}. \tag{2.39}$$

Here

$$\sigma_{\mathcal{L}} = \{\lambda \in \mathbb{C} : \max_{x\in\mathbb{R}}\left(|U(x)|, |V(x)|\right) < \infty\}, \tag{2.40}$$

or

$$U, V \in C_b^0(\mathbb{R}). \tag{2.41}$$

In order to have spectral stability, we need to demonstrate that the spectrum $\sigma_{\mathcal{L}}$ does not enter into the right half of the complex λ plane. Since (2.1) is Hamiltonian [4], the spectrum of its linearization is symmetric with respect to both the real and imaginary axis [71]. In other words, proving spectral stability for elliptic solutions to (2.1) amounts to proving that the stability spectrum lies strictly on the imaginary axis. In our case, we show that none of the elliptic solutions are spectrally stable, as we demonstrate spectral elements in the right-half plane near the origin for any choice of the parameters b and k.

2.4   The Lax pair

We wish to obtain an analytical representation for the spectrum $\sigma_{\mathcal{L}}$. As mentioned in the introduction, this analytical representation comes from the squared eigenfunction connection between the linear stability problem (2.33) and its Lax pair. We begin by formulating (2.1) in a traveling frame, by defining

$$\Psi(x,t) = e^{-i\omega t}\psi(x,t), \tag{2.42}$$

so that ψ satisfies

$$i\psi_t = -\omega\psi - \frac{1}{2}\psi_{xx} - \psi|\psi|^2. \tag{2.43}$$

This equation is equivalent to the compatibility condition $\chi_{xt} = \chi_{tx}$ of the following Lax pair [74]:

$$\chi_x = \begin{pmatrix} -i\zeta & \psi \\ -\psi^* & i\zeta \end{pmatrix}\chi, \tag{2.44}$$

$$\chi_t = \begin{pmatrix} -i\zeta^2 + \frac{i}{2}|\psi|^2 + \frac{i}{2}\omega & \zeta\psi + \frac{i}{2}\psi_x \\ -\zeta\psi^* + \frac{i}{2}\psi_x^* & i\zeta^2 - \frac{i}{2}|\psi|^2 - \frac{i}{2}\omega \end{pmatrix}\chi, \tag{2.45}$$

where * represents the complex conjugate $[1, 12]$. Regarding (2.44) as a spectral problem with ζ as the spectral parameter:

$$\begin{pmatrix} i\partial_x & -i\psi \\ -i\psi^* & -i\partial_x \end{pmatrix}\chi = \zeta\chi, \tag{2.46}$$

we see that it is not self adjoint [49]. This means that the spectral parameter ζ is not necessarily confined to the real axis as it was for defocusing NLS [12] which makes our analysis more difficult. Since the elliptic solutions are given by $\psi(x,t) = \phi(x)$, we restrict the Lax pair to elliptic solutions by writing

$$\chi_x = \begin{pmatrix} -i\zeta & \phi \\ -\phi^* & i\zeta \end{pmatrix}\chi, \tag{2.47}$$

$$\chi_t = \begin{pmatrix} -i\zeta^2 + \frac{i}{2}|\phi|^2 + \frac{i}{2}\omega & \zeta\phi + \frac{i}{2}\phi_x \\ -\zeta\phi^* + \frac{i}{2}\phi_x^* & i\zeta^2 - \frac{i}{2}|\phi|^2 - \frac{i}{2}\omega \end{pmatrix} \chi. \tag{2.48}$$

Henceforth we refer to the spectrum of (2.47) as σ_L or informally as the Lax spectrum. Specifically, σ_L consists of all ζ for which (2.47) has a bounded (in x) eigenfunction solution. To determine σ_L we start by rewriting (2.48) in the short-hand form

$$\chi_t = \begin{pmatrix} A & B \\ C & -A \end{pmatrix} \chi, \tag{2.49}$$

where

$$A = -i\zeta^2 + \frac{i}{2}|\phi|^2 + \frac{i}{2}\omega, \tag{2.50}$$

$$B = \zeta\phi + \frac{i}{2}\phi_x, \tag{2.51}$$

$$C = -\zeta\phi^* + \frac{i}{2}\phi_x^*. \tag{2.52}$$

Since A, B, and C are independent of t, we separate variables. Let

$$\chi(x,t) = e^{\Omega t}\varphi(x), \tag{2.53}$$

with Ω being independent of t but possibly depending on x. Substituting (2.53) into (2.49) and canceling the exponential, we find

$$\begin{pmatrix} A - \Omega & B \\ C & -A - \Omega \end{pmatrix} \varphi = 0. \tag{2.54}$$

In order to have nontrivial solutions we require the determinant of (2.54) to be zero. Using the definitions of A, B and C, we get

$$\Omega^2 = A^2 + BC = -\zeta^4 + \omega\zeta^2 + c\zeta + \frac{1}{16}\left(-4\omega b - 3b^2 - k'^4\right), \tag{2.55}$$

where $k' = \sqrt{1 - k^2}$. We notice that Ω is not only independent of t but also of x. Thus Ω is strictly a function of ζ and the solution parameters.

To satisfy (2.54), we let

$$\varphi(x) = \gamma(x) \begin{pmatrix} -B(x) \\ A(x) - \Omega \end{pmatrix}, \tag{2.56}$$

where $\gamma(x)$ is a scalar function. By construction of $\varphi(x)$, $\chi(x,t)$ satisfies (2.48). Since (2.47) and (2.48) commute, it is possible to choose $\gamma(x)$ such that χ also satisfies (2.47). Indeed, $\gamma(x)$ satisfies a first-order linear equation, whose solution is given by

$$\gamma(x) = \gamma_0 \exp\left(-\int \frac{(A - \Omega)\phi + B_x + i\zeta B}{B} \, \mathrm{d}x\right). \tag{2.57}$$

For almost every $\zeta \in \mathbb{C}$, we have explicitly determined the two linearly independent solutions of (2.47), *i.e.*, those corresponding to the positive and negative signs of Ω in (2.55). Assuming $\Omega \neq 0$ these two solutions are by construction linearly independent. In the case where ζ corresponds to $\Omega = 0$ the second solution to (2.47) can be determined via the reduction-of-order method.

Since (2.47) and (2.48) share their eigenfunctions, σ_L is the set of all $\zeta \in \mathbb{C}$ such that (2.56) is bounded for all $x \in \mathbb{R}$. Indeed, the vector part of φ is bounded for all x, so we only need that the scalar function $\gamma(x)$ is bounded as $x \to \pm\infty$. A necessary and sufficient condition for this is

$$\left\langle \mathrm{Re}\left(\frac{(A - \Omega)\phi + B_x + i\zeta B}{B}\right) \right\rangle = 0, \tag{2.58}$$

where $\langle \cdot \rangle$ is the average over one period $2\mathcal{K}(k)$ of the integrand, and Re denotes the real part. At this point, the integral condition (2.58) completely determines the Lax spectrum σ_L.

2.5 The squared eigenfunction connection

A connection between the eigenfunctions of the Lax pair (2.47) and (2.48) and the eigenfunctions of the linear stability problem (2.33) using a squared eigenfunctions is well known [1]. We prove the following theorem.

Theorem 2.5.1. *The vector*

$$\begin{pmatrix} u \\ v \end{pmatrix} = \begin{pmatrix} e^{-i\theta(x)}\chi_1^2 - e^{i\theta(x)}\chi_2^2 \\ -ie^{-i\theta(x)}\chi_1^2 - ie^{i\theta(x)}\chi_2^2 \end{pmatrix} \tag{2.59}$$

satisfies the linear stability problem (2.33). Here $\chi = (\chi_1, \chi_2)^T$ is any solution of the Lax pair (2.44-2.45) corresponding by direct calculation to the elliptic solution $\phi(x) = R(x)e^{i\theta(x)}$.

Proof. The proof is done by direct calculation. For the left-hand side of (2.33), evaluate (u_t, v_t) using the product rule and (2.45). Eliminate x-derivatives of u and v (up to order 2) using (2.44). Upon substitution and using (2.47) and (2.48), the left-hand side and right-hand side of (2.33) are equal, finishing the proof. $\square$

To establish the connection between the $\sigma_{\mathcal{L}}$ spectrum and the σ_L spectrum we examine the right- and left-hand sides of (2.38). Substituting in (2.59) and (2.53) to the left-hand side of (2.38) we find

$$e^{2\Omega t} \begin{pmatrix} e^{-i\theta(x)}\varphi_1^2 - e^{i\theta(x)}\varphi_2^2 \\ -ie^{-i\theta(x)}\varphi_1^2 - ie^{i\theta(x)}\varphi_2^2 \end{pmatrix} = e^{\lambda t} \begin{pmatrix} U \\ V \end{pmatrix}, \tag{2.60}$$

and we conclude that

$$\lambda = 2\Omega(\zeta), \tag{2.61}$$

with eigenfunctions given by

$$\begin{pmatrix} U \\ V \end{pmatrix} = \begin{pmatrix} e^{-i\theta(x)}\varphi_1^2 - e^{i\theta(x)}\varphi_2^2 \\ -ie^{-i\theta(x)}\varphi_1^2 - ie^{i\theta(x)}\varphi_2^2 \end{pmatrix}. \tag{2.62}$$

This gives the connection between the σ_L spectrum and the $\sigma_{\mathcal{L}}$ spectrum. It is also necessary to check that indeed all solutions of (2.39) are obtained through (2.60). This is not shown explicitly here, but is done analogous to the work in [12].

Although in principle the above construction determines $\sigma_{\mathcal{L}}$, it remains to be seen how practical this determination is. In the following section we discuss a technique for explicitly integrating (2.58) using Weierstrass elliptic functions, leading to a more explicit characterization of $\sigma_{\mathcal{L}}$.

2.6 The Lax spectrum in terms of elliptic functions

In terms of Weierstrass elliptic functions,

$$\Omega^2 = -\zeta^4 + \omega\zeta^2 + K_1\zeta + \frac{1}{4}\left(-\omega^2 - \frac{K_2}{4}\right), \tag{2.63}$$

while (2.58) becomes

$$\text{Re} \int_0^{2\omega_1} \frac{(A - \Omega)\phi_w + B_x + i\zeta B}{B} \mathrm{d}x = 0, \tag{2.64}$$

with A and B given in (2.50) and (2.51). Substituting for ϕ_w we find that (2.64) is of the form

$$\text{Re} \int_0^{2\omega_1} \frac{C_1 + C_2\wp(x) + C_3\wp'(x)}{C_4 + C_5\wp(x)} \mathrm{d}x = 0, \tag{2.65}$$

here $\wp(x) = \wp(x + x_w, g_2, g_3)$ with the dependence on x_w, g_2, and g_3 suppressed. The C_j's depend on ζ but are independent of x. They are given by

$$C_1 = -\frac{2\omega\zeta}{3} - \frac{K_1}{2} + \zeta^3 - \frac{\omega\zeta}{6} - i\zeta\Omega(\zeta),$$
$$C_2 = -\frac{\zeta}{2}, \qquad\qquad C_3 = \frac{i}{4}, \tag{2.66}$$
$$C_4 = -\Omega(\zeta) - i\zeta^2 + i\frac{\omega}{6}, \quad C_5 = -\frac{i}{2}.$$

We can evaluate the integral in (2.65) explicitly [35]. We find

$$\text{Re}\left[\frac{2\omega_1 C_2}{C_5} + \frac{4(C_1 C_5 - C_2 C_4)}{\wp'(\alpha)C_5^2}\left(\zeta_w(\alpha)\omega_1 - \zeta_w(\omega_1)\alpha\right)\right] = 0, \tag{2.67}$$

with

$$\alpha = \alpha(\zeta) = \wp^{-1}\left(-\frac{C_4(\zeta)}{C_5(\zeta)}, g_2, g_3\right). \tag{2.68}$$

Here $\wp^{-1}$ is a multivalued function, but for the sake of our analysis α is chosen as any value such that $\wp(\alpha) = -C_4(\zeta)/C_5(\zeta)$. Substituting for the C_j's, (2.65) becomes

$$\text{Re}\left[-2i\zeta\omega_1 + \frac{4i\left(-K_1 + 4\zeta^3 - 2\zeta\omega - 4i\zeta\Omega(\zeta)\right)}{\wp'(\alpha)}\left(\zeta_w(\alpha)\omega_1 - \zeta_w(\omega_1)\alpha\right)\right] = 0. \tag{2.69}$$

We simplify this further by recognizing that

$$\wp'^2(\alpha) = 4\wp^3(\alpha) - g_2\wp(\alpha) - g_3 = 4\left(-\frac{C_4(\zeta)}{C_5(\zeta)}\right)^3 - g_2\left(-\frac{C_4(\zeta)}{C_5(\zeta)}\right) - g_3. \tag{2.70}$$

Substituting for $C_4(\zeta)$ and $C_5(\zeta)$, changing g_2 and g_3 to K_1 and K_2 via (2.18) and (2.19) respectively, and substituting in (2.63) for higher powers of $\Omega(\zeta)$ gives

$$\wp'^2(\alpha) = -4\left(-K_1 + 4\zeta^3 - 2\zeta\omega - 4i\zeta\Omega(\zeta)\right)^2. \tag{2.71}$$

Thus (2.69) simplifies to

$$\mathrm{Re}\left(-2i\zeta\omega_1 + 2\tau\left(\zeta_w(\alpha)\omega_1 - \zeta_w(\omega_1)\alpha\right)\right) = 0, \tag{2.72}$$

where $\tau = \mathrm{sgn}\left(\mathrm{Re}\left(-K_1 + 4\zeta^3 - 2\zeta\omega - 4i\zeta\Omega(\zeta)\right)\right).$

Under the mapping (2.29), and applying the formula for the Weierstrass ζ function evaluated at a half period [17], $\zeta_w(\omega_1) = \sqrt{e_1 - e_3}\left(\mathcal{E}(k) - \frac{e_1}{e_1 - e_3}\mathcal{K}(k)\right)$, (2.72) becomes

$$\mathrm{Re}\left[-2i\zeta\mathcal{K}(k) + 2\tau\left(\zeta_w(\alpha)\mathcal{K}(k) - \left(\mathcal{E}(k) - \frac{1}{3}\left(2 - k^2\right)\mathcal{K}(k)\right)\alpha\right)\right] = 0. \tag{2.73}$$

Here

$$\mathcal{E}(k) = \int_0^{\pi/2}\sqrt{1 - k^2\sin^2 y}\,dy, \tag{2.74}$$

is the complete elliptic integral of the second kind. At this point, we have simplified the integral condition (2.64) as much as possible. Thus $\zeta \in \sigma_L$ if and only if (2.73) is satisfied. To simply notation, let

$$I(\zeta) = -2i\zeta\omega_1 + 2\tau\left(\zeta_w(\alpha)\omega_1 - \zeta_w(\omega_1)\alpha\right), \tag{2.75}$$

so that (2.73) is

$$\mathrm{Re}\left[I(\zeta)\right] = 0. \tag{2.76}$$

Next, we wish to examine the level sets of the left-hand side of (2.76). To this end, we differentiate $I(\zeta)$ with respect to ζ. To evaluate this derivative we use the chain rule and note that

$$\frac{\partial}{\partial\zeta}\zeta_w(\alpha) = -\wp(\alpha)\frac{\partial\alpha}{\partial\zeta} = \frac{C_4(\zeta)}{C_5(\zeta)}\frac{\mathrm{d}\wp^{-1}}{\mathrm{d}\zeta}\left(-\frac{C_4(\zeta)}{C_5(\zeta)}, g_2, g_3\right)\left(-\frac{C_4(\zeta)}{C_5(\zeta)}\right)'. \tag{2.77}$$

Since

$$\frac{\mathrm{d}}{\mathrm{d}z}\wp^{-1}\left(-\frac{C_4(\zeta)}{C_5(\zeta)}, g_2, g_3\right) = \frac{1}{\wp'\left(\wp^{-1}\left(-\frac{C_4(\zeta)}{C_5(\zeta)}, g_2, g_3\right)\right)} = \frac{1}{\wp'(\alpha)}, \tag{2.78}$$

we can use (2.71) to obtain

$$\frac{\mathrm{d}I(\zeta)}{\mathrm{d}\zeta} = \frac{2\mathcal{E}(k) - (1 + b - k^2 + 4\zeta^2)\,\mathcal{K}(k)}{2\Omega(\zeta)}. \tag{2.79}$$

Simply taking the real part of (2.79) does not give another characterization of the spectrum. Instead, if we think of (2.73) as restricting ourselves to the zero level set of the left-hand side. Then we use (2.79) to determine a tangent vector field which allows us to map out level curves originating from any point. This is explained in more detail in Section 2.8. Additionally, there we see that (2.79) is useful in determining the boundary regions in parameter space corresponding to qualitatively different parts of the spectrum.

2.7 The $\sigma_\mathcal{L}$ spectrum on the imaginary axis

In this section we discuss $\sigma_\mathcal{L} \cap i\mathbb{R}$. As we demonstrate, this corresponds to the part of σ_L lying on the real axis. Using (2.73) we obtain analytic expressions for $\sigma_L \cap \mathbb{R}$, and thus for $\sigma_\mathcal{L} \cap i\mathbb{R}$.

First, we consider $\zeta \in \mathbb{R}$. As we demonstrate below, (2.73) is satisfied for any real ζ. Using (2.63) and (2.61), we determine the corresponding parts of $\sigma_\mathcal{L}$.

Theorem 2.7.1. *The condition (2.73) is satisfied for all $\zeta \in \mathbb{R}$.*

Proof. Since k, $\mathcal{K}(k)$, and $\mathcal{E}(k)$ are real, it suffices to show that $\alpha \in i\mathbb{R}$ and $\zeta_w(\alpha) \in i\mathbb{R}$. Since ζ_w with $g_2, g_3 \in \mathbb{R}$ takes real values to real values and purely imaginary values to purely imaginary values [55], it suffices to show that $\alpha = \wp^{-1}\left(-\frac{C_4(\zeta)}{C_5(\zeta)}, g_2, g_3\right) \in i\mathbb{R}$. For $g_2, g_3 \in \mathbb{R}$, $\wp(\mathbb{R}, g_2, g_3)$ maps to $[e_1, \infty)$, and since $\wp(ix, g_2, g_3) = -\wp(x, g_2, -g_3)$ we have that $\wp(i\mathbb{R}, g_2, g_3)$ maps to $(-\infty, e_3]$. Thus we need to show that ζ, $-\frac{C_4(\zeta)}{C_5(\zeta)} \leq e_3$. Substituting for $C_4(\zeta)$ and $C_5(\zeta)$, we want to show

$$\frac{1}{6}\left(2\omega - 12\zeta^2 - 3\sqrt{1 - 3b^2 + k^4 - 16c\zeta - 8\zeta^2 + 16\zeta^4 - 2k^2(1 + 4\zeta^2) + 2b(1 + k^2 + 12\zeta^2)}\right) \leq e_3. \tag{2.80}$$

Simplifying the left- and right- hand sides of this expression yields

$$4\zeta^2 + \sqrt{(1 + k^2 - b - 4\zeta^2)^2 + 4\left(2\sqrt{b}\zeta - \sqrt{(1 - b)(b - k^2)}\right)^2} \geq 1 + k^2 - b. \tag{2.81}$$

There are two cases. If $4\zeta^2 \geq 1 + k^2 - b$ we are done, as the square root term is nonnegative. If $4\zeta^2 < 1 + k^2 - b$, we have

$$4\zeta^2 + \sqrt{\left(1 + k^2 - b - 4\zeta^2\right)^2 + 4\left(2\zeta\sqrt{b} - \sqrt{(1-b)(b-k^2)}\right)^2} \geq 4\zeta^2 + \sqrt{\left(1 + k^2 - b - 4\zeta^2\right)^2}.$$
(2.82)

Since $1 + k^2 - b - 4\zeta^2 > 0$, this gives (2.81) as we wished to prove. $\qquad\square$

At this point, we know that $\mathbb{R} \subset \sigma_L$. We wish to see what this corresponds to for $\sigma_{\mathcal{L}}$. Looking at (2.63), we notice that

$$\Omega^2 = -\frac{1}{16}\left(\left(1 + k^2 - b - 4\zeta^2\right)^2 + 4\left(2\zeta\sqrt{b} - \sqrt{(1-b)(b-k^2)}\right)^2\right).$$
(2.83)

For convenience define

$$S_\Omega = \left\{\Omega : \Omega^2 = -\frac{1}{16}\left(\left(1 + k^2 - b - 4\zeta^2\right)^2 + 4\left(2\zeta\sqrt{b} - \sqrt{(1-b)(b-k^2)}\right)^2\right) \text{ and } \zeta \in \sigma_L\right\}.$$
(2.84)

Thus when $\zeta \in \mathbb{R}$, $\Omega(\zeta) \in i\mathbb{R}$ necessarily, since $\Omega^2(\zeta) < 0$. Applying (2.61), we see that $\zeta \in \mathbb{R}$ corresponds to imaginary spectral elements of $\sigma_{\mathcal{L}}$. Representative plots of Ω^2 are shown in Figure 2.3. The subset of S_Ω corresponding to $\zeta \in \mathbb{R}$ consists of $(-\infty, -i|\Omega_m|] \cup [i|\Omega_m|, \infty)$, where Ω_m is the maximum value of Ω. The set S_Ω is in general at least double covered as for almost every value of Ω there are at least two values of ζ which map to it. The spectrum on the imaginary axis is quadruple covered if the quartic (2.63) has four distinct real roots ζ, as is the case in Figure 2.3(d) for $\Omega^2 \in (-0.0639, -0.0243)$.

The condition for a subset of the spectrum to have a quadruple covering is readily determined. We require that the quartic $\Omega^2(\zeta)$ has three critical values, *i.e.*, that its derivative has three distinct roots. Examining the discriminant of (2.63) with respect to ζ, we see that if

$$k^2 < b < \frac{1 + 3k^2 + 3k^4 + k^6}{9(1 - k^2 + k^4)},$$
(2.85)

then there is a region of the imaginary axis which is quadruple covered. We show a plot of parameter space separated into two distinct regions by this condition in Figure 2.4. In the
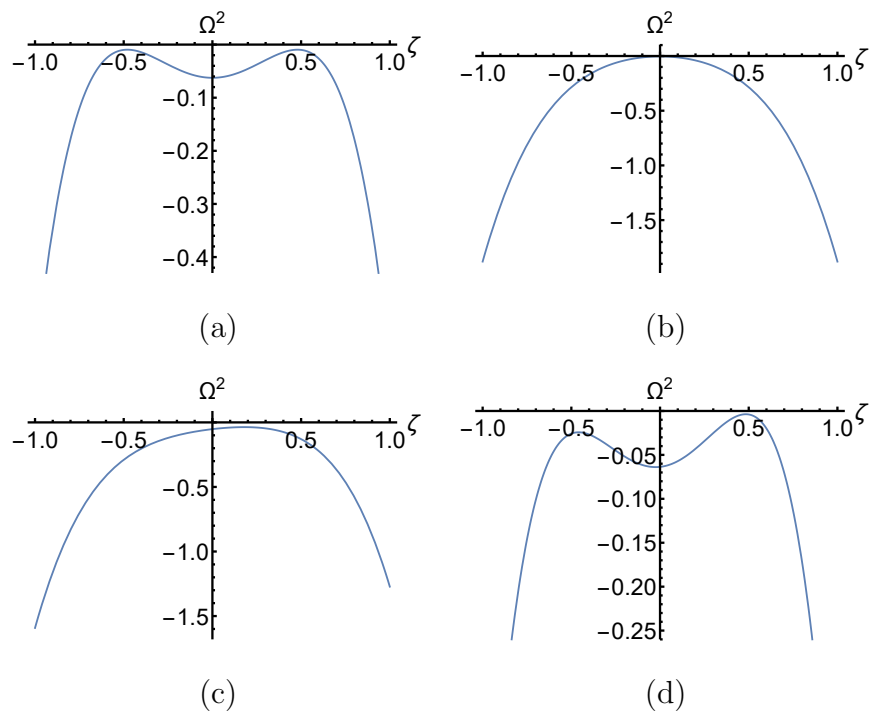
Figure 2.3: Ω^2 as a function of real ζ for various values of b and k: (a) cn case with $(k, b) = (0.2, 0.04)$; (b) dn case with $(k, b) = (0.5, 1)$; (c) general nontrivial-phase case with one maximum with $(k, b) = (0.8, 0.8)$; (d) general nontrivial-phase case with two maxima with $(k, b) = (0.2, 0.05)$.
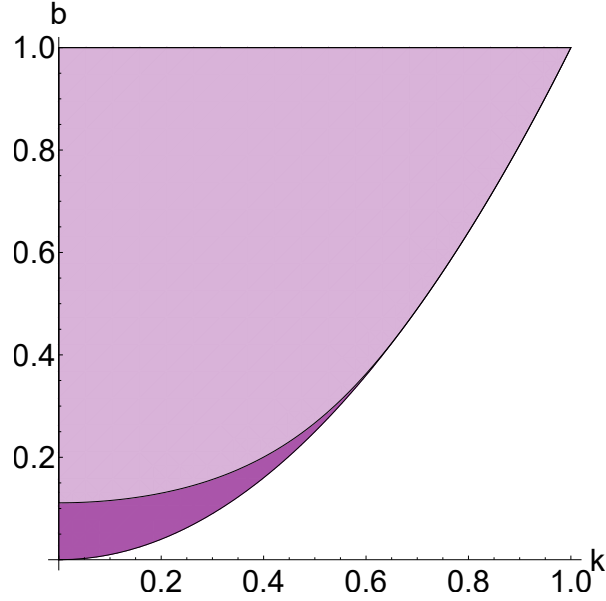
Figure 2.4: Parameter space split using (2.85) in the region for which a subset of $\sigma_{\mathcal{L}} \cup i\mathbb{R}$ is quadruple covered given by (2.85) (dark lower region), and only double covered (light upper region). The lower region region comes to a point at $(k, b) = (\sqrt{2}/2, 1/2)$.

upper region, the subset of $\sigma_{\mathcal{L}}$ on the imaginary axis has no quadruple covering. In the lower region there is a quadruple covering.

To explicitly determine the location of the covering on the imaginary axis, we need the local extrema of Ω^2. In the case when (2.85) is satisfied, the three extrema Ω_c^2 of Ω^2 satisfy the cubic in Ω_c^2

$$
\begin{aligned}
&-16k^4(-1 + k^2)^2 - 32\left(-4k^2 + 32k^4 - 4k^6 + 27bg_3\right)\Omega_c^2 + \\
&256(-1 - 18b + 27b^2 + 10k^2 - 18bk^2 - k^4)\Omega_c^4 - 4096\Omega_c^6 = 0.
\end{aligned}
\tag{2.86}
$$

Labeling the real roots as Ω_{c1}^2, Ω_{c2}^2, Ω_{c3}^2, with $\Omega_{c1}^2 < \Omega_{c2}^2 < \Omega_{c3}^2$, we have that the $\sigma_{\mathcal{L}}$ spectrum is double covered on the region $\left(-i\infty, -2\sqrt{\Omega_{c3}^2}\right) \cup \left(-2\sqrt{\Omega_{c2}^2}, -2\sqrt{\Omega_{c1}^2}\right) \cup \left(2\sqrt{\Omega_{c1}^2}, 2\sqrt{\Omega_{c2}^2}\right) \cup \left(2\sqrt{\Omega_{c3}^2}, i\infty\right)$, and quadruple covered on the region $\left(-2\sqrt{\Omega_{c3}^2}, -2\sqrt{\Omega_{c2}^2}\right) \cup \left(2\sqrt{\Omega_{c2}^2}, 2\sqrt{\Omega_{c3}^2}\right)$. If (2.85) is not satisfied, the $\sigma_{\mathcal{L}}$ spectrum has no quadruple covering, and is double covered on the region $\left(-i\infty, 2\sqrt{\Omega_{c*}^2}\right) \cup \left(2\sqrt{\Omega_{c*}^2}, i\infty\right)$, where Ω_{c*}^2 is the only real root of (2.86).

The extent of the spectrum $\sigma_{\mathcal{L}}$ on the imaginary axis vastly simplifies for the cnoidal wave, the dnoidal wave, and the Stokes wave solutions because (2.63) is biquadratic in the former two cases, and because $k = 0$ in the latter case. We detail these boundary cases below giving the $\sigma_{\mathcal{L}}$ spectrum. For dn solutions, the imaginary axis is double covered on the region $(-i\infty, -ik^2/2) \cup (ik^2/2, i\infty)$. This confirms results in [24, 48]. For cn solutions, if $k < \sqrt{2}/2$, the imaginary axis is double covered from $(-i\infty, -i/2) \cup (i/2, i\infty)$, and quadruple covered from $\left(-i/2, -ik\sqrt{1-k^2}\right) \cup \left(ik\sqrt{1-k^2}, i/2\right)$. Finally, for the Stokes wave solutions, if $b > 1/9$, then $i\mathbb{R} \subset \sigma_{\mathcal{L}}$ and is double covered. If $b < 1/9$, then the imaginary axis is still fully double covered except from $(-S_+, -S_-) \cup (S_-, S_+)$, where it is quadruple covered, here

$$S_\pm = \frac{\sqrt{-1 \mp \sqrt{(1-9b)(1-b)} + 9b\left(-2 \pm \sqrt{(1-9b)(1-b) + 3b}\right)}}{2\sqrt{2}}. \qquad (2.87)$$

2.8 Qualitatively different parts of the spectrum

Up to this point we have discussed only the subset of $\sigma_{\mathcal{L}}$ that is on the imaginary axis. In this section we discuss the rest of the spectrum. In general, for all choices of the parameters b and k, a part of the spectrum $\sigma_{\mathcal{L}}$ is in the right-half plane (corresponding to unstable modes). We split parameter space into five regions where $\overline{\sigma_{\mathcal{L}} \setminus i\mathbb{R}}$ is qualitatively different. Here $\overline{\sigma_{\mathcal{L}} \setminus i\mathbb{R}}$ refers to the closure of $\sigma_{\mathcal{L}}$ not on the imaginary axis.

We refer to Figure 2.5, which shows (k, b) parameter space with curves that split it into regions where $\overline{\sigma_{\mathcal{L}} \setminus i\mathbb{R}}$ spectrum is qualitatively different. The exact curves splitting up the regions, as well as their derivations, are given below. In Figure 2.6(1) we show representative plots of $\sigma_{\mathcal{L}}$ for the trivial-phase solutions on the boundary of parameter space, and in Figure 2.6(2) we show the corresponding σ_L spectrum. Additionally, we plot the ζ choices for which $\Omega(\zeta) \in i\mathbb{R}$. These curves are used to split up parameter space. The stability of trivial-phase solutions has been well studied in the literature [24, 34, 42, 48]. The Stokes wave solutions have constant magnitude and their stability problem has constant coefficients. Thus it is significantly easier to analyze.
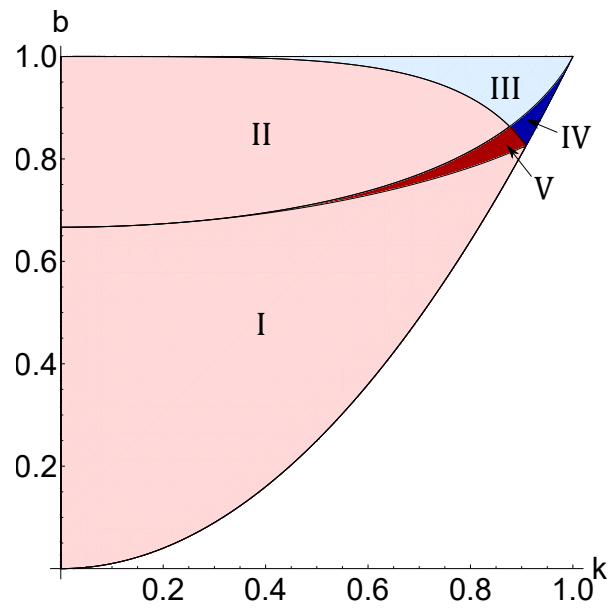
Figure 2.5: A colored plot of parameter space with regions corresponding to different qualitative behavior in the linear stability spectrum. Regions I and II: two nested figure 8s; region III: non-self-intersecting butterflies; region IV: self-intersecting butterflies; region V: one triple-figure 8 inside of a figure 8.

For the dn solutions, $\overline{\sigma_{\mathcal{L}} \setminus i\mathbb{R}}$ consists of a quadruple covered finite interval on the real axis. For Stokes wave solutions $\overline{\sigma_{\mathcal{L}} \setminus i\mathbb{R}}$ consists of a single-covered figure 8, and $\overline{\sigma_{\mathcal{L}} \setminus i\mathbb{R}}$ for cn solutions consists of a double covered figure 8. There are two cases for the cn solutions. Either $\sigma_{\mathcal{L}} \cap i\mathbb{R}$ pierces the figure 8 (see Figure 2.6(1c)), or it does not (see Figure 2.6(1d)). The exact value of k separating the closure of the regions is given below.

For these trivial-phase cases, much can be proven and quantified explicitly, *i.e.*, not in terms of special functions. Specifically, for the spectrum in the Stokes wave case we give a parametric description for the figure 8 curve. For the spectrum for the dn case we calculate the extent of the covering of $\sigma_{\mathcal{L}} \cap i\mathbb{R}$. For the spectrum in the piercing cn case, we give an explicit expression for where the top (or bottom) of the figure 8 crosses the imaginary axis. Additionally, we have an explicit expression for the tangents to $\sigma_{\mathcal{L}}$ leaving the origin in both cn cases. In fact, we are able to approximate the spectrum at the origin using a Taylor series to arbitrary order. These series give a good approximation to the greatest real part of the figure 8 using only a few terms.

In the interior of parameter space we examine the nontrivial-phase solutions. Four cases appear and plots of the $\sigma_{\mathcal{L}}$ spectrum for representative choices of k and b are seen in Figure 2.7. The cases are as follows

(2.7-1a) $\overline{\sigma_{\mathcal{L}} \setminus i\mathbb{R}}$ consists of two single-covered figure 8s, resulting in the degenerate double covered case of $\overline{\sigma_{\mathcal{L}} \setminus i\mathbb{R}}$ for cn solutions.

(2.7-1b) We have a single-covered non-self-intersecting butterfly. As $b \to 1$ the wings of this butterfly collapse to the real axis and the spectrum for dn solutions is seen with a quadruple covering on the real axis.

(2.7-1c) $\overline{\sigma_{\mathcal{L}} \setminus i\mathbb{R}}$ is a single-covered triple-figure 8 inside of a single-covered figure 8.

(2.7-1d) $\overline{\sigma_{\mathcal{L}} \setminus i\mathbb{R}}$ consists of a single-covered self-intersecting butterfly, which is seen as a perturbation of $\overline{\sigma_{\mathcal{L}} \setminus i\mathbb{R}}$ for the cn solutions as the double covered figure 8 splits apart horizontally.

(1a) (1b) (1c) (1d)

(2a) (2b) (2c) (2d)
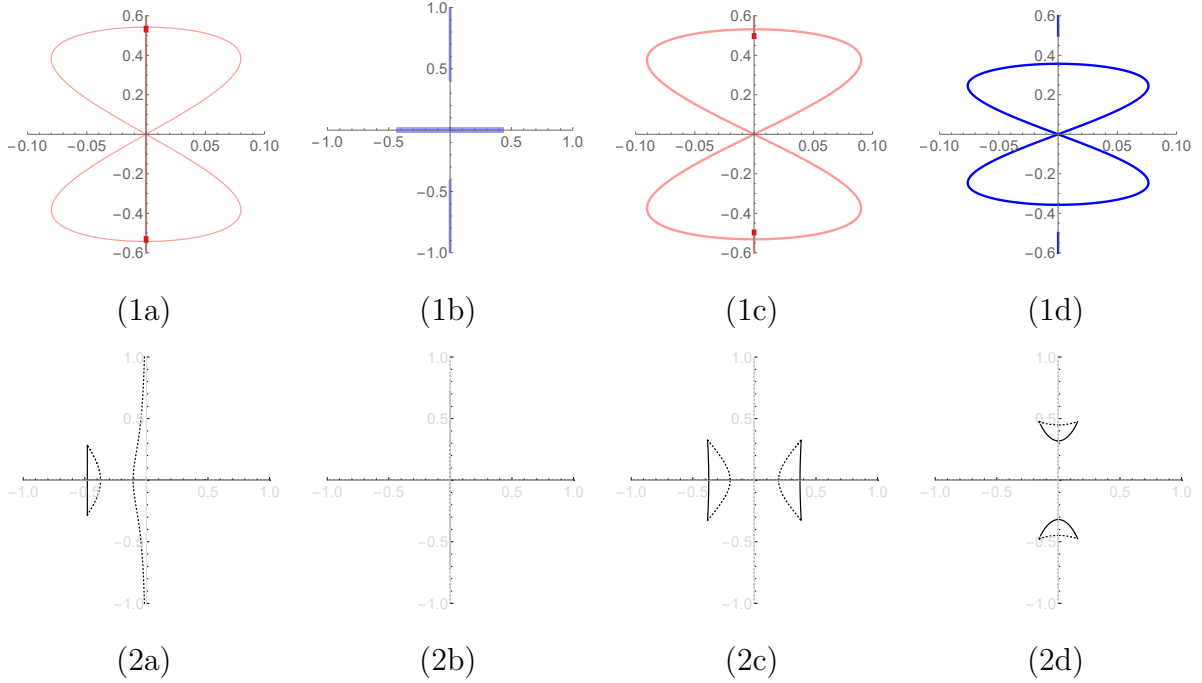
Figure 2.6: (1) $\sigma_{\mathcal{L}}$ for the trivial-phase cases and (2) the corresponding σ_L spectra (solid lines), values for which $\mathrm{Re}\,(\Omega(\zeta)) = 0$ (dotted). In (1), color corresponds to region in Figure 2.5 and thickness of curves corresponds to single, double, or quadruple covering going from thinnest to thickest. (a) Stokes wave solution, regions I and II, $(k, b) = (0, 0.08)$; (b) dn solution, region III, $(k, b) = (0.9, 1)$; (c) cn solution with piercing, region I, $(k, b) = (0.65, 0.4225)$; (d) cn solution without piercing, region IV, $(k, b) = (0.95, 0.9025)$.

In fact, there are two non-connected regions in parameter space for which we have two single-covered figure 8s, but qualitatively the spectrum is the same so we do not show samples from both regions.

For the nontrivial-phase case less can be determined explicitly. That said, we present an explicit expression for the slope of the spectrum for any nontrivial-phase solution as it leaves the origin. Since at least some of these slopes are finite, this settles the conjecture of Rowlands [60] that *all* stationary solutions of (2.1) are unstable. Moreover, a Taylor series expansion around the origin can be obtained for all cases and it well approximates the largest real part with a small number of terms. Additionally, explicit expressions for the tops (or bottoms) of the figure 8s in both cases with figure 8s are given.

A starting point for solving (2.73) for ζ is to recognize that if ζ satisfies $\Omega^2(\zeta) = 0$, then ζ must satisfy (2.73). This is due to the fact that the origin is always included in $\sigma_{\mathcal{L}}$ and hence in S_Ω. In fact, the four roots of the quartic $\Omega^2 = 0$ corresponds to the fact that $0 \in \sigma_{\mathcal{L}}$ with multiplicity four. This is seen from the symmetries of (2.1) and by applying Noether's Theorem [47, 65].

It may be instructive to see this explicitly. In the general case, the roots of $\Omega^2(\zeta)$ are

$$\zeta_c = \left\{ \frac{\sqrt{1-b}}{2} \pm i \frac{\sqrt{b} - \sqrt{b-k^2}}{2}, \; -\frac{\sqrt{1-b}}{2} \pm i \frac{\sqrt{b} + \sqrt{b-k^2}}{2} \right\}. \tag{2.88}$$

These roots are seen in Figures 2.6-2.8 (bottom) as the intersections between the solid and dotted lines lying off of the real axis. Indeed, as long as $b, k > 0$, these points have nonzero imaginary part, and other $\zeta \in \overline{\sigma_L \setminus \mathbb{R}}$ can be found by following the level curves of (2.73) originating from these points. For convenience we label these four roots $\zeta_1, \zeta_2, \zeta_3, \zeta_4$, where the subscript corresponds to the quadrant on the real and imaginary plane the root is in.

To better examine this we look at the tangent vector field to the level curve (2.76). If we let $\zeta = \zeta_r + i\zeta_r$, then

$$I(\zeta) = I(\zeta_r + i\zeta_i) = -2i(\zeta_r + i\zeta_i)\mathcal{K}(k) \pm 2 \left(\zeta_w(\alpha)\mathcal{K}(k) - \left(\mathcal{E}(k) - \frac{1}{3}\left(2 - k^2\right)\mathcal{K}(k) \right) \alpha \right). \tag{2.89}$$

The level curve $\{ \zeta \in \mathbb{C} : \text{Re}\left[I(\zeta) \right] = 0 \}$, is exactly the condition for $\zeta \in \sigma_L$. Taking derivatives with respect to ζ_r and ζ_i gives a normal vector field to the level curves of the general condition $\text{Re}\left[I(\zeta) \right] = C$ for any constant C, specifically, the normal vector is given by

$$\left(\frac{\mathrm{d}\text{Re}\left[I(\zeta_r + i\zeta_i) \right]}{\mathrm{d}\zeta_r}, \frac{\mathrm{d}\text{Re}\left[I(\zeta_r + i\zeta_i) \right]}{\mathrm{d}\zeta_i} \right).$$

Thus, the tangent vector field is

$$\left(-\frac{\mathrm{d}\text{Re}\left[I(\zeta_r + i\zeta_i) \right]}{\mathrm{d}\zeta_i}, \frac{\mathrm{d}\text{Re}\left[I(\zeta_r + i\zeta_i) \right]}{\mathrm{d}\zeta_r} \right).$$

By applying the chain rule and using the fact that $\text{Re}[iz] = -\text{Im}[z]$, we have that the tangent vector field to the level curves is

$$\left(\text{Im}\left[\frac{\mathrm{d}I}{\mathrm{d}\zeta} \right], \text{Re}\left[\frac{\mathrm{d}I}{\mathrm{d}\zeta} \right] \right).$$

(1a)　　　　(1b)　　　　(1c)　　　　(1d)

(2a)　　　　(2b)　　　　(2c)　　　　(2d)
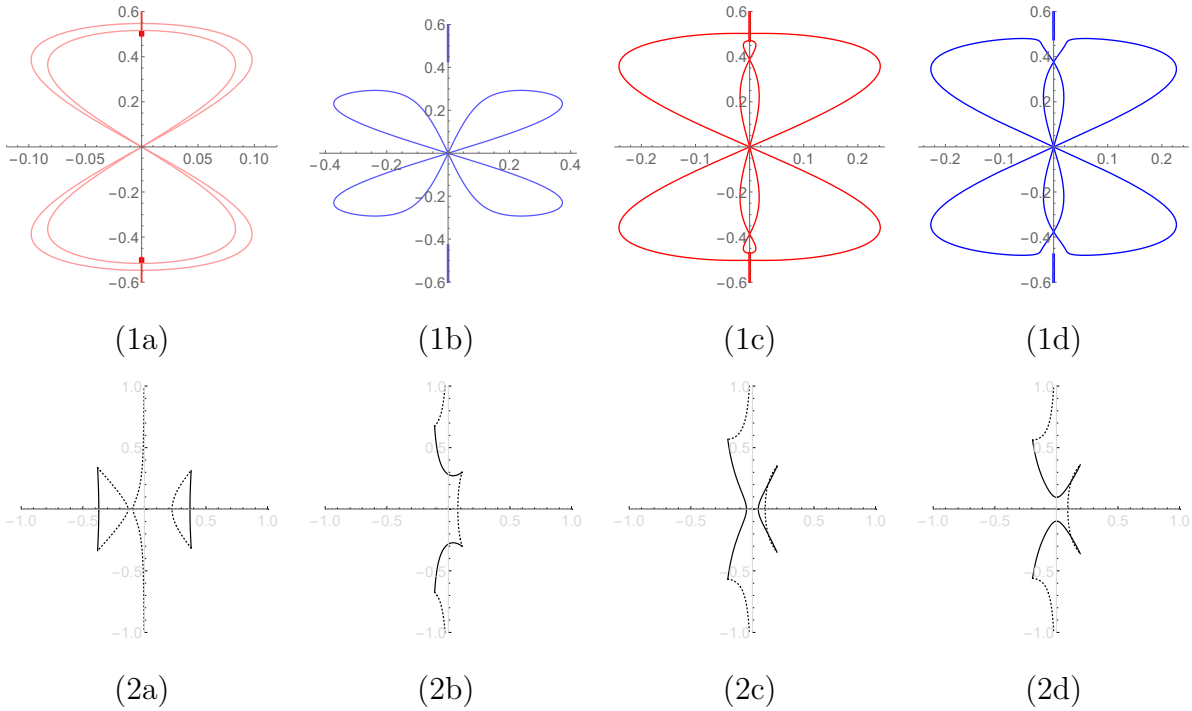
Figure 2.7: (1) $\sigma_{\mathcal{L}}$ for the nontrivial-phase cases and (2) the corresponding σ_L spectra (solid lines), values for which $\operatorname{Re}(\Omega(\zeta)) = 0$ (dotted). In (1), color corresponds to region in Figure 2.5. (a) Double-figure 8 solution, regions I and II, $(k, b) = (0.65, 0.423)$; (b) non-self-intersecting butterfly solution, region III, $(k, b) = (0.9, 0.95)$; (c) triple-figure 8 solution, region V, $(k, b) = (0.89, 0.84)$; (d) self-intersecting butterfly solution, region IV, $(k, b) = (0.9, 0.85)$.

Substituting this back into (2.79), the tangent vectors are

$$\left(\text{Im}\left[\frac{2\mathcal{E}(k) - (1 + b - k^2 + 4\zeta^2)\,\mathcal{K}(k)}{2\Omega(\zeta)}\right],\text{Re}\left[\frac{2\mathcal{E}(k) - (1 + b - k^2 + 4\zeta^2)\,\mathcal{K}(k)}{2\Omega(\zeta)}\right]\right). \quad (2.90)$$

Thus, given a point in the σ_L spectrum (lying on the 0 level curve of $\text{Re}\left[I(\zeta)\right]$), we can follow the tangent vector field to find other points in the σ_L spectrum.

2.8.1 Stokes wave case

Applying this idea to the Stokes wave case, we see that generically

$$\zeta_c = \frac{\sqrt{1 - b}}{2},\ \frac{\sqrt{1 - b}}{2},\ -\frac{\sqrt{1 - b}}{2} \pm i\sqrt{b},$$

i.e., there is a double root on the real axis and two conjugate roots. Following level curves we see that

$$\forall \zeta_i \in [-\sqrt{b}, \sqrt{b}],\quad -\frac{\sqrt{1 - b}}{2} + i\zeta_i \in \sigma_L. \quad (2.91)$$

Substituting this into (2.63), we find that the $\sigma_{\mathcal{L}}$ spectrum for Stokes waves is given parametrically as a single-covered figure 8:

$$\lambda = \pm\left(2\sqrt{b\zeta_i^2 - \zeta_i^4} + 2i\,\text{sgn}(\zeta_i)\sqrt{(1 - b)(b - \zeta_i^2)}\right) \text{ for } \zeta_i \in [-\sqrt{b}, \sqrt{b}]. \quad (2.92)$$

Plots of the σ_L and the $\sigma_{\mathcal{L}}$ spectra are seen in Figure 2.6(a) for $k = 0$, $b = 0.08$.

2.8.2 dn case

Similarly, in the dn case we find that

$$\left[-\frac{1 + \sqrt{1 - k^2}}{2}i, -\frac{1 - \sqrt{1 - k^2}}{2}i\right] \cup \left[\frac{1 - \sqrt{1 - k^2}}{2}i, \frac{1 + \sqrt{1 - k^2}}{2}i\right] \in \sigma_L, \quad (2.93)$$

where $[\cdot, \cdot]$ corresponds to the straight line segment between its two endpoints. Mapping this back to $\sigma_{\mathcal{L}}$ via (2.63), we find that there is a quadruple covering of the real axis

$$\left[-\sqrt{1 - k^2}, \sqrt{1 - k^2}\right] \in \sigma_{\mathcal{L}}. \quad (2.94)$$

Representative plots of these spectrum are seen in Figure 2.6(b). This corrects a typo in [48], and confirms the conjecture made in [24].

2.8.3   cn case

For the cn case, less is known explicitly. Representative plots of the σ_L spectrum are shown in Figure 2.6(2c,2d). In both cases we have a quadrafold symmetry. The distinguishing factor between the two cases in (c) and (d) is whether or not $\overline{\sigma_L \setminus \mathbb{R}}$ leaving ζ_c crosses the real axis or the imaginary axis. Examining (2.90) on the real axis we can determine the condition for a vertical tangent to occur. This happens when

$$\zeta = \pm \frac{\sqrt{2\mathcal{E}(k) - \mathcal{K}(k)}}{2\sqrt{\mathcal{K}(k)}}. \tag{2.95}$$

Equating $\zeta = 0$, we solve for k such that the vertical tangent occurs at the origin. With $2E(k^*) - K(k^*) = 0$, we find that $k^* \approx 0.908909$. This gives two cases: if $k < k^*$ then $\overline{\sigma_L \setminus \mathbb{R}}$ crosses the real axis, and if $k > k^*$ then $\overline{\sigma_L \setminus \mathbb{R}}$ crosses the imaginary axis. When $k < k^*$ we know the crossing of the real axis occurs when ζ satisfies (2.95). Mapping this back to $\sigma_{\mathcal{L}}$, we see that this point corresponds to the top (or bottom) of the figure 8

$$\lambda = \pm i \frac{\sqrt{(1 - k^2)\mathcal{K}^2(k) - 2(1 - k^2)\mathcal{E}(k)\mathcal{K}(k) + \mathcal{E}^2(k)}}{\mathcal{K}(k)}. \tag{2.96}$$

For all $k < k^*$ the figure 8 is pierced by the covering on the imaginary axis as seen in Figure 2.6(1c), but as $k \to k^*$, (2.96) approaches $\pm i/2$ which is the extent of the covering on the imaginary axis as seen in Section 2.7. Thus for $k > k^*$, the figure 8 is no longer pierced by $\sigma_{\mathcal{L}} \cap i\mathbb{R}$, as is the case in Figure 2.6(1d).

2.8.4   Nontrival-phase cases

Plots of generic cases of the σ_L spectrum are seen in Figure 2.7(2a-d). The idea of whether $\overline{\sigma_L \setminus \mathbb{R}}$ crosses the real or imaginary axis still applies. The same analysis as above yields conditions on when ζ crosses the real axis. We find that when

$$\zeta = \pm \frac{\sqrt{2\mathcal{E}(k) - \mathcal{K}(k) - (b - k^2)\mathcal{K}(k)}}{2\sqrt{\mathcal{K}(k)}}, \tag{2.97}$$

$\overline{\sigma_L \setminus \mathbb{R}}$ crosses the real axis. Mapping this back to $\sigma_{\mathcal{L}}$, this corresponds to the top (or bottom) of the outside figure 8:

$$\lambda = \pm i \sqrt{\frac{\mathcal{E}^2(k)}{\mathcal{K}^2(k)} - 2(1-b)\frac{\mathcal{E}(k)}{\mathcal{K}(k)} + (1 - 2b^2 - k^2 + 2bk^2) + 2c\sqrt{2\frac{\mathcal{E}(k)}{\mathcal{K}(k)} + k^2 - b - 1}}, \quad (2.98)$$

and the top (or bottom) of the enclosed figure 8 (or triple-figure 8):

$$\lambda = \pm i \sqrt{\frac{\mathcal{E}^2(k)}{\mathcal{K}^2(k)} - 2(1-b)\frac{\mathcal{E}(k)}{\mathcal{K}(k)} + (1 - 2b^2 - k^2 + 2bk^2) - 2c\sqrt{2\frac{\mathcal{E}(k)}{\mathcal{K}(k)} + k^2 - b - 1}}. \quad (2.99)$$

We note that $\zeta < 0$ in (2.97) corresponds to the top (or bottom) of the outside figure 8 in (2.98), while $\zeta > 0$ in (2.97) corresponds to the top (or bottom) of the enclosed figure 8 in (2.99). This is difficult to show directly, but is seen from the more general result that for any $\zeta \in \mathbb{R}$, $\Omega^2(-|\zeta|) > \Omega^2(|\zeta|)$, which is derived directly from (2.83).

Equating $\zeta = 0$ in (2.97) gives the condition for differentiating between figure 8's and butterflies:

$$b = -1 + k^2 + \frac{2\mathcal{E}(k)}{\mathcal{K}(k)}. \quad (2.100)$$

If b is less than this value the spectrum looks like in Figure 2.7(1a or 1c), and if b is greater than this value the spectrum looks like in Figure 2.7(1b or 1d). In Figure 2.8(a) we show the case when (2.100) is exactly satisfied.

Next we examine the slopes of the $\sigma_{\mathcal{L}}$ curves at the origin. Because $\sigma_{\mathcal{L}} = 2S_\Omega$ it suffices to examine the slopes for the set S_Ω. We let $\Omega = \Omega_r + i\Omega_i$, and we consider ζ_i as a function of ζ_r so that $\Omega(\zeta_r, \zeta_i(\zeta_r))$. Applying the chain rule we have that the slope at any point in the set S_Ω is

$$\frac{\mathrm{d}\Omega_i}{\mathrm{d}\Omega_r} = \frac{\mathrm{d}\Omega_i/\mathrm{d}\zeta_r}{\mathrm{d}\Omega_r/\mathrm{d}\zeta_r} = \frac{\frac{\mathrm{d}\Omega_i}{\mathrm{d}\zeta_r} + \frac{\mathrm{d}\Omega_i}{\mathrm{d}\zeta_i}\frac{\mathrm{d}\zeta_i}{\mathrm{d}\zeta_r}}{\frac{\mathrm{d}\Omega_r}{\mathrm{d}\zeta_r} + \frac{\mathrm{d}\Omega_r}{\mathrm{d}\zeta_i}\frac{\mathrm{d}\zeta_i}{\mathrm{d}\zeta_r}}, \quad (2.101)$$

where

$$\frac{\mathrm{d}\zeta_i}{\mathrm{d}\zeta_r} = -\frac{\mathrm{d}\mathrm{Re}(I)/\mathrm{d}\zeta_r}{\mathrm{d}\mathrm{Re}(I)/\mathrm{d}\zeta_i}. \quad (2.102)$$

(1a)   (1b)   (1c)   (1d)

(2a)   (2b)   (2c)   (2d)
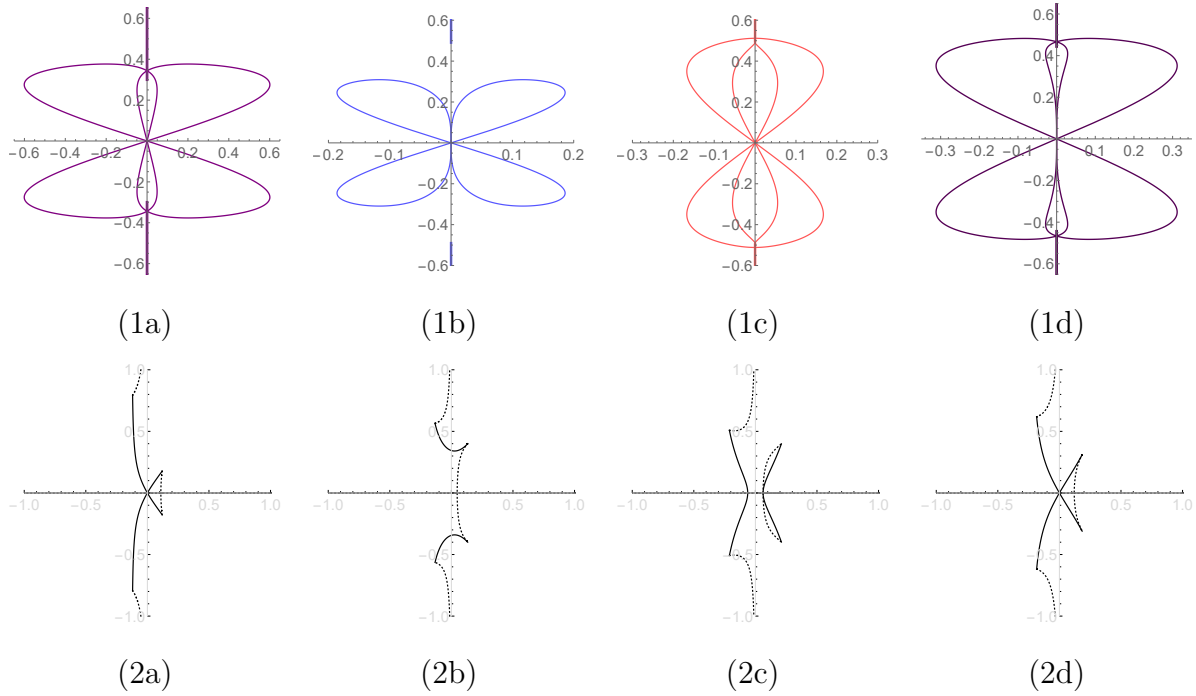
Figure 2.8: (1) $\sigma_{\mathcal{L}}$ for the cases separating regions and (2) the corresponding σ_L spectra (solid lines), values for which $\mathrm{Re}\,(\Omega(\zeta)) = 0$ (dotted). In (1), color corresponds to location in Figure 2.5. (a) Split between figure 8s and butterflies, $(k, b) = (0.75, 0.942384)$; (b) split between self-intersecting and non-self-intersecting butterflies, $(k, b) = (0.95, 0.929542)$; (c) lower split between figure 8 and triple-figure 8, $(k, b) = (0.9, 0.821993)$; (d) four-corners point, $(k, b) = (0.876430, 0.863399)$.

We examine (2.101) near where $\Omega = 0$ and $\zeta = \zeta_c$. The slopes around the origin are

$$\frac{d\Omega_i}{d\Omega_r} = \pm \frac{\left(2\sqrt{b(1-b)(b-k^2)} + \sqrt{1-b}(k^2 - 2b)\right)\mathcal{E}(k)}{\left(\sqrt{b-k^2} - \sqrt{b}\right)\left(\left(b-1-\sqrt{b(b-k^2)}\right)\mathcal{E}(k) + (1-k^2)\mathcal{K}(k)\right)}, \tag{2.103}$$

$$\frac{d\Omega_i}{d\Omega_r} = \pm \frac{\left(2\sqrt{b(1-b)(b-k^2)} - \sqrt{1-b}(k^2 - 2b)\right)\mathcal{E}(k)}{\left(\sqrt{b-k^2} + \sqrt{b}\right)\left(-\left(b-1-\sqrt{b(b-k^2)}\right)\mathcal{E}(k) + (1-k^2)\mathcal{K}(k)\right)}. \tag{2.104}$$

In the cn case $(b = k^2)$ the slopes at the origin simplify to

$$\frac{d\Omega_i}{d\Omega_r} = \pm \frac{k\mathcal{E}(k)}{\sqrt{1-k^2}(\mathcal{E}(k) - \mathcal{K}(k))}. \tag{2.105}$$

For the cn solutions, these slopes are always finite. This is not necessarily the case for nontrivial-phase solutions. Specifically, while the slopes in (2.104) are always finite, the slopes in (2.103) can be infinite if

$$\left(b - 1 - \sqrt{b(b-k^2)}\right)\mathcal{E}(k) + (1-k^2)\mathcal{K}(k) = 0. \tag{2.106}$$

Spectra corresponding to solutions for which this condition is satisfied are shown in in Figure 2.8(b). The condition corresponds to the splitting between the two butterfly regions, as well as the upper splitting between the triple-figure 8 and the figure 8s regions. See Figure 2.5. Further application of the chain rule can yield expressions for derivatives around the origin of any order, and the same technique can be applied around the top of the figure 8s. In doing this we can obtain Taylor series approximations of $\sigma_{\mathcal{L}}$ to any order.

Finally, an expression is obtained for the lower boundary of the triple-figure 8s and figure 8s regions. A representative example of this case is seen in Figure 2.8(c). The boundary between these regions occurs at the bifurcation when $\sigma_{\mathcal{L}} \cap i\mathbb{R}$ and $\overline{\sigma_{\mathcal{L}} \setminus i\mathcal{R}}$ have a threefold intersection, see Figure 2.9(b). This occurs when

$$\text{Rt(b,k)} = \sqrt{\frac{2\mathcal{E}(k) - \mathcal{K}(k) - b\mathcal{K}(k) + k^2\mathcal{K}(k)}{4\mathcal{K}(k)}}, \tag{2.107}$$

where Rt(b,k) is the smallest real root of the cubic equation

$$-c + \left(-1 + 3b - k^2\right)Y + 4Y^3 = 0. \tag{2.108}$$
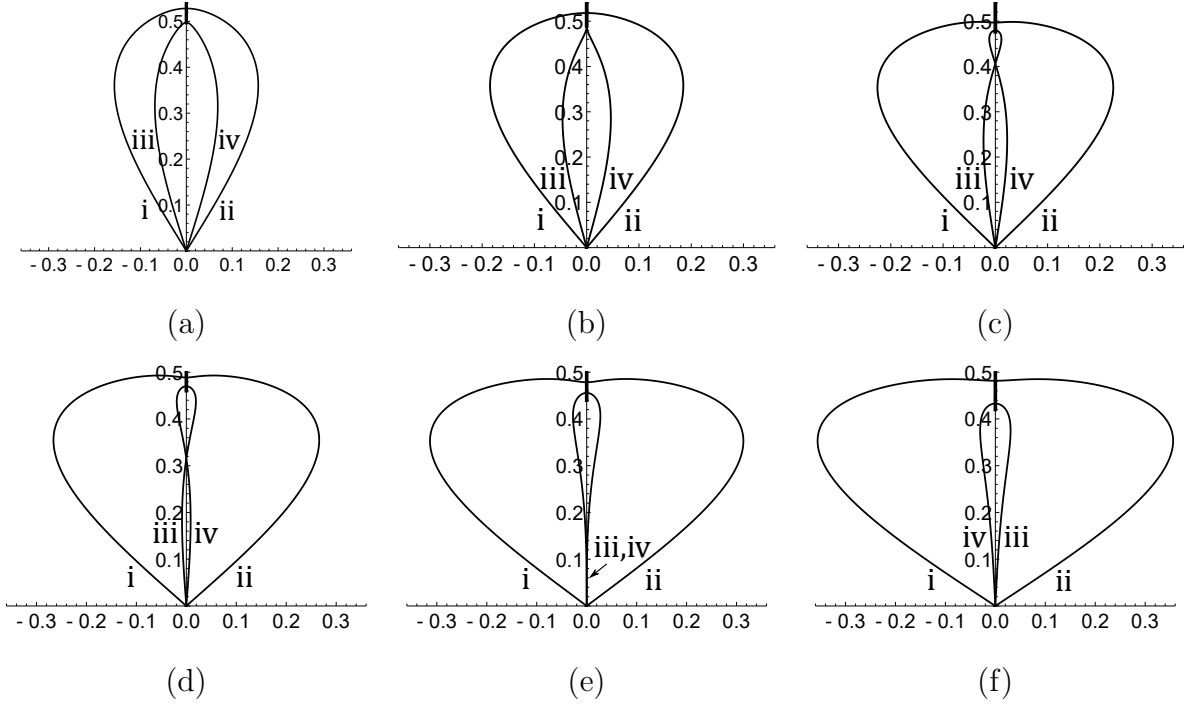
Figure 2.9: (1) $\sigma_{\mathcal{L}}$ in the upper-half plane for a sequence of parameter values demonstrating the boundaries of the triple-figure 8 region. (a) Two figure 8s, lower region, $(k, b) = (0.89, 0.8)$; (b) lower boundary of triple-figure 8 region, $(k, b) = (0.895, 0.819747)$, the enclosed figure 8 is not smooth at the top; (c) triple-figure 8 near lower boundary, $(k, b) = (0.895, 0.84)$; (d) triple-figure 8 near upper boundary, $(k, b) = (0.887, 0.85)$; (e) upper boundary of the triple-figure 8 region, $(k, b) = (0.875, 0.862349)$; (f) Two figure 8s, upper region, $(k, b) = (0.86, 0.87)$.

This is seen directly as the left-hand side of (2.107) gives the point when $\text{Re}(\Omega) = 0$ intersects the real axis and the right-hand side is (2.97), the point where $\overline{\sigma_L \setminus \mathbb{R}}$ intersects the real axis.

In Figure 2.9, we plot $\sigma_{\mathcal{L}} \cap \mathbb{C}^+$. In $\mathbb{C}^+$ there are two lobes to the triple-figure 8, one near the origin and one away from the origin, see Figure 2.9(c,d). For triple-figure 8s near the lower boundary of the region as in Figure 2.9(c), the lobe of $\overline{\sigma_{\mathcal{L}} \setminus i\mathbb{R}}$ near the origin is larger than the lobe away from the origin. In contrast, for triple-figure 8s near the upper boundary of the region, see Figure 2.9(d), the lobe of $\overline{\sigma_{\mathcal{L}} \setminus i\mathbb{R}}$ away from the origin is larger.

We also mention the four curves of $\overline{\sigma_{\mathcal{L}} \setminus i\mathbb{R}}$ near the origin which we label i, ii, iii and iv in Figure 2.9. These curves give a distinguishing feature between regions I and II in Figure 2.5

both with two figure 8s. Specifically, the curves iii and iv of $\overline{\sigma_\mathcal{L} \setminus i\mathbb{R}}$ for the enclosed figure 8 near the origin switch places. This is seen from examining the slopes of these curves in (2.103) and also by comparing the relative positions of curves c and d in Figure 2.9(a) and Figure 2.9(f).

Lastly, we mention the four-corners point seen in Figure 2.8(d). This point occurs at the intersection of (2.100) and (2.106), the intersection of all four nontrivial-phase regions. At this point, $\overline{\sigma_\mathcal{L} \setminus i\mathbb{R}}$ has vertical tangents at the origin as well as a four-way intersection point on the imaginary axis corresponding to $\zeta = 0$ in σ_L.

2.9   *Floquet theory and subharmonic perturbations*

We examine $\sigma_\mathcal{L}$ using a Floquet parameter description. We use this to prove some spectral stability results with respect to perturbations of an integer multiple of the fundamental period of the solution, *i.e.*, subharmonic perturbations.

Note that the solutions to the stationary problem (2.3) are not periodic in general, as they may have a nontrivial phase. On the other hand, (2.39) is a spectral problem with periodic coefficients since it depends only on $R(x)$.

We write the eigenfunctions from (2.39) using a Floquet-Bloch decomposition

$$\begin{pmatrix} U(x) \\ V(x) \end{pmatrix} = e^{i\mu x} \begin{pmatrix} \hat{U}(x) \\ \hat{V}(x) \end{pmatrix}, \quad \hat{U}(x + T(k)) = \hat{U}(x), \quad \hat{V}(x + T(k)) = \hat{V}(x). \quad (2.109)$$

with $\mu \in [-\pi/T(k), \pi/T(k))$ [12, 24]. Here $T(k) = 2\mathcal{K}(k)$ for all solutions, except $T(k) = 4\mathcal{K}(k)$ for the cn solution. From Floquet's Theorem [24], all bounded solutions of (2.39) are of this form, and our analysis includes perturbations of an arbitrary period. Specifically, $\mu = 2m\pi/T(k)$ for $m \in \mathbb{Z}$ corresponds to perturbations of the same period $T(k)$ of our solutions, and in general,

$$\mu = \frac{2m\pi}{PT(k)}, \quad m, P \in \mathbb{Z}, \quad (2.110)$$

corresponds to perturbations of period $PT(k)$. The choice of the specific range of μ is arbitrary, as long as it is of length $2\pi/T(k)$. For added clarity in this section, we plot some

figures using the larger range $[-2\pi/T(k), 2\pi/T(k))$, before modding out, reducing the μ interval to $[-\pi/T(k), \pi/T(k))$.

In the previous sections $\sigma_{\mathcal{L}}$ is parameterized in terms of ζ. We wish to parameterize $\sigma_{\mathcal{L}}$ in terms of μ. We examine the U eigenfunction from (2.109). From the periodicity of $\hat{U}$ we have

$$e^{i\mu T(k)} = \frac{U(x + T(k))}{U(x)}. \tag{2.111}$$

Using (2.62), (2.56), and (2.57), we have

$$e^{i\mu T(k)} = \exp\left(-2\int_0^{T(k)} \frac{(A(x) - \Omega)\phi + B_x(x) + i\zeta B(x)}{B(x)}dx\right) \exp\left(i\theta(T(k))\right), \tag{2.112}$$

where we have used the periodicity properties

$$A\left(x + T(k)\right) = A(x), \quad B\left(x + T(k)\right) = B(x)e^{i\theta(T(k))}, \quad \theta\left(x + T(k)\right) = \theta(x) + \theta\left(T(k)\right). \tag{2.113}$$

Using (2.73),

$$\mu(\zeta) = \frac{2iI(\zeta)}{T(k)} + \frac{\theta\left(T(k)\right)}{T(k)} + \frac{2\pi n}{T(k)}, \tag{2.114}$$

where $I(\zeta)$ is given in (2.89), $n \in \mathbb{Z}$, and

$$\theta(T(k)) = \begin{cases} \int_0^{T(k)} \frac{\sqrt{b(1-b)(b-k^2)}}{b - k^2 \mathrm{sn}^2(y,k)}dy, & \text{if } b > k^2, \\ \pi, & \text{if } b = k^2, \end{cases} \tag{2.115}$$

from (2.7). Equation (2.114) relates the two spectral parameters ζ and μ.

In what follows we discuss the stability of solutions with respect to perturbations of integer multiples of their fundamental periods, so-called subharmonic perturbations [39]. The expression (2.114) gives an easy way to do this. Specifically, from (2.110) we know which values of μ correspond to perturbations of what type. For stability, we need all spectral elements associated with a given μ value to have zero real part. In Figure 2.10 we plot the real part of $\sigma_{\mathcal{L}}$ as a function of $\mu T(k)$ using (2.61), (2.63), and (2.114). We rescale
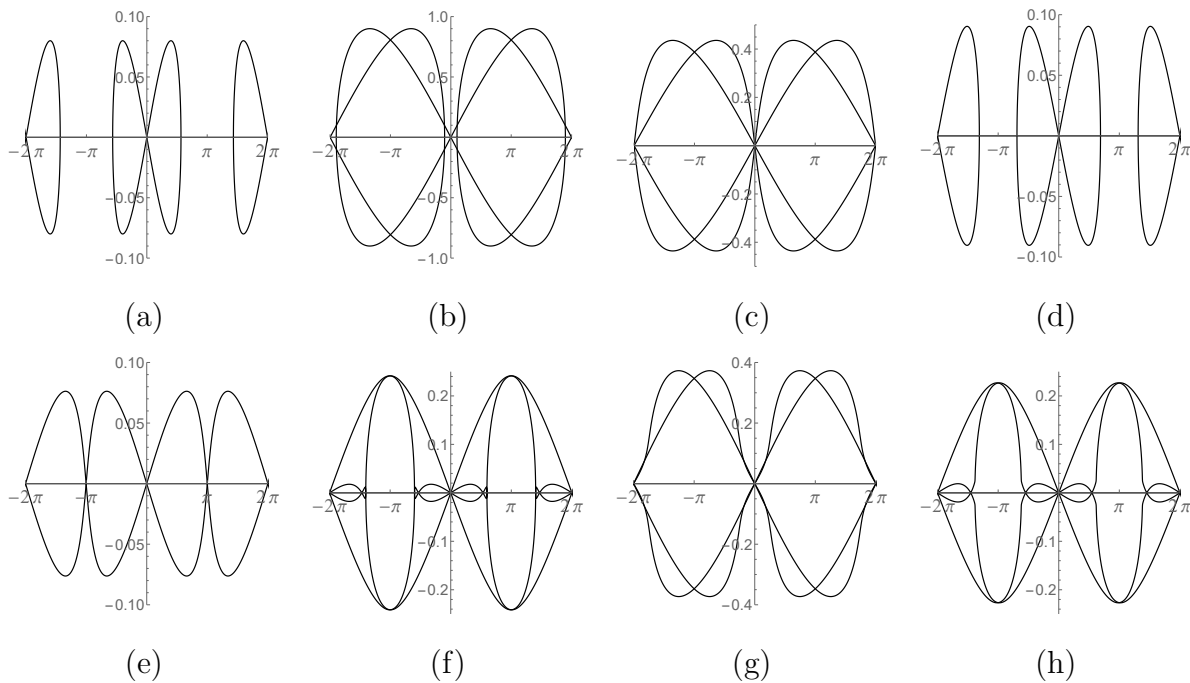
Figure 2.10: The real part of the spectrum $\mathrm{Re}(\lambda)$ (vertical axis) as a function of $\mu T(k)$ (horizontal axis). $T(k)\mu = 2m\pi/P$ for integers m and P corresponds to perturbations of period P times the period of the underlying solution. (a) Stokes wave solution, $(k,b) = (0, 0.08)$; (b) Stokes wave solution, $(k,b) = (0, 0.9)$; (c) dn solution, $(k,b) = (0.9, 1)$; (d) cn solution, $(k,b) = (0.65, 0.4225)$; (e) cn solution, $(k,b) = (0.95, 0.9025)$; (f) triple-figure 8 solution, $(k,b) = (0.89, 0.84)$; (g) non-self-intersecting butterfly solution, $(k,b) = (0.9, 0.95)$; (h) self-intersecting butterfly solution, $(k,b) = (0.9, 0.85)$.

μ by the fundamental period $T(k)$ for consistency in our figures. Specifically,

$$\mu T(k) = \frac{2\pi m}{P},$$

corresponds to perturbations of $PT(k)$ for any integer n. In what follows, we omit $\sigma_{\mathcal{L}} \cap i\mathbb{R}$.

2.9.1 Stokes wave case

We begin with the spectrum for Stokes waves (see Figures 2.10(a,b)). After simplification,

$$\mu T(k) = -2\pi \text{sgn}(s)\sqrt{b - s^2} + 2\pi n, \qquad (2.116)$$

$$\text{Re}(\lambda) = \pm 2\sqrt{bs^2 - s^4}, \qquad (2.117)$$

for $s \in [-\sqrt{b}, \sqrt{b}]$ and $n \in \mathbb{Z}$. Qualitatively, for any value of n, the parametric plot of $\text{Re}(\sigma_{\mathcal{L}})$ as a function of $\mu T(k)$ looks like a figure 8 on its side. Specifically, The figure 8 is centered at $(2\pi n, 0)$ and extends left and right to $(2\pi n \pm 2\pi\sqrt{b}, 0)$, with non-zero values in between, see Figures 2.10(a,b). This leads to the following theorem:

Theorem 2.9.1. *For any positive integer P, Stokes wave solutions to (2.1) with $b \leq 1/P^2$ are stable with respect to perturbations of period $P\pi$.*

Proof. First, $T(k) = T(0) = \pi$. Let $P \in \mathbb{N}_0$. For stability with respect to perturbations of period $PT(k)$ we need that for $\mu T(k) = \frac{2\pi m}{P}$, the spectral elements $\lambda \in \sigma_{\mathcal{L}}$ have zero real part, *i.e.*, for $\mu T(k) = 0, \frac{2\pi}{P}, \ldots, \frac{2\pi(P-1)}{P}$, $\text{Re}(\lambda) = 0$. From (2.116), $\mu T(k) = 0$ only when $s = \pm\sqrt{b}$, which corresponds to $\text{Re}(\lambda) = 0$ from (2.117). Thus it suffices to consider $\mu T(k) = \frac{2\pi}{P}, \ldots, \frac{2\pi(P-1)}{P}$. Qualitatively, we have figure 8s centered at $\mu T(k) = 2\pi n$ extending over $[2\pi n - 2\pi\sqrt{b}, 2\pi n + 2\pi\sqrt{b}]$. Specifically, as s ranges from $-\sqrt{b}$ to 0, $\mu T(k)$ monotonically increases from $2\pi n$ to $2\pi(n+\sqrt{b})$. Over the same range, $|\text{Re}(\lambda)|$ increases from 0 (at $s = -\sqrt{b}$) to b (at $s = -\sqrt{b/2}$) then decreases back down to 0 (at $s = 0$) mapping out the right-half of the figure 8. For $s \in (0, \sqrt{b})$, the left-half of the figure 8 is produced symmetrically. Relevant to the interval $[0, 2\pi)$ are the figure 8s centered at 0 and 2π. If the right-most edge of the figure 8 centered at $\mu T(k) = 0$ is less than $2\pi/P$ and the left most edge of the figure 8

centered at $\mu T(k) = 2\pi$ is greater than $2\pi(P-1)/P$, then the real part of the spectrum at $\mu T(k) = \frac{2\pi}{P}, \ldots, \frac{2\pi(P-1)}{P}$ is zero. These conditions are

$$2\pi\sqrt{b} \le \frac{2\pi}{P} \text{ and } 2\pi - 2\pi\sqrt{b} \ge \frac{2\pi(P-1)}{P}. \tag{2.118}$$

Simplifying both conditions gives $0 \le b \le 1/P^2$, completing the proof. $\qquad\square$

For more intuition about this result, one can examine Figure 2.10. In Figure 2.10(a), $b = 0.08$. Here $b < 1/P^2$ for $P = 1, 2, 3$ so this Stokes wave solution is stable with respect to perturbations of periods $\pi, 2\pi, 3\pi$. This is readily seen in Figure 2.10(a) where the figure 8 centered at the origin extends to $\mu T(k) = \pm 2\pi\sqrt{0.08} \approx 0.567\pi$, so $\text{Re}(\lambda) = 0$ when $\mu T(k) = 0, 2\pi/3, \pi, 4\pi/3, 2\pi$. In Figure 2.10(b), $b < 1/P^2$ only for $P = 1$, so the Stokes wave solution is only stable with respect to perturbations of the fundamental period π. Indeed, the figure 8 centered at the origin extends to $\mu T(k) = \pm 2\pi\sqrt{0.9} \approx 1.90\pi$, so $\text{Re}(\lambda) = 0$ only for $\mu T(k) = 0$.

In order to proceed with results for the dn, cn, and general nontrivial-phase solutions we provide the following useful lemma:

Lemma 2.9.2. *For any analytic function $f(z) = u(x,y) + iv(x,y)$, on a contour where $u(x,y) = constant$, $v(x,y)$ is strictly monotone, provided the contour does not traverse a saddle point.*

Proof. This is an immediate consequence of the Cauchy-Riemann relations [10]. $\qquad\square$

Thus along contours where $\text{Re}(I(\zeta)) = 0$, if there are no saddle points, then $\text{Im}(I(\zeta))$ is monotone. If we fix b and k, using (2.114) we see that $\mu(\zeta)$ is also monotone along curves with $\text{Re}(\zeta) = 0$.

2.9.2 dn case

A representative plot of $\mu T(k)$ vs $\text{Re}(\lambda)$ for a dn solution is shown in Figure 2.10c. We prove the following theorem:

Theorem 2.9.3. *The* dn *solutions to (2.1) are stable with respect to co-periodic perturbations, but not to subharmonic perturbations.*

Proof. It suffices to consider values of ζ in the range given by (2.93), as these are the only ζ which correspond to λ with positive real part. We can limit our study to

$$\zeta \in \left[\frac{1 - \sqrt{1 - k^2}}{2}i, \frac{1 + \sqrt{1 - k^2}}{2}i\right] := [\zeta_b, \zeta_t],$$

as ζ with negative imaginary part correspond to symmetric values of $\mu T(k)$. For $\zeta = \zeta_t$, $\mu T(k) = 0$, and $\text{Re}(\lambda) = 0$. Similarly, for $\zeta = \zeta_b$, $\mu T(k) = 2\pi$, and $\text{Re}(\lambda) = 0$. From Lemma 2.9.2 we know that $\mu T(k)$ increases monotonically as ζ ranges from ζ_t to ζ_b, and since $\text{Re}(\lambda(\zeta)) > 0$ in that range we have that some ζ in the range will correspond to a λ with positive real part. Hence, dn solutions are unstable with respect to perturbations other than their fundamental period. Additionally, since ζ_t and ζ_b are the only values of ζ corresponding to $\mu T(k) = 2\pi n$ we have that dn solutions are stable with respect to perturbations of their fundamental period. □

2.9.3   cn case

Note that $T(k) = 4\mathcal{K}(k)$ for cn solutions.

Theorem 2.9.4. *The* cn *solutions with $k < k^*$ are stable with respect to perturbations of period $PT(k)$, if they satisfy the condition:*

$$\pi - 2iI(-\zeta_t) \leq \frac{2\pi}{P}, \tag{2.119}$$

for

$$\zeta_t = \frac{\sqrt{2\mathcal{E}(k) - \mathcal{K}(k)}}{2\sqrt{\mathcal{K}(k)}}. \tag{2.120}$$

Proof. We examine $\zeta \in \sigma_L$ that satisfy (2.73), see Figure 2.6(2c). The figure 8 spectrum is double covered, so without loss of generality, we consider only values of ζ in the left-half plane. Specifically we consider values of ζ ranging from $\zeta_- = -\frac{\sqrt{1-k^2}}{2} - \frac{k}{2}i$ to $\zeta_+ = \frac{\sqrt{1-k^2}}{2} - \frac{k}{2}i$ passing

along the level curve through $\zeta = -\zeta_t$. At ζ_-, $\mu T(k) = 0$ and $\mathrm{Re}(\lambda) = 0$. As ζ moves from ζ_- to $-\zeta_t$, $\mu T(k)$ monotonically increases (Lemma 2.9.2) until it reaches $\mu_t T(k) = \pi - 2iI(-\zeta_t)$ at $\zeta = -\zeta_t$. At $-\zeta_t$, $\mathrm{Re}(\lambda) = 0$. Note that we are only considering the lower-left quarter plane. The analysis for ζ ranging from ζ_+ to ζ_t is symmetric in $\mu T(k)$.

The only values of ζ which have $\mathrm{Re}(\lambda) > 0$ are within the ranges $[2\pi n - \mu_t, 2\pi n + \mu_t]$. As in Theorem 2.9.1, relevant to the interval $[0, 2\pi)$ are the figure 8s centered at 0 and 2π. For stability the right-most edge of the figure 8 centered at $\mu T(k) = 0$ needs to be less than $2\pi/P$ and the left-most edge of the figure 8 centered at $\mu T(k) = 2\pi$ to be greater than $2\pi(P-1)/P$. These conditions are

$$\mu_t \leq \frac{2\pi}{P} \text{ and } 2\pi - \mu_t \geq \frac{2\pi(P-1)}{P}, \tag{2.121}$$

which are the same conditions as (2.119). $\qquad\square$

Theorem 2.9.5. *The* cn *solutions with $k > k^*$ are stable with respect to perturbations of period $T(k)$ and period $2T(k)$.*

Proof. We examine $\zeta \in \sigma_L$ that satisfy (2.73), see Figure 2.6 (2d). Similar to the proof of Theorem 2.9.4 we consider ζ in the lower-left quarter plane only. The parameter ζ ranges from ζ_3 to ζ_t with $\zeta_t \in i\mathbb{R}$. At ζ_3, $\mu T(k) = 0$, and $\mathrm{Re}(\lambda) = 0$. As ζ moves to ζ_t, we know that $\mu T(k)$ increases monotonically (Lemma 2.9.2) until it reaches ζ_t. We do not know explicitly where on the imaginary axis ζ_t is, but it satisfies (2.73). For any ζ on the imaginary axis, we can compute directly $\mu T(k) = \pi$, $\mathrm{Re}(\lambda) = 0$. Thus the figure 8 centered at $\mu T(k) = 0$ extends outward to $\mu T(k) = \pi$. Similarly, using symmetries, the figure 8 centered at $\mu T(k) = 2\pi$ extends backward to $\mu T(k) = \pi$, see Figure 2.10(e). Both figure 8s have $\mathrm{Re}(\lambda) = 0$ at $\mu T(k) = 0$ and $\mu T(k) = \pi$, so we have stability with respect to perturbations of periods $2T(k)$ and $T(k)$. $\qquad\square$

2.9.4 Nontrivial-phases cases

Theorem 2.9.6. *Nontrivial-phase solutions in the figure 8s region and the triple-figure 8 region are stable with respect to subharmonic perturbations of period $PT(k)$ if they satisfy*

the condition

$$\theta(T(k)) - 2iI(-\zeta_t) \leq \frac{2\pi}{P}, \tag{2.122}$$

with

$$\zeta_t = \frac{\sqrt{2\mathcal{E}(k) - \mathcal{K}(k) - (b - k^2)\mathcal{K}(k)}}{2\sqrt{\mathcal{K}(k)}}. \tag{2.123}$$

Proof. We examine $\zeta \in \sigma_L$ which satisfy (2.73), see Figure 2.7(2a,2c). Recall that ζ_i corresponds to the root of $\Omega^2(\zeta)$ in the ith quadrant from (2.88). The ζ spectrum has three components which we examine separately:

1. ζ *strictly real, corresponding to* $\sigma_\mathcal{L} \cap i\mathbb{R}$.

   ζ strictly real corresponds to λ strictly imaginary, so these values do not need to be examined further.

2. ζ *ranging between* ζ_3 *and* ζ_2, *corresponding to the outside figure 8.*

   For ζ ranging between ζ_3 and ζ_2 we follow identical steps from the proof of Theorem 2.9.4. Taking the right-most edge of the outside figure 8 centered at $\mu T(k) = 0$ to be less than $2\pi/P$ and the left-most edge of the outside figure 8 centered at $\mu T(k) = 2\pi$ to be greater than $2\pi(P - 1)/P$, we arrive at analogous conditions to (2.121) which reduce to (2.123) as desired. Note that we have shown only that (2.123) is a necessary condition.

3. ζ *ranging between* ζ_4 *and* ζ_1, *corresponding to the enclosed figure 8 or the triple-figure 8.*

   For ζ ranging between ζ_4 and ζ_1, we know from Section 2.8 that this corresponds to the enclosed figure 8 (or triple-figure 8). Specifically, the top of this figure 8 (or triple-figure 8) is lower than the top of the other figure 8. It suffices to show that the extent of this figure 8 (or triple-figure 8) in $\mu T(k)$ is less than that of the larger figure 8. Indeed, if the enclosed figure 8 (or triple-figure 8) extends less in $\mu T(k)$ than the larger figure 8 does, then the stability bounds above are sufficient.
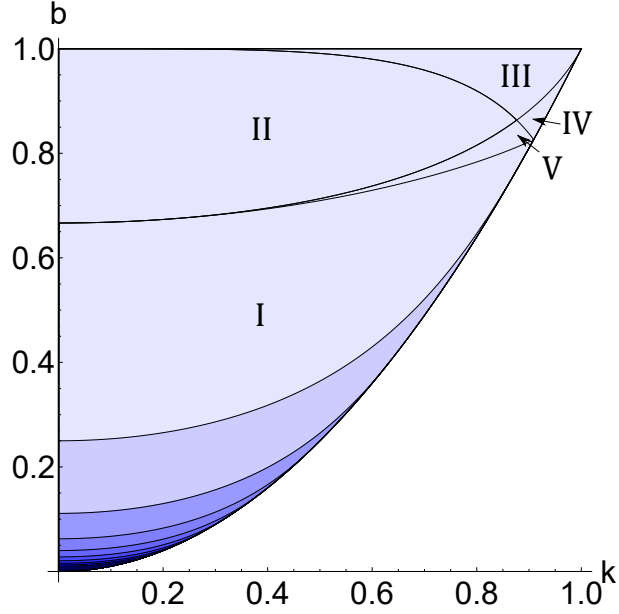
Figure 2.11: A plot of parameter space showing the spectral stability of solutions with respect to various subharmonic perturbations. Lightest blue or darker (entire region): solutions stable with respect to perturbations of the fundamental period. Second lightest blue or darker: solutions stable with respect to perturbations of two times the fundamental period. Third lightest blue or darker: solutions stable with respect to perturbations of three times the fundamental period. Etc.

It suffices to show that $-2iI(\zeta_t) < -2iI(-\zeta_t)$. Let $g(\zeta) = -2iI(\zeta)$. We know $g(\zeta)$ is a real-valued function with real coefficients for $\zeta \in \mathbb{R}$. Furthermore, from (2.79),

$$\frac{\mathrm{d}g(\zeta)}{\mathrm{d}\zeta} = \frac{2\mathcal{E}(k) - (1 + b - k^2 + 4\zeta^2)\,\mathcal{K}(k)}{i\Omega(\zeta)}. \tag{2.124}$$

The only roots of $\mathrm{d}g(\zeta)/\mathrm{d}\zeta$ are $\zeta = \pm\zeta_t$. By checking $\mathrm{d}^2 g(\zeta)/\mathrm{d}\zeta^2$ we see that $g(\zeta_t)$ is a local minimum and $g(-\zeta_t)$ is a local maximum. Since there are no other extrema, $g(-\zeta_t) > g(\zeta_t)$ and (2.123) is a sufficient condition.

$\square$

Theorem 2.9.7. *Nontrivial-phase solutions of butterfly type are stable with respect to perturbations of the fundamental period.*

Proof. We examine $\zeta \in \sigma_L$ satisfying (2.73), see Figure 2.7(2b,2d). The ζ spectrum consists of three components:

1. ζ strictly real, corresponding to $\sigma_{\mathcal{L}} \subset i\mathbb{R}$.

2. ζ ranging between ζ_3 and ζ_4, corresponding to two of the butterfly wings.

3. ζ ranging between ζ_2 and ζ_1, corresponding to the other two butterfly wings.

Case 1 consists only of values of ζ corresponding to λ with zero real part so it need not be examined. Cases 2 and 3 are symmetric in μ so it suffices to look at case 2. With $\zeta = \zeta_3$, $\mu T(k) = 0$ with $\text{Re}(\lambda) = 0$. Then, from Lemma 2.9.2, $\mu T(k)$ increases monotonically as ζ varies from ζ_3 to ζ_4. At $\zeta = \zeta_4$, $\mu T(k) = 2\pi$, with $\text{Re}(\lambda) = 0$. Because of the monotone increase in $\mu T(k)$, ζ_3 and ζ_4 are the only possible values of ζ which correspond to $\mu T(k) = 0, 2\pi$. Since $\text{Re}(\lambda) = 0$ for both of these values of ζ, we have stability for perturbations of period $T(k)$ as desired. $\qquad\square$

The above results are summarized in Figure 2.11 where we plot the different regions of parameter space corresponding to spectral stability with respect to different classes of subharmonic perturbations.

2.10 Approximating the greatest real part of the spectrum

In this section we find an approximation to the value of the spectral element $\sigma_{max} \in \sigma_{\mathcal{L}}$ with greatest real part. This value is significant because it corresponds to the eigenfunction with the fastest growth rate. For the Stokes wave case and for the dn solution case $\text{Re}(\sigma_{max})$ is known explicitly, so in this section we focus on approximating σ_{max} for the cn solutions and nontrivial-phase solutions. In the Stokes wave case $\text{Re}(\sigma_{max}) = b$. This is seen from maximizing the real component of (2.92). For the dn solution case, from (2.94) we know that the spectrum extends to $\text{Re}(\sigma_{max}) = \sqrt{1 - k^2}$.

From (2.101) and (2.102) we have an expression for the slope at any point in the set S_Ω. σ_{max} occurs when the slope at that point is infinity, *i.e.*, when the denominator in (3.108) is identically zero:

$$\frac{\mathrm{d}\Omega_r}{\mathrm{d}\zeta_r} + \frac{\mathrm{d}\Omega_r}{\mathrm{d}\zeta_i}\frac{\mathrm{d}\zeta_i}{\mathrm{d}\zeta_r} = 0. \tag{2.125}$$

To simplify this equation we note that the expressions for $\mathrm{d}\Omega_r/\mathrm{d}\zeta_r$ and $\mathrm{d}\Omega_r\mathrm{d}\zeta_i$ are found using (2.83) by substituting in $\Omega = \Omega_r + i\Omega_i$ and $\zeta = \zeta_r + i\zeta_i$, taking real and imaginary parts, and differentiating with respect to ζ_r and ζ_i. For the expression $\mathrm{d}\zeta_i/\mathrm{d}\zeta_r$ we use (3.109) and the fact that

$$\frac{\mathrm{dRe}(I)}{\mathrm{d}\zeta_r} = \mathrm{Re}\left[\frac{\mathrm{d}I}{\mathrm{d}\zeta}\right], \tag{2.126}$$

$$\frac{\mathrm{dRe}(I)}{\mathrm{d}\zeta_i} = -\mathrm{Im}\left[\frac{\mathrm{d}I}{\mathrm{d}\zeta}\right], \tag{2.127}$$

from Section 2.8. Using (2.79), we find the real and imaginary components of $\mathrm{d}I/\mathrm{d}\zeta$ as

$$\mathrm{Re}\left[\frac{\mathrm{d}I}{\mathrm{d}\zeta}\right] = \frac{2\mathcal{E}(k)\Omega_r + \mathcal{K}(k)\left(-8\zeta_i\zeta_r\Omega_i - \left(1 + b - k^2 + 4\zeta_r^2 - 4\zeta_i^2\right)\Omega_r\right)}{2\left(\Omega_i^2 + \Omega_r^2\right)}, \tag{2.128}$$

$$\mathrm{Im}\left[\frac{\mathrm{d}I}{\mathrm{d}\zeta}\right] = -\frac{2\mathcal{E}(k)\Omega_i - \mathcal{K}(k)\left(-8\zeta_i\zeta_r\Omega_r + \left(1 + b - k^2 + 4\zeta_r^2 - 4\zeta_i^2\right)\Omega_i\right)}{2\left(\Omega_i^2 + \Omega_r^2\right)}, \tag{2.129}$$

Using (2.83), (2.128), and (2.129) we simplify (2.125):

$$\begin{aligned}
&\left(-1 + 3b^2 + k^4 + 16\zeta_i^4 - 2b\left(-1 + 2k^2 + 8\zeta_i^2\right)\right.\\
&\left.+ 8c\zeta_r + 16\zeta_r^2 + 32\zeta_i^2\zeta_r^2 + 16\zeta_r^4 + 8k^2(\zeta_i^2 - \zeta_r^2)\right)\mathcal{K}(k)\\
&+ \left(2 - 6b + 2k^2 + 8\zeta_i^2 - 24\zeta_r^2\right)\mathcal{E}(k) = 0.
\end{aligned} \tag{2.130}$$

This equation gives a condition on the real and imaginary parts of ζ. By construction, if (2.130) and (2.73) are satisfied, then $\zeta \in \sigma_L$ maps to σ_{max}. We denote such ζ as ζ_{max}. We note that in the trivial-phase case, (2.130) is an equation for a conic section in the variables ζ_r^2 and ζ_i^2. In Figure 2.12 we plot values of (ζ_r, ζ_i) which satisfy (2.130) along with values of $\zeta = \zeta_r + i\zeta_i$ satisfying (2.73). The intersection of these curves gives ζ_{max}.

By simultaneously solving (2.130) and (2.73) and substituting into (2.61) and (2.63) we have an exact expression for σ_{max}. For the rest of this section we generate series expansions
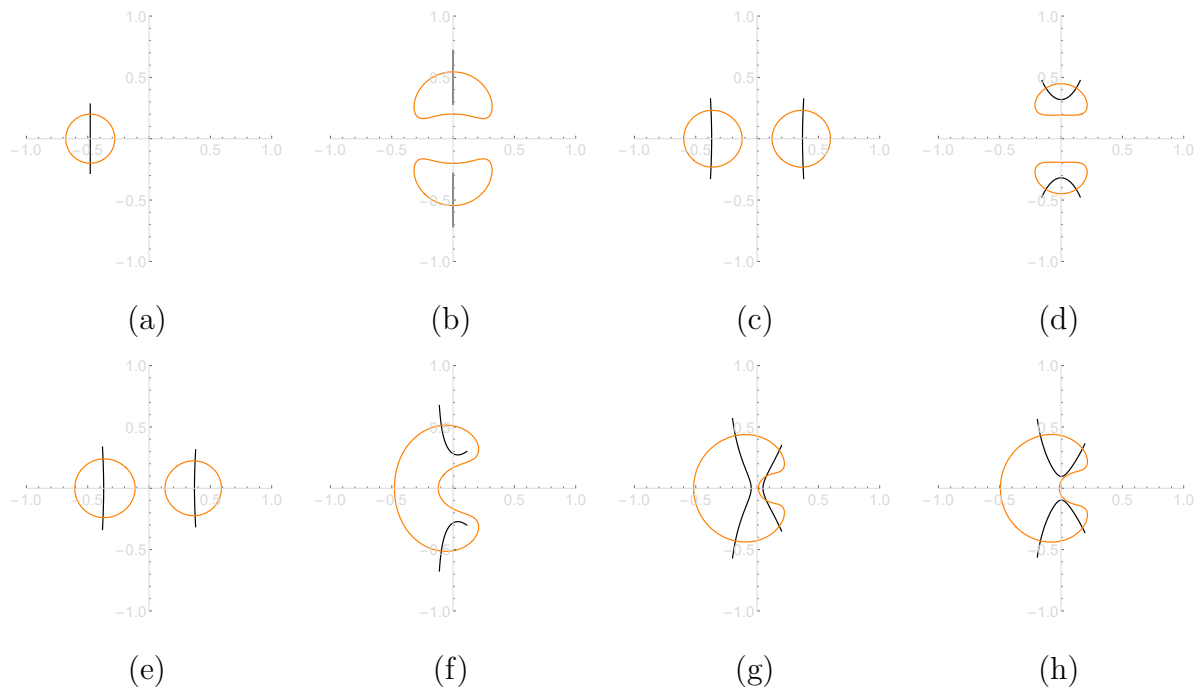
Figure 2.12: The σ_L spectrum (black) along with the curve corresponding to greatest real part of the $\sigma_{\mathcal{L}}$ spectrum (orange) satisfying (2.130). (a) Stokes wave solution, $(k, b) = (0, 0.08)$; (b) dn solution, $(k, b) = (0.9, 1)$; (c) cn solution with piercing, $(k, b) = (0.65, 0.4225)$; (d) cn solution without piercing, $(k, b) = (0.95, 0.9025)$; (e) double-figure 8 solution, $(k, b) = (0.65, 0.423)$; (f) non-self-intersecting butterfly solution, $(k, b) = (0.9, 0.95)$; (g) triple-figure 8 solution, $(k, b) = (0.89, 0.84)$; (h) self-intersecting butterfly solution, $(k, b) = (0.9, 0.85)$.

for (2.73) and show that even using low-order approximations we are able to reproduce much of the spectrum, including σ_{max}.

From Section 2.8, we know a few points of σ_L explicitly. Because the functions we are working with are analytic, we can perform series expansions around these explicitly known points. The points we have explicit expressions for are ζ_c, *i.e.*, the ζ corresponding to $\lambda = 0$, and ζ_t, the ζ corresponding to the tops of the figure 8 or triple-figure 8. In what follows we outline a procedure for finding an approximation to points in S_Ω around these explicitly known points. These expansions provide approximations to the set S_Ω, and using the mapping (2.61) and (2.63), results in approximations to the $\sigma_{\mathcal{L}}$ spectrum.

Procedure for finding a series approximation to ζ satisfying (2.73) around ζ_c:

1. Expand the expression inside the real part of (2.73) around ζ_c in a Puiseux series [30] to give:

$$\mathrm{Re}\left((a_1 + b_1 i)(\zeta - \zeta_c)^{1/2} + (a_2 + b_2 i)(\zeta - \zeta_c)^{3/2} + (a_3 + b_3 i)(\zeta - \zeta_c)^{5/2} + \ldots\right) = 0,$$

(2.131)

where $a_i, b_i \in \mathbb{R}$ are the real and imaginary parts of the coefficients of the terms in the Puiseux series.

2. Let

$$\delta = \delta_r + i\delta_i = (\zeta - \zeta_c)^{1/2},$$

(2.132)

for $\delta_r, \delta_i \in \mathbb{R}$. Then (2.131) becomes

$$\mathrm{Re}\left((a_1 + b_1 i)\delta + (a_2 + b_2 i)\delta^3 + (a_3 + b_3 i)\delta^5 + O(\delta^7)\right) = 0.$$

(2.133)

3. Near $\zeta = \zeta_c$, δ is small. Let $\delta = \delta_r(\delta_i) + i\delta_i$, with

$$\delta_r(\delta_i) = \delta_1 \delta_i + \delta_3 \delta_i^3 + \delta_5 \delta_i^5 + O(\delta_i^7).$$

(2.134)

4. Substituting (2.134) into (2.133) and simplifying the expression on the left-hand side, we equate powers of δ_i to solve for $\delta_1, \delta_3, \delta_5, \ldots$ sequentially. We find

$$\delta_1 = \frac{b_1}{a_1}, \tag{2.135}$$

$$\delta_3 = \frac{3a_1^2 a_3 b_1 - a_3 b_1^3 - a_1^3 b_3 + 3a_1 b_1^2 b_3}{a_1^4}, \tag{2.136}$$

$$\delta_5 = \frac{1}{a_1^7} \left(a_1^6 b_5 - a_1^5 (3a_3 b_3 + 5a_5 b_1) + a_1^4 b_1 \left(9a_3^2 - 10b_1 b_5 - 6b_3^2 \right) + 10a_1^3 b_1^2 (3a_3 b_3 + a_5 b_1) \right.$$
$$\left. + a_1^2 b_1^3 \left(-12a_3^2 + 5b_1 b_5 + 18b_3^2 \right) - a_1 b_1^4 (15a_3 b_3 + a_5 b_1) + 3a_3^2 b_1^5 \right), \tag{2.137}$$

. . .

5. Solving (2.132) for ζ results in an approximation for ζ as a function of δ_i in terms of its real and imaginary parts:

$$\zeta = \delta_r(\delta_i)^2 - \delta_i^2 + \text{Re}(\zeta_c) + (2\delta_r(\delta_i)\delta_i + \text{Im}(\zeta_c))\, i. \tag{2.138}$$

We call (2.138) an nth-order expansion where n is the largest power of ζ_i from (2.134) included. For instance, a third-order expansion for ζ is

$$\zeta = \left(\delta_1 \delta_i + \delta_3 \delta_i^3 \right)^2 - \delta_i^2 + \text{Re}(\zeta_c) + \left(2 \left(\delta_1 \delta_i + \delta_3 \delta_i^3 \right) \delta_i + \text{Im}(\zeta_c) \right) i. \tag{2.139}$$

First- and third-order approximations to (2.73) around ζ_c are shown in Figure 2.13 for the two types of cn solutions. Although the expansion is only guaranteed to be valid around ζ_c, the first-order expansion approximates σ_L well up to (and past) the point where σ_{max} occurs. With this in mind, we present Figure 2.14, comparing the exact value of the greatest real part of the spectrum and the approximate value. From this figure, generally the approximation performs better in the piercing case ($k < k^*$) than in the non-piercing case ($k > k^*$). Also, with just the first-order approximation we get a maximum relative error of less than 18%. For third-order, the maximum relative error is less than 1%, and for fifth-order this decreases to less than 0.1%.

(a)   (b)
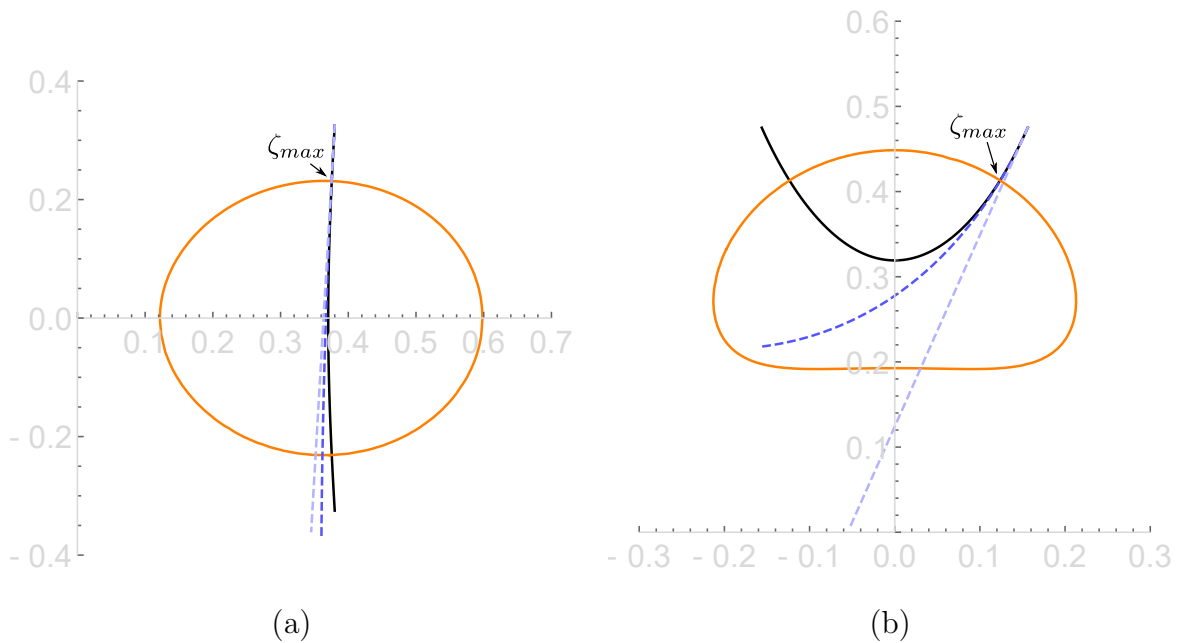
Figure 2.13: Approximating the σ_L spectrum for cn solutions. Shown are the σ_L spectrum (black solid curve), the curve corresponding to greatest real part of the $\sigma_{\mathcal{L}}$ spectrum (orange solid curve), ζ_{max} at the intersection point of the black and orange curves, the first-order approximation to σ_L around ζ_1 (light-blue dotted curve), third-order approximation to σ_L around ζ_1 (dark-blue dotted curve). (a) A cn solution with piercing, $(k, b) = (0.65, 0.4225)$; (b) cn solution without piercing, $(k, b) = (0.95, 0.9025)$.
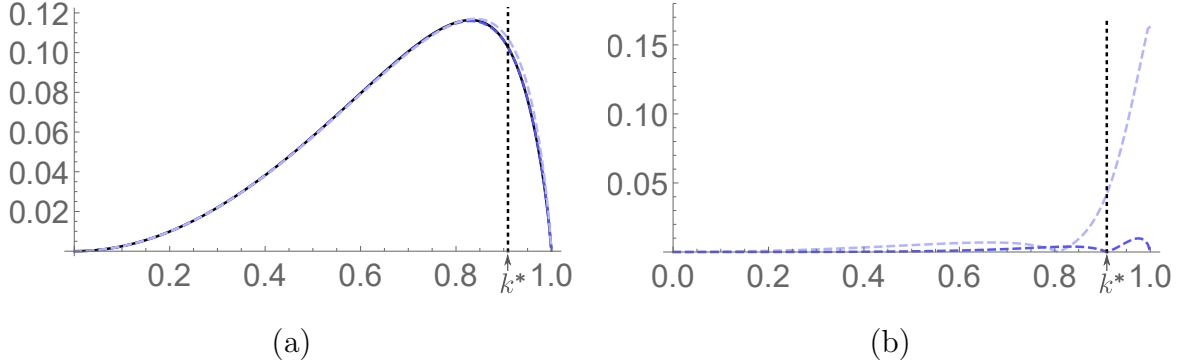
Figure 2.14: (a) Comparison of the exact value for the greatest real part of $\sigma_{\mathcal{L}}$ for cn solutions (black solid curve) with a first-order approximation (dark blue dotted curve) and a third-order approximation (light blue dotted curve). (b) The relative error of the approximations: |(approximation-exact)/exact|.

Using the approximations to σ_{max} we can obtain an approximation to the eigenfunction profile with the largest growth rate. This is achieved by substituting ζ_{max} into (2.62) using (2.56) and (2.57). The approximation for ζ_{max} does not exactly satisfy (2.58) and in order to find a bounded eigenfunction we subtract the left-hand side of (2.58) from the exponent in (2.57). Indeed, with ζ_{max} in Figure 2.13 the left-hand side of (2.58) is small in magnitude. For example, when $k = 0.65$, the left-hand side of (2.58) is 0.0014 for the first-order approximation and 0.00034 for the third-order approximation. These values should be compared with 0.22 when ζ is chosen to correspond to a point in the middle of the figure 8.

In addition to expanding around ζ_c, we can also expand (2.73) around $\zeta = \zeta_t$, corresponding to the top of the figure 8 or triple-figure 8. Note that we cannot do so if we are in the butterfly region or in the cn region without piercing, thus we require

$$b + 1 - k^2 - \frac{2\mathcal{E}(k)}{\mathcal{K}(k)} < 0. \tag{2.140}$$

Since we are expanding around a point where the expression inside the real part of (2.73) is analytic, we can use a Taylor series instead of a Puiseux series which vastly simplifies the analysis.

Procedure for finding an approximation to ζ satisfying (2.73) around ζ_t:

1. Expand the expression inside the real part of (2.73) around ζ_t in a Taylor series to give

$$\text{Re}\left[(a_1 + b_1 i)(\zeta - \zeta_t) + (a_2 + b_2 i)(\zeta - \zeta_t)^2 + (a_3 + b_3 i)(\zeta - \zeta_t)^3 + \ldots\right] = 0, \quad (2.141)$$

where $a_i, b_i \in \mathbb{R}$ are the real and imaginary parts of the coefficients of the terms in the Taylor series. In fact, all a_i's are identically zero, and $b_1 = 0$ so that

$$\text{Re}\left[b_2 i(\zeta - \zeta_t)^2 + b_3 i(\zeta - \zeta_t)^3 + \ldots\right] = 0. \quad (2.142)$$

2. Let

$$\delta = \delta_r + i\delta_i = \zeta - \zeta_t, \quad (2.143)$$

for $\delta_r, \delta_i \in \mathbb{R}$. Then (2.142) becomes

$$\text{Re}\left[b_2 i\delta^2 + b_3 i\delta^3 + O(\delta^4)\right] = 0. \quad (2.144)$$

3. Near $\zeta = \zeta_c$, δ is small. Let $\delta = \delta_r(\delta_i) + \delta_i$, with

$$\delta_r(\delta_i) = \delta_1\delta_i + \delta_2\delta_i^2 + \delta_3\delta_i^3 + O(\delta_i^4). \quad (2.145)$$

4. Substituting (2.145) into (2.144) and simplifying the expression on the left-hand side, we equate powers of δ_i to solve for $\delta_1, \delta_2, \delta_3, \ldots$. We find that $\delta_i = 0$ for i odd and

$$\delta_2 = \frac{b_3}{2b_2}, \quad (2.146)$$

$$\delta_4 = \frac{-3b_3^3 + 8b_2 b_3 b_4 - 4b_2^2 b_5}{8b_2^3}, \quad (2.147)$$

$$\delta_6 = \frac{9b_3^5 - 40b_2 b_4 b_3^3 + 32b_2^2 b_5 b_3^2 + 32b_2^2 b_4^2 b_3 - 24b_2^3 b_6 b_3 - 16b_2^3 b_4 b_5 + 8b_2 r^4 b_7}{16b_2^5}, \quad (2.148)$$

$$\ldots$$

5. Solving (2.143) for ζ we obtain an approximation for ζ as a function of δ_i in terms of its real and imaginary parts:

$$\zeta = (\delta_r(\delta_i) + \zeta_t) + i\delta_i. \quad (2.149)$$
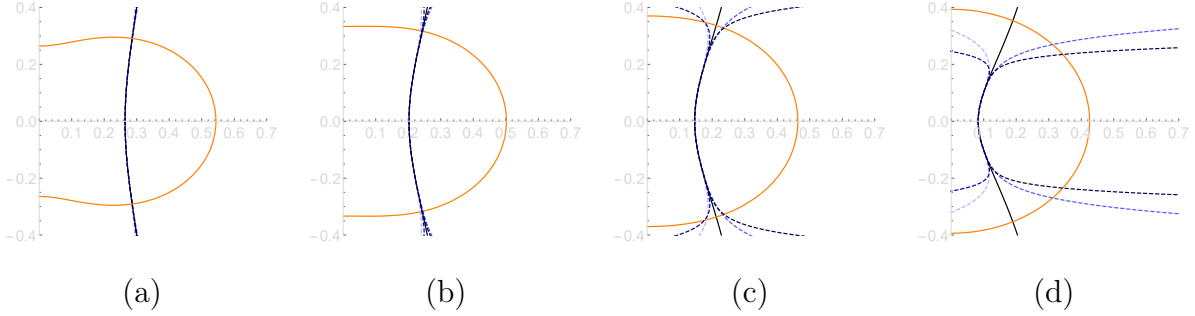
Figure 2.15: Approximating σ_L for cn solutions around the top of the figure 8. Shown are σ_L (black solid curve), the curve corresponding to the greatest real part of $\sigma_{\mathcal{L}}$ (orange solid curve), the first-order approximation to σ_L around ζ_1 (lightest-blue dotted curve), third-order approximation to σ_L around ζ_1 (light-blue dotted curve, fifth-order approximation to σ_L around ζ_1 (dark-blue dotted curve, seventh-order approximation to σ_L around ζ_1 (darkest-blue dotted curve). (a) A cn solution, $(k,b) = (0.8, 0.64)$; (b) cn solution, $(k,b) = (0.85, 0.7225)$; (c) cn solution, $(k,b) = (0.88, 0.7744)$; (d) cn solution, $(k,b) = (0.9, 0.81)$.

As before, call (2.149) an nth-order expansion where n is the largest power of ζ_i from (2.145) included. For instance, a fourth-order approximation for ζ is

$$\zeta = \left(\delta_2 \delta_i^2 + \delta_4 \delta_i^4 + \zeta_t\right) + i\delta_i. \tag{2.150}$$

The fourth-, sixth-, eighth-, and tenth-order approximations to (2.73) are shown in Figure 2.15 for piercing cn solutions as k approaches k^*. We see that these approximations quickly diverge from the σ_L spectrum as k approaches k^*. The results here are shown for cn solutions but hold in the nontrivial-phase case as well. For small values of k and b satisfying (2.140) we are able to approximate σ_{max} well using this Taylor series approach, but as the left-hand side of (2.140) approaches 0 this approximation fails. In general, the Puiseux expansions around ζ_c serve as more robust approximations than the Taylor expansions around ζ_t.

2.11 Conclusion

We obtained an analytical expression for the linear operator associated with focusing NLS. The expression allowed us to obtain various quantitative and qualitative results about the

spectrum. Specifically, we split the solution parameter space into four regions of distinct qualitative behavior of the spectrum. Additionally, we found regions of parameter space for which solutions are spectrally stable with respect to perturbations of a small integer multiple of their fundamental period. We also provided a procedure for approximating the greatest real part of the spectrum. The techniques used in this chapter may extend to other non self adjoint problems and would be worthwhile investigating in future work. Regarding the stability results in Section 2.9, it would be interesting to examine whether we have nonlinear stability when one restricts oneself to subharmonic perturbations.

Chapter 3

THE STABILITY SPECTRUM FOR ELLIPTIC SOLUTIONS TO THE SINE-GORDON EQUATION

In this chapter, I present an analysis of the stability spectrum for all stationary periodic solutions to the sine-Gordon equation. An analytical expression for the spectrum is given. From this expression, various quantitative and qualitative results about the spectrum are derived. Specifically, the solution parameter space is shown to be split into regions of distinct qualitative behavior of the spectrum, in one of which the solutions are stable. Additional results on the stability of solutions with respect to perturbations of an integer multiple of the solution period are given. This chapter follows the same format as Chapter 2 and applies the methods used there to the sine-Gordon equation. This chapter consists of work submitted for publication and was done as a collaboration with Peter McGill at the University College London [25].

3.1 Introduction

The sine-Gordon equation in laboratory coordinates is given by

$$u_{tt} - u_{xx} + \sin u = 0. \tag{3.1}$$

Here, $u(x,t)$ is a real-valued function. This equation was first introduced to study surfaces of constant Gaussian curvature in light cone form [13]. Since its introduction it has appeared in various applications including the description of the magnetic flux in long superconducting Josephson junctions [59, 61, 63], the modeling of fermions in the Thirring model [20], the study of the stability of structures found in galaxies [53, 66, 67], mechanical vibrations of a ribbon pendulum [68], propagation of crystal dislocation [32], propagation of deformations

along DNA double helix [72], among others. A comprehensive discussion of many of these applications is found in the review paper by Barone [7].

We consider general traveling wave solutions to (3.1). Defining $z = x - ct$, $\tau = t$, and introducing $v(z, \tau) = u(x, t)$,

$$(c^2 - 1)v_{zz} - 2cv_{z\tau} + v_{\tau\tau} + \sin(v) = 0. \tag{3.2}$$

For subsequent discussion we assume that $c \neq 1$. We proceed to look for stationary solutions to (3.2) of the form

$$v(z, \tau) = f(z), \tag{3.3}$$

leading to

$$(c^2 - 1)f''(z) + \sin(f(z)) = 0, \tag{3.4}$$

where $'$ denotes a derivative with respect to z. Integrating once,

$$\frac{1}{2}(c^2 - 1)f'(z)^2 + 1 - \cos(f(z)) = E, \tag{3.5}$$

where E is a constant of integration referred to as the total energy. The stationary solutions in this chapter are the elliptic solutions to (3.5) and their limits. These solutions are periodic in z and limit to the well-known kink solutions as their period goes to infinity [22, 54].

We call stationary solutions $f(z)$ with waves speeds satisfying $c^2 < 1$ (respectively $c^2 > 1$) subluminal (superluminal). Representative phase portraits of subluminal and superluminal solutions to (3.5) are shown in Figure 3.1. Additionally, we call solutions $f(z)$ whose orbits in phase space lie within the separatrix librational, and those whose orbits lie outside the separatrix rotational. This distinction is illustrated in Figure 3.1 in both the subluminal and superluminal cases. Librational waves correspond to $E \in (0, 2)$. For rotational waves, $E < 0$ for subluminal waves and $E > 2$ for superluminal waves.

Scott [62] was the first to study the stability of periodic traveling wave solutions to (3.1). He classified subluminal rotational waves as spectrally stable and determined spectral instability for all other types of waves, but these instability results were based on an incorrect

(a) Subluminal: $c^2 < 1$ (b) Superluminal: $c^2 > 1$
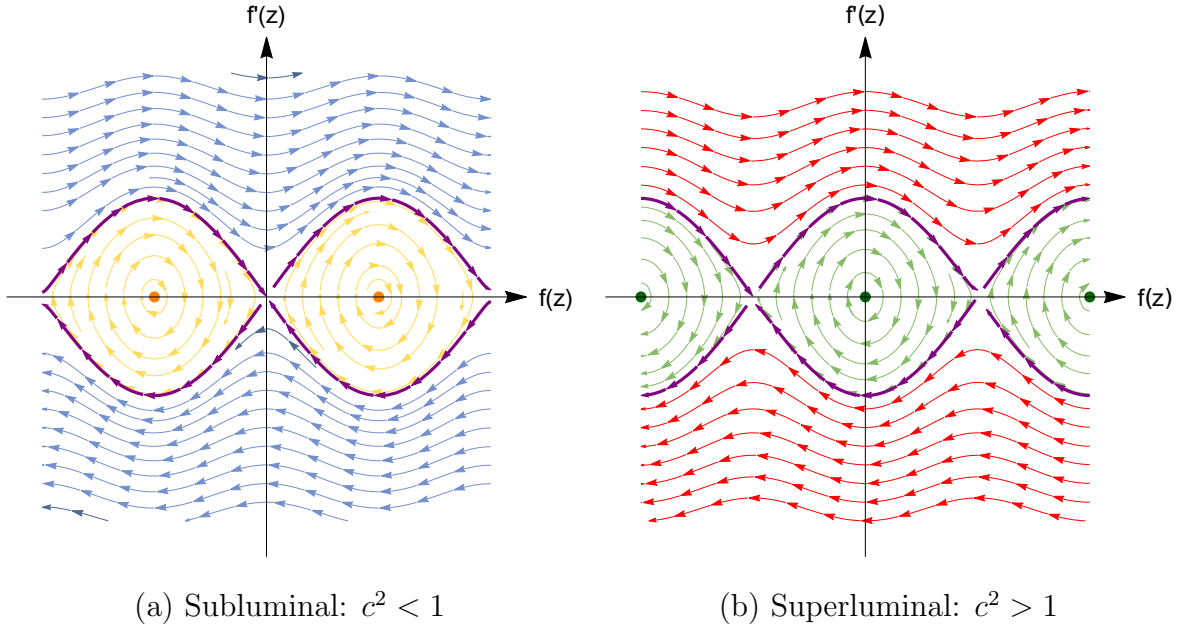
Figure 3.1: Phase portraits of the solutions showing both librational waves (closed orbits inside the separatrix) in yellow for (a) and green for (b) and rotational waves (orbits outside the separatrix) in blue for (a) and red for (b). The separatrix is denoted in purple.

claim that the spectrum in all cases was strictly confined to the real and imaginary axes. His proof has been corrected [45] and extended to the Klein-Gordon equation [46]. Using entirely different methods, we confirm the results in [45] and explicitly characterize all of parameter space. We also provide stability results for solutions perturbed by integer multiples of their fundamental period.

In Section 3.2 we present the elliptic solutions to (3.5) in Jacobi elliptic form from [45], and then reformulate the solutions into Weierstrass elliptic form. In Sections 3.3, 3.4 and 3.5, using the same methods as [11,12,26,27], we exploit the integrability of (3.1) to associate the spectrum of the linear stability problem with the Lax spectrum using the squared eigenfunction connection [1]. This allows us to obtain an analytical expression for the spectrum of the operator associated with the linearization of (3.1) in the form of a condition on the real part of an integral over one period of some integrand. Similar to [27], we proceed by integrating
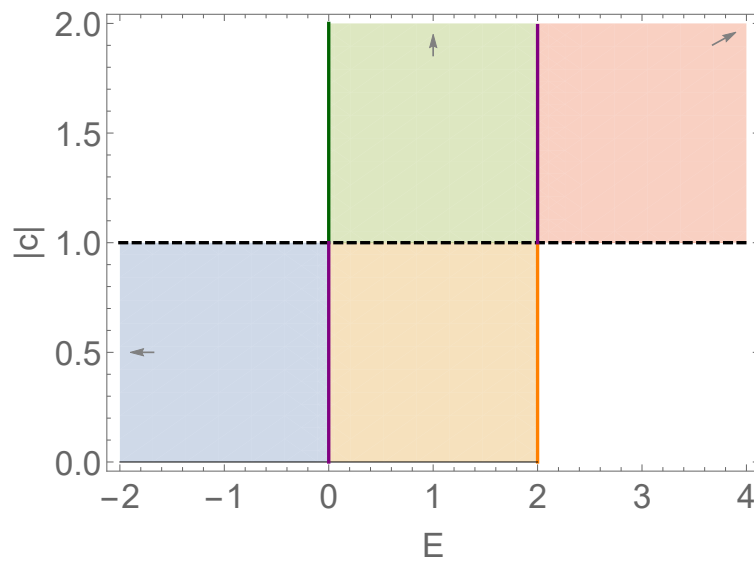
Figure 3.2: Subregions of Parameter space. Colors correspond to solutions in Figure 3.1. Blue: subluminal rotational ($0 \leq |c| < 1$, $E < 0$), orange: subluminal librational ($0 \leq |c| < 1$, $0 < E \leq 2$), green: superluminal librational ($|c| > 1$, $0 \leq E < 2$), red: superluminal rotational ($0 \leq |c| > 1$, $E > 2$). Subregions extend to infinity in directions of arrows. Subluminal kink solutions occur for $E = 0, 0 \leq |c| < 1$, and superluminal kink solutions occur for $E = 2, |c| > 1$.

the integrand explicitly in Section 3.6. Next, using the expressions obtained, we prove results concerning the location of the stability spectrum on the imaginary axis in Section 3.7. In Section 3.8, we present analytical results about the spectrum, and we make use of the integral condition to split parameter space into different regions where the spectrum shows qualitatively different behavior. Finally, in Section 3.9 we examine the spectral stability of solutions with respect to perturbations of an integer multiple of their fundamental period and prove various stability results.

3.2 Elliptic solutions

The derivation of the solutions is presented in the appendix of [45]. We limit our presentation to what is necessary for the following sections. For solutions to be real and nonsingular for real z we require the following constraints:

$$\text{subluminal, rotational:} \qquad 0 \leq |c| < 1, \qquad\qquad E < 0, \qquad (3.6)$$

$$\text{superluminal, rotational:} \qquad |c| > 1, \qquad\qquad E > 2, \qquad (3.7)$$

$$\text{subluminal, librational:} \qquad 0 \leq |c| < 1, \qquad 0 < E \leq 2, \qquad (3.8)$$

$$\text{superluminal, librational:} \qquad |c| > 1, \qquad 0 < E \leq 2. \qquad (3.9)$$

Solutions to (3.5) are of the form

$$\cos\left(f(z)\right) = \alpha + \beta \text{sn}^2(\lambda z, k), \qquad (3.10)$$

with the following parameter values for the various cases:

$$\text{subluminal, rotational:} \quad \alpha = -1, \quad \beta = 2, \qquad \lambda = \sqrt{\frac{2-E}{2(1-c^2)}}, \quad k = \sqrt{\frac{2}{2-E}}, \quad (3.11)$$

$$\text{superluminal, rotational:} \quad \alpha = 1, \quad \beta = -2, \qquad \lambda = \sqrt{\frac{E}{2(c^2-1)}}, \quad k = \sqrt{\frac{2}{E}}, \qquad (3.12)$$

$$\text{subluminal, librational:} \quad \alpha = -1, \quad \beta = 2-E, \quad \lambda = \sqrt{\frac{1}{1-c^2}}, \qquad k = \sqrt{\frac{2-E}{2}}, \quad (3.13)$$

$$\text{superluminal, librational:} \quad \alpha = 1, \quad \beta = -E, \qquad \lambda = \sqrt{\frac{1}{c^2-1}}, \qquad k = \sqrt{\frac{E}{2}}. \qquad (3.14)$$

Here $\text{sn}(x, k)$ is the Jacobi elliptic sn function with elliptic modulus k [17,52,55,70]. We are neglecting to include a horizontal shift in z. This additional parameter does not change the qualitative results and it is not included here.

Of some importance are the limits of these solutions on the boundaries of their regions of validity. On the boundaries for subluminal waves and superluminal waves the rotational and librational solutions limit to kink solutions. For subluminal waves that limit occurs when $E = 0$:

$$\cos\left(f(z)\right) = -1 + 2\tanh^2\left(\frac{z}{\sqrt{1 - c^2}}\right), \tag{3.15}$$

while for superluminal waves the limit is when $E = 2$:

$$\cos\left(f(z)\right) = 1 - 2\tanh^2\left(\frac{z}{\sqrt{c^2 - 1}}\right). \tag{3.16}$$

These solutions are seen as the separatices in Figure 3.1 in purple and are on the purple curves in parameter space in Figure 3.2. The other limits for librational waves are when solutions limit to a constant. In the subluminal cases this occurs when $E = 2$ and $\cos\left(f(z)\right) = -1$, or in the superluminal case when $E = 0$ and $\cos\left(f(z)\right) = 1$. For a general solution which is not on the boundary in parameter space, the solutions in (3.11-3.14) are periodic in z with period $2\mathcal{K}(k)$ where

$$\mathcal{K}(k) = \int_0^{\pi/2} \frac{1}{\sqrt{1 - k^2 \sin^2 y}} dy, \tag{3.17}$$

the complete elliptic integral of the first kind.

We reformulate our elliptic solutions to (3.1) using Weierstrass elliptic functions [55] rather than Jacobi elliptic functions. This will simplify working with the integral condition (3.53) in Section 3.4, as formulas for integrating Weierstrass elliptic functions are well documented [17, 35]. It is important to note that nothing is lost by switching to Weierstrass elliptic functions, as we can map any Weierstrass elliptic function to a Jacobi elliptic function, and visa versa [27,55]. Let

$$\wp(z + \omega_3, g_2, g_3) - e_3 = \left(\frac{\mathcal{K}(k)k}{\omega_1}\right)^2 \text{sn}^2\left(\frac{\mathcal{K}(k)z}{\omega_1}, k\right), \tag{3.18}$$

with g_2 and g_3 the lattice invariants of the Weierstrass $\wp$ function, e_1, e_2, and e_3 the zeros of the polynomial $4t^3 - g_2 t - g_3$, and ω_1 and ω_3 the half-periods of the Weierstrass lattice given by

$$\omega_1 = \int_{e_1}^{\infty} \frac{dz}{\sqrt{4z^3 - g_2 z - g_3}}, \tag{3.19}$$

$$\omega_3 = i \int_{-e_3}^{\infty} \frac{dz}{\sqrt{4z^3 - g_2 z + g_3}}. \tag{3.20}$$

Using (3.18) we convert our general solution in terms of Jacobi elliptic functions (3.10) to one in terms of Weierstrass elliptic functions:

$$\cos\left(f(z)\right) = \alpha + \frac{\beta}{k^2 \lambda^2} \left(\wp(z + \omega_3, g_2, g_3) - e_3\right), \tag{3.21}$$

with

$$g_2 = \frac{4}{3} \left(1 - k^2 + k^4\right) \lambda^4, \tag{3.22}$$

$$g_3 = \frac{4}{27} \left(2 - 3k^2 - 3k^4 + 2k^6\right) \lambda^6, \tag{3.23}$$

$$e_1 = \frac{1}{3} \left(2 - k^2\right) \lambda^2, \quad e_2 = \frac{1}{3} \left(-1 + 2k^2\right) \lambda^2, \quad e_3 = \frac{1}{3}(-1 - k^2)\lambda^2, \tag{3.24}$$

$$\omega_1 = \frac{\mathcal{K}(k)}{\lambda}, \quad \omega_3 = \frac{i\mathcal{K}'(k)}{\lambda}, \tag{3.25}$$

where $\mathcal{K}'(k)$ is the complement to $\mathcal{K}(k)$ given by $\mathcal{K}'(k) = \mathcal{K}(1 - k^2)$. For all cases,

$$g_2 = \frac{4 - 2E + E^2}{3(c^2 - 1)^2}, \tag{3.26}$$

$$g_3 = \frac{8 - 6E - 3E^2 + E^3}{27(c^2 - 1)^3}. \tag{3.27}$$

One motivation for using Weierstrass elliptic functions instead of Jacobi elliptic functions is that there is a unique expression for the lattice invariants g_2 and g_3 see (3.26-3.27) which holds for all cases, as opposed to Jacobi elliptic functions where a different elliptic modulus k is used for each case see (3.11-3.14). The zeros of the polynomial $4s^3 - g_2 s - g_3$ are

$$s = \frac{E - 1}{3(c^2 - 1)}, \quad s = \frac{E + 2}{6(1 - c^2)}, \quad s = \frac{4 - E}{6(c^2 - 1)}. \tag{3.28}$$

These roots correspond to e_1, e_2, and e_3 where $e_1 > e_2 > e_3$. For the various cases:

$$\text{subluminal, rotational:} \quad e_1 = \frac{E-1}{3(c^2-1)}, \quad e_2 = \frac{E+2}{6(1-c^2)}, \quad e_3 = \frac{4-E}{6(c^2-1)}, \quad (3.29)$$

$$\text{superluminal, rotational:} \quad e_1 = \frac{E-1}{3(c^2-1)}, \quad e_2 = \frac{4-E}{6(c^2-1)}, \quad e_3 = \frac{E+2}{6(1-c^2)}, \quad (3.30)$$

$$\text{subluminal, librational:} \quad e_1 = \frac{E+2}{6(1-c^2)}, \quad e_2 = \frac{E-1}{3(c^2-1)}, \quad e_3 = \frac{4-E}{6(c^2-1)}, \quad (3.31)$$

$$\text{superluminal, librational:} \quad e_1 = \frac{4-E}{6(c^2-1)}, \quad e_2 = \frac{E-1}{3(c^2-1)}, \quad e_3 = \frac{E+2}{6(1-c^2)}. \quad (3.32)$$

3.3 The linear stability problem

To examine the linear stability of our solutions, we consider

$$v(z,\tau) = f(z) + \epsilon w(z,\tau) + \mathcal{O}\left(\epsilon^2\right), \quad (3.33)$$

where ϵ is a small parameter. Substituting (3.33) into (3.2), we obtain at order ϵ

$$(c^2-1)w_{zz} - 2cw_{z\tau} + w_{\tau\tau} + \cos\left(f(z)\right)w = 0. \quad (3.34)$$

Letting $w_1(z,\tau) = w(z,\tau)$ and $w_2(z,\tau) = w_\tau(z,\tau)$ we rewrite (3.34) as a first-order system of equations

$$\frac{\partial}{\partial \tau}\begin{pmatrix} w_1 \\ w_2 \end{pmatrix} = \mathcal{L}\begin{pmatrix} w_1 \\ w_2 \end{pmatrix} = \begin{pmatrix} 0 & 1 \\ -(c^2-1)\partial_z^2 - \cos\left(f(z)\right) & 2c\partial_z \end{pmatrix}\begin{pmatrix} w_1 \\ w_2 \end{pmatrix}. \quad (3.35)$$

An elliptic solution $f(z)$ is linearly stable if for all $\epsilon > 0$ there exists a $\delta > 0$ such that if $||w(z,0)|| < \delta$ then $||w(z,\tau)|| < \epsilon$ for all $\tau > 0$. This definition depends on the choice of norm $||\cdot||$, which is specified in the definition of the spectrum in (3.38) below.

Since (3.35) is autonomous in τ, we separate variables to look for solutions of the form

$$\begin{pmatrix} w_1(z,\tau) \\ w_2(z,\tau) \end{pmatrix} = e^{\lambda\tau}\begin{pmatrix} W_1(z) \\ W_2(z) \end{pmatrix}, \quad (3.36)$$

resulting in the spectral problem

$$\lambda\begin{pmatrix} W_1 \\ W_2 \end{pmatrix} = \mathcal{L}\begin{pmatrix} W_1 \\ W_2 \end{pmatrix} = \begin{pmatrix} 0 & 1 \\ -(c^2-1)\partial_z^2 - \cos\left(f(z)\right) & 2c\partial_z \end{pmatrix}\begin{pmatrix} W_1 \\ W_2 \end{pmatrix}. \quad (3.37)$$

Here

$$\sigma_{\mathcal{L}} = \{\lambda \in \mathbb{C} : \max_{x \in \mathbb{R}} \left(|W_1(x)|, |W_2(x)| \right) < \infty\}, \tag{3.38}$$

or

$$W_1, W_2 \in C_b^0(\mathbb{R}). \tag{3.39}$$

For spectral stability, we need to demonstrate that the spectrum $\sigma_{\mathcal{L}}$ does not enter the open right half of the complex λ plane. Since (3.1) is Hamiltonian [4], the spectrum of its linearization is symmetric with respect to both the real and imaginary axis [71]. In other words, proving spectral stability for elliptic solutions to (3.1) amounts to proving that the stability spectrum lies strictly on the imaginary axis. We show that the elliptic solutions are spectrally stable only in the subluminal rotational case. We demonstrate spectral elements in the right-half plane near the origin for all choices of the parameters E and c outside the subluminal rotational regime.

3.4   The Lax problem

We wish to obtain an analytical representation for the spectrum $\sigma_{\mathcal{L}}$. As mentioned in the introduction, this analytical representation comes from the squared eigenfunction connection between the linear stability problem (3.37) and the Lax pair of (3.1). The Lax pair for sine-Gordon is well known [1,2,4,50]. The compatibility condition $\chi_{xt} = \chi_{tx}$ of the Lax pair,

$$\chi_x = \begin{pmatrix} -\dfrac{i\zeta}{2} + \dfrac{i\cos(u)}{8\zeta} & \dfrac{i\sin(u)}{8\zeta} - \dfrac{1}{4}\left(u_x + u_t\right) \\ \dfrac{i\sin(u)}{8\zeta} + \dfrac{1}{4}\left(u_x + u_t\right) & \dfrac{i\zeta}{2} - \dfrac{i\cos(u)}{8\zeta} \end{pmatrix} \chi, \tag{3.40}$$

$$\chi_t = \begin{pmatrix} -\dfrac{i\zeta}{2} - \dfrac{i\cos(u)}{8\zeta} & -\dfrac{i\sin(u)}{8\zeta} - \dfrac{1}{4}\left(u_x + u_t\right) \\ -\dfrac{i\sin(u)}{8\zeta} + \dfrac{1}{4}\left(u_x + u_t\right) & \dfrac{i\zeta}{2} + \dfrac{i\cos(u)}{8\zeta} \end{pmatrix} \chi, \tag{3.41}$$

is (3.1). We transform the Lax pair by moving into a traveling reference frame letting $z = x - ct$, $\tau = t$, and $v(z, \tau) = u(x, t)$. Additionally, to examine the stationary solutions we

let $v(z, \tau) = f(z)$ so that

$$\chi_z = \begin{pmatrix} C & D \\ -D^* & -C \end{pmatrix} \chi,$$ (3.42)

$$\chi_\tau = \begin{pmatrix} A & B \\ -B^* & -A \end{pmatrix} \chi,$$ (3.43)

where $*$ represents the complex conjugate, and

$$A = -\frac{i\left(4(1+c)\zeta^2 - (c-1)\cos(f(z))\right)}{8\zeta},$$ (3.44)

$$B = \frac{(c-1)\left(i\sin(f(z)) + 2(c+1)\zeta f'(z)\right)}{8\zeta},$$ (3.45)

$$C = -\frac{i\zeta}{2} + \frac{i\cos(f(z))}{8\zeta},$$ (3.46)

$$D = \frac{i\sin(f(z))}{8\zeta} - \frac{f'(z)}{4} + \frac{cf'(z)}{4},$$ (3.47)

whose compatibility condition $\chi_{z\tau} = \chi_{\tau z}$ is (3.4). We define σ_L, or informally the Lax spectrum, as the set of all ζ for which (3.42) has a bounded (in z) solution. Examining (3.43), since A and B are independent of τ, we separate variables. Let

$$\chi(z, \tau) = e^{\Omega \tau} \varphi(z),$$ (3.48)

with Ω being independent of τ, but possibly depending on z. Substituting (3.48) into (3.43) and canceling the exponential, we find

$$\begin{pmatrix} A - \Omega & B \\ -B^* & -A - \Omega \end{pmatrix} \varphi = 0.$$ (3.49)

To have nontrivial solutions, we require the determinant of (3.49) to be zero. Using the definitions of A and B, we get

$$\Omega^2 = A^2 - BB^* = \frac{1}{64}\left(-8(c^2-1)(E-1) - \frac{(c-1)^2}{\zeta^2} - 16(c+1)^2\zeta^2\right).$$ (3.50)

As expected, Ω is independent of both τ (by construction) and z (by integrability). Thus Ω is strictly a function of ζ and the solution parameters c and E. We remark that Ω takes the form (3.50) for all values of c and E regardless of where we are in parameter space.

To satisfy (3.49), we let

$$\varphi(z) = \gamma(z) \begin{pmatrix} -B(z) \\ A(z) - \Omega \end{pmatrix}, \tag{3.51}$$

where $\gamma(z)$ is a scalar function. By construction of $\varphi(z)$, $\chi(z, \tau)$ satisfies (3.43). Since (3.42) and (3.43) commute, it is possible to choose $\gamma(z)$ such that χ also satisfies (3.42). Indeed, $\gamma(z)$ satisfies a first-order linear equation, whose solution is given by

$$\gamma(z) = \gamma_0 \exp\left(\int \frac{-C(A - \Omega) + BD^* - A_z}{A - \Omega} dz\right). \tag{3.52}$$

For almost every $\zeta \in \mathbb{C}$, we have explicitly determined the two linearly independent solutions of (3.42), *i.e.*, those corresponding to the positive and negative signs of Ω in (3.50). Assuming $\Omega \neq 0$ these two solutions are, by construction, linearly independent. In the case where ζ is a root of Ω, the second solution to (3.42) can be determined via the reduction-of-order method.

Since (3.42) and (3.43) share eigenfunctions, σ_L is the set of all $\zeta \in \mathbb{C}$ such that (3.51) is bounded for all $z \in \mathbb{R}$. The vector part of φ is bounded for all z, so we only need that the scalar function $\gamma(z)$ is bounded as $z \to \pm\infty$. A necessary and sufficient condition for this is

$$\left\langle \mathrm{Re}\left(\frac{-C(A - \Omega) + BD^* - A_z}{A - \Omega}\right)\right\rangle = 0, \tag{3.53}$$

where $\langle \cdot \rangle$ is the average over one period $2\mathcal{K}(k)$ of the integrand, and Re denotes the real part. The integral condition (3.53) completely determines the Lax spectrum σ_L.

3.5 The squared eigenfunction connection

A connection between the eigenfunction of the Lax pair (3.42) and (3.43) and the eigenfunctions of the linear stability problem (3.37) using squared eigenfunctions is well known [1]. We prove the following theorem.

Theorem 3.5.1. *The sum of squares,*

$$w(z, \tau) = \chi_1(z, \tau)^2 + \chi_2(z, \tau)^2, \tag{3.54}$$

satisfies the linear stability problem (3.34) for $f(z)$. Here $\chi = (\chi_1, \chi_2)^T$ is any solution of (3.42-3.43).

Proof. The proof is done by direct calculation. Substitute $w(z, \tau)$ into the left-hand side of (3.34). Eliminate z-derivatives of χ_1 and χ_2 (up to order 2) using (3.42) and eliminate τ-derivatives of χ_1 and χ_2 (up to order 2) using (3.43). The resulting expression for the left-hand side is 0, thus demonstrating that (3.34) is satisfied, finishing the proof. □

To establish the connection between $\sigma_{\mathcal{L}}$ and σ_L, we examine the right- and left-hand sides of (3.36). Substituting (3.54) and (3.48) to the left hand side of (3.36) we find

$$e^{2\Omega\tau} \begin{pmatrix} \varphi_1^2 + \varphi_2^2 \\ 2\Omega \left(\varphi_1^2 + \varphi_2^2 \right) \end{pmatrix} = e^{\lambda\tau} \begin{pmatrix} W_1(z) \\ W_2(z) \end{pmatrix}, \tag{3.55}$$

so we conclude that

$$\lambda = 2\Omega(\zeta), \tag{3.56}$$

with eigenfunctions given by

$$\begin{pmatrix} W_1(z) \\ W_2(z) \end{pmatrix} = \begin{pmatrix} \varphi_1^2 + \varphi_2^2 \\ 2\Omega \left(\varphi_1^2 + \varphi_2^2 \right) \end{pmatrix}. \tag{3.57}$$

This gives the connection between the σ_L spectrum and the $\sigma_{\mathcal{L}}$ spectrum. It is also necessary to check that indeed all solutions of (3.37) are obtained through (3.55). This is not shown explicitly here, but is done analogous to the work in [11, 12].

Although in principle the above construction determines $\sigma_{\mathcal{L}}$, it remains to be seen whether this determination is practical. In the following section we discuss a technique for explicitly integrating (3.53) using Weierstrass elliptic functions, leading to a more explicit characterization of $\sigma_{\mathcal{L}}$.

3.6 The Lax spectrum in terms of elliptic functions

In terms of Weierstrass elliptic functions, (3.53) becomes

$$\text{Re} \int_0^{2\omega_1} \frac{-C(A - \Omega) + BD^* - A_z}{A - \Omega} \mathrm{d}z = 0, \tag{3.58}$$

with A, B, C, and D given in (3.46-3.47). Substituting in for $f(z)$ using (3.21) we find that (3.58) is

$$\text{Re} \int_0^{2\omega_1} \frac{C_1 + C_2\wp(z) + C_3\wp'(z)}{C_4 + C_5\wp(z)} \mathrm{d}z = 0, \tag{3.59}$$

with $\wp(z) = \wp(z + \omega_3, g_2, g_3)$ with the dependence on ω_3, g_2, and g_3 suppressed. The C_j's depend on ζ but are independent of z. Like $\Omega(\zeta)$, the C_j's take one form regardless of where the solution is in parameter space. They are given by

$$C_1 = \frac{1}{3}\left(-3i - 16i(E-1)\zeta^2 + 48i\zeta^4 + 3ic\left(1 + 8(E-1)\zeta^2 + 16\zeta^4\right)\right. \tag{3.60}$$

$$\left. + \left(8(e-1)\zeta + 96\zeta^3\right)\Omega(\zeta)\right), \tag{3.61}$$

$$C_2 = 16(c^2 - 1)\zeta\left(i\zeta + \Omega(\zeta)\right), \tag{3.62}$$

$$C_3 = -8(c-1)^2(c+1)\zeta, \tag{3.63}$$

$$C_4 = \frac{8}{3}\zeta\left((c-1)(E-1) + 12(c+1)\zeta^2 - 24i\zeta\Omega(\zeta)\right), \tag{3.64}$$

$$C_5 = 16(c-1)^2(c+1)\zeta. \tag{3.65}$$

We evaluate the integral in (3.59) explicitly [35]. We find

$$\text{Re}\left[\frac{2\omega_1 C_2}{C_5} + \frac{4\left(C_1 C_5 - C_2 C_4\right)}{\wp'(\rho)C_5^2}\left(\zeta_w(\rho)\omega_1 - \zeta_w(\omega_1)\rho\right)\right] = 0, \tag{3.66}$$

with

$$\rho = \rho(\zeta) = \wp^{-1}\left(-\frac{C_4(\zeta)}{C_5(\zeta)}, g_2, g_3\right), \tag{3.67}$$

and ζ_w is the Weierstrass Zeta function [55]. Note that $\wp^{-1}$ is a multivalued function, but for our analysis ρ is chosen as any value such that $\wp(\rho) = -C_4(\zeta)/C_5(\zeta)$. Substituting for the C_j's (3.66) becomes

$$\text{Re}\left[\frac{2\omega_1\left(i\zeta + \Omega(\zeta)\right)}{c-1} + \frac{4\zeta\left(-i(c-1)(E-1) - 4i(c+1)\zeta^2 - 8\zeta\Omega(\zeta)\right)}{(c-1)^3(c+1)\wp'(\rho)}\left(\zeta_w(\rho)\omega_1 - \zeta_w(\omega_1)\rho\right)\right] = 0. \tag{3.68}$$

We simplify this further by recognizing that

$$\wp'^2(\rho) = 4\wp^3(\rho) - g_2\wp(\rho) - g_3 = 4\left(-\frac{C_4(\zeta)}{C_5(\zeta)}\right)^3 - g_2\left(-\frac{C_4(\zeta)}{C_5(\zeta)}\right) - g_3. \tag{3.69}$$

Substituting in for $C_4(\zeta)$ and $C_5(\zeta)$ gives

$$\wp'^2(\rho) = 4\left(\frac{\zeta\left(-i(c-1)(E-1) - 4i(c+1)\zeta^2 - 8\zeta\Omega(\zeta)\right)}{(c-1)^3(c+1)}\right)^2. \qquad (3.70)$$

Thus (3.68) simplifies to

$$\mathrm{Re}\left(\frac{2\omega_1\left(i\zeta + \Omega(\zeta)\right)}{c-1} + 2\nu\left(\zeta_w(\rho)\omega_1 - \zeta_w(\omega_1)\rho\right)\right) = 0, \qquad (3.71)$$

where

$$\nu = \begin{cases} +1 & \text{if } -\frac{\pi}{2} < \arg\left(\frac{\zeta\left(-i(c-1)(E-1) - 4i(c+1)\zeta^2 - 8\zeta\Omega(\zeta)\right)}{(c-1)^3(c+1)}\right) \leq \frac{\pi}{2}, \\ -1 & \text{otherwise.} \end{cases} \qquad (3.72)$$

Using (3.25), and applying the formula for the Weierstrass ζ function evaluated at a half period [17], $\zeta_w(\omega_1) = \sqrt{e_1 - e_3}\left(\mathcal{E}(k) - \frac{e_1}{e_1 - e_3}\mathcal{K}(k)\right)$, (3.71) becomes

$$\mathrm{Re}\left[\frac{2\mathcal{K}(k)\left(i\zeta + \Omega(\zeta)\right)}{c-1} + 2\nu\left(\zeta_w(\rho)\mathcal{K}(k) - \sqrt{e_1 - e_3}\left(\mathcal{E}(k) - \frac{e_1}{e_1 - e_3}\mathcal{K}(k)\right)\rho\right)\right] = 0. \qquad (3.73)$$

Here

$$\mathcal{E}(k) = \int_0^{\pi/2}\sqrt{1 - k^2\sin^2 y}\,\mathrm{d}y, \qquad (3.74)$$

is the complete elliptic integral of the second kind. We have simplified the integral condition (3.58) significantly. Thus $\zeta \in \sigma_L$ if and only if (3.73) is satisfied. To simplify notation, let

$$I(\zeta) = \frac{2\omega_1\left(i\zeta + \Omega(\zeta)\right)}{c-1} + 2\nu\left(\zeta_w(\rho)\omega_1 - \zeta_w(\omega_1)\rho\right), \qquad (3.75)$$

so that (3.73) is

$$\mathrm{Re}\left[I(\zeta)\right] = 0. \qquad (3.76)$$

Next, we wish to examine the level sets of the left-hand side of (3.76). To this end, we differentiate $I(\zeta)$ with respect to ζ. To evaluate this derivative we use the chain rule and note that

$$\frac{\partial}{\partial\zeta}\zeta_w(\rho) = -\wp(\rho)\frac{\partial\rho}{\partial\zeta} = \frac{C_4(\zeta)}{C_5(\zeta)}\frac{\mathrm{d}\wp^{-1}}{\mathrm{d}\zeta}\left(-\frac{C_4(\zeta)}{C_5(\zeta)}, g_2, g_3\right)\left(-\frac{C_4(\zeta)}{C_5(\zeta)}\right)'. \qquad (3.77)$$

Since

$$\frac{\mathrm{d}}{\mathrm{d}z}\wp^{-1}\left(-\frac{C_4(\zeta)}{C_5(\zeta)},g_2,g_3\right) = \frac{1}{\wp'\left(\wp^{-1}\left(-\frac{C_4(\zeta)}{C_5(\zeta)},g_2,g_3\right)\right)} = \frac{1}{\wp'(\rho)}, \tag{3.78}$$

we use (3.70) to obtain

$$\frac{\mathrm{d}I(\zeta)}{\mathrm{d}\zeta} = \frac{3(c-1)\omega_1 - 48(c+1)\zeta^4\omega_1 - 8\zeta^2\left(6(c^2-1)\zeta_w(\omega_1) + (1-E)\omega_1\right)}{96\zeta^3\Omega(\zeta)}. \tag{3.79}$$

Taking the real part of (3.79) does not give another characterization of the spectrum. Instead, if we think of (3.73) as restricting to the zero level set of the left-hand side. Then we use (3.79) to determine a tangent vector field which allows us to map out level curves originating from any point. This is explained in more detail in Section 3.7.

3.7 The $\sigma_{\mathcal{L}}$ spectrum on the imaginary axis

In this section we discuss $\sigma_{\mathcal{L}} \cap i\mathbb{R}$. As we demonstrate, this corresponds to the part of σ_L lying on the real axis for both rotational and librational waves, as well as a part of σ_L lying on the imaginary axis for rotational waves. Using (3.73) we obtain analytic expressions for σ_L corresponding to $\sigma_{\mathcal{L}} \cap i\mathbb{R}$.

We begin by considering $\zeta \in \mathbb{R}$. As we demonstrate below, (3.73) is satisfied for any real ζ. Using (3.50) and (3.56), we determine the corresponding parts of $\sigma_{\mathcal{L}}$.

Theorem 3.7.1. *The condition (3.73) is satisified for $\zeta \in \mathbb{R}$.*

Proof. Since k, c, $\mathcal{K}(k)$, and $\mathcal{E}(k)$ are real, it suffices to show that $\Omega(\zeta) \in i\mathbb{R}$, $\rho \in i\mathbb{R}$, and $\zeta_w(\rho) \in i\mathbb{R}$. Rewriting (3.50) in the superluminal case,

$$\Omega^2(\zeta) = -\frac{1}{64}\left(\left(-4(1+c)\zeta + \frac{c-1}{\zeta}\right)^2 + 8E(c^2-1)\right), \tag{3.80}$$

and in the subluminal case,

$$\Omega^2(\zeta) = -\frac{1}{64}\left(\left(-4(1+c)\zeta - \frac{c-1}{\zeta}\right)^2 + 8(2-E)(1-c^2)\right). \tag{3.81}$$

In either case $\Omega^2 \leq 0$ and $\Omega(\zeta) \in i\mathbb{R}$. Since ζ_w with $g_2, g_3 \in \mathbb{R}$ takes real values to real values and purely imaginary values to purely imaginary values [55], to prove $\zeta_w(\rho) \in i\mathbb{R}$ it suffices to show that $\rho = \wp^{-1}\left(-\frac{C_4(\zeta)}{C_5(\zeta)}, g_2, g_3\right) \in i\mathbb{R}$. For $g_2, g_3 \in \mathbb{R}$, $\wp(\mathbb{R}, g_2, g_3)$ maps to $[e_1, \infty)$, and since $\wp(ix, g_2, g_3) = -\wp(x, g_2, -g_3)$ we have that $\wp(i\mathbb{R}, g_2, g_3)$ maps to $(-\infty, e_3]$. Thus we need to show that for $\zeta \in \mathbb{R}$, $-\frac{C_4(\zeta)}{C_5(\zeta)} \leq e_3$. Again we split into cases. In the superluminal case, we want to show

$$\frac{(c-1)(E-1) + 12(c+1)\zeta^2 - 24i\zeta\Omega(\zeta)}{6(c-1)(1-c^2)} \leq \frac{E+2}{6(1-c^2)}. \tag{3.82}$$

Substituting in for $\Omega(\zeta)$ using (3.80) and simplifying the left- and right-hand sides of this expression yields

$$\frac{4(c+1)\zeta^2}{c-1} + \frac{\sqrt{(-4(1+c)\zeta^2 + (c-1))^2 + 8E(c^2-1)\zeta^2}}{c-1} \geq 1. \tag{3.83}$$

Since $\sqrt{(-4(1+c)\zeta^2 + (c-1))^2 + 8E(c^2-1)\zeta^2} \geq \sqrt{(-4(1+c)\zeta^2 + (c-1))^2}$, (3.83) is satisfied. For the subluminal case we proceed in a similar manner, noting the different value of e_3 from (3.29-3.32). We want to show

$$\frac{(c-1)(E-1) + 12(c+1)\zeta^2 - 24i\zeta\Omega(\zeta)}{6(c-1)(1-c^2)} \leq \frac{E-4}{6(1-c^2)}. \tag{3.84}$$

Substituting in for $\Omega(\zeta)$ using (3.81) and simplifying the left- and right-hand sides of this expression yields

$$\frac{4(c+1)\zeta^2 + \sqrt{(-4(c+1)\zeta^2 + (1-c))^2 + 8(2-E)(1-c^2)\zeta^2}}{1-c} \geq 1. \tag{3.85}$$

Since $\sqrt{(-4(c+1)\zeta^2 + (1-c))^2 + 8(2-E)(1-c^2)\zeta^2} \geq \sqrt{(-4(c+1)\zeta^2 + (1-c))^2}$, (3.85) is satisfied. $\qquad\square$

At this point, we know that $\mathbb{R} \subset \sigma_L$. We wish to see what this corresponds to for $\sigma_{\mathcal{L}}$. For convenience define

$$S_\Omega = \left\{\Omega : \Omega^2 = \frac{1}{64}\left(-8(c^2-1)(E-1) - \frac{(c-1)^2}{\zeta^2} - 16(c+1)^2\zeta^2\right) \text{ and } \zeta \in \sigma_L\right\}. \tag{3.86}$$

(a) Subluminal: $c^2 < 1$ (b) Superluminal: $c^2 > 1$
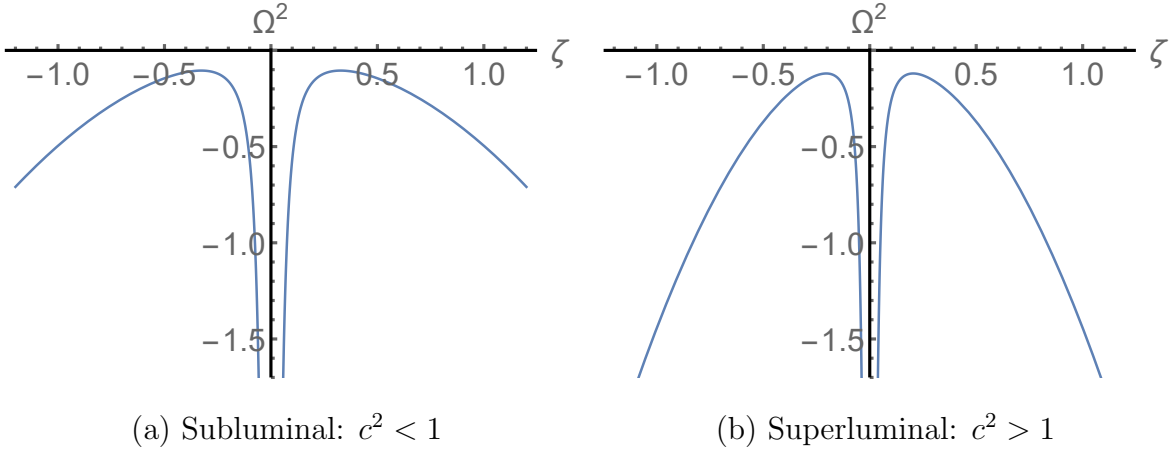
Figure 3.3: Ω^2 as a function of real ζ for subluminal and superluminal waves: (a) subluminal: $c = 0.4$ and $E = 1$, and (b) superluminal: $c = 1.4$ and $E = 1$.

As was seen in the proof of Theorem 3.7.1, when $\zeta \in \mathbb{R}$, $\Omega(\zeta) \in i\mathbb{R}$. Applying (3.56), we see that $\zeta \in \mathbb{R}$ corresponds to $\sigma_\mathcal{L} \cup i\mathbb{R}$. Representative plots of Ω^2 are shown in Figure 3.3. The subset of S_Ω corresponding to $\zeta \in \mathbb{R}$ consists of $(-i\infty, -i|\Omega_m|] \cup [i|\Omega_m|, i\infty)$, where Ω_m^2 is the maximum value of Ω^2. The set S_Ω corresponding to $\zeta \in \mathbb{R}$ is quadruple covered as for all values of Ω there are four values of ζ which map to it, except at $\Omega = \pm\Omega_m$, where just two values of ζ map to it. Ω_m can be found explicitly by finding the extrema of $\Omega^2(\zeta)$. In the subluminal case, $\Omega^2(\zeta)$ reaches its maxima at

$$\zeta_m = \pm\sqrt{\frac{1-c}{4(1+c)}}, \quad \Omega_m^2 = -\frac{1}{8}(1-c^2)(2-E), \tag{3.87}$$

and in the superluminal case, $\Omega^2(\zeta)$ reaches its maxima at

$$\zeta_m = \pm\sqrt{\frac{c-1}{4(1+c)}}, \quad \Omega_m^2 = -\frac{1}{8}(c^2-1)E. \tag{3.88}$$

Applying (3.56) we have $(-i\infty, -\lambda_1] \cup [\lambda_1, i\infty) \subset \sigma_\mathcal{L}$ where

$$\lambda_1 = i\sqrt{\frac{(1-c^2)(2-E)}{2}}, \tag{3.89}$$

in the subluminal case, and

$$\lambda_1 = i\sqrt{\frac{E(c^2-1)}{2}}, \tag{3.90}$$

in the superluminal case.

If ζ satisfies $\Omega^2(\zeta) = 0$, then ζ must satisfy (3.73). This is due to the fact that the origin is always included in $\sigma_{\mathcal{L}}$ and hence in S_Ω. The fact that there are four roots of $\Omega^2(\zeta) = 0$ corresponds to the fact that $0 \in \sigma_{\mathcal{L}}$ with multiplicity four. This is seen from the symmetries of (3.1) and by applying Noether's Theorem [47,65]. For rotational waves, the roots of $\Omega^2(\zeta)$ lie on the imaginary axis. For the subluminal rotational case the roots are:

$$\zeta_c = \left\{ \frac{\sqrt{1-c^2}}{2\sqrt{2}(c+1)} \left(\sqrt{-E} \pm \sqrt{2-E} \right) i, -\frac{\sqrt{1-c^2}}{2\sqrt{2}(c+1)} \left(\sqrt{-E} \pm \sqrt{2-E} \right) i \right\}, \qquad (3.91)$$

and in the superluminal rotational case the roots are:

$$\zeta_c = \left\{ \frac{\sqrt{c^2-1}}{2\sqrt{2}(c+1)} \left(\sqrt{E} \pm \sqrt{E-2} \right) i, -\frac{\sqrt{c^2-1}}{2\sqrt{2}(c+1)} \left(\sqrt{E} \pm \sqrt{E-2} \right) i \right\}. \qquad (3.92)$$

We label the four roots ζ_1, ζ_2, ζ_3, and ζ_4 where $\mathrm{Im}(\zeta_1) < \mathrm{Im}(\zeta_2) < \mathrm{Im}(\zeta_3) < \mathrm{Im}(\zeta_4)$. They are labeled for reference in Figure 3.4.

Theorem 3.7.2. *For rotational waves, the condition (3.73) is satisified for all $\zeta \in i\mathbb{R}$ such that $\mathrm{Im}(\zeta_1) \leq \mathrm{Im}(\zeta) \leq \mathrm{Im}(\zeta_2)$ or $\mathrm{Im}(\zeta_3) \leq \mathrm{Im}(\zeta) \leq \mathrm{Im}(\zeta_4)$.*

Proof. The level curve (3.76), is exactly the condition (3.73). We examine the tangent vector field to (3.76). If we let $\zeta = \zeta_r + i\zeta_i$, then

$$I(\zeta) = I(\zeta_r + i\zeta_i) = \frac{2\omega_1 \left(i(\zeta_r + i\zeta_i) + \Omega(\zeta_r + i\zeta_i) \right)}{c-1} + 2\nu \left(\zeta_w(\rho)\omega_1 - \zeta_w(\omega_1)\rho \right). \qquad (3.93)$$

Taking derivatives with respect to ζ_r and ζ_i gives a normal vector field to level curves of the general condition $\mathrm{Re}\left[I(\zeta)\right] = C$ for any constant C, specifically, the normal vector is given by

$$\left(\frac{d\mathrm{Re}\left[I(\zeta_r + i\zeta_i)\right]}{d\zeta_r}, \frac{d\mathrm{Re}\left[I(\zeta_r + i\zeta_i)\right]}{d\zeta_i} \right).$$

Thus, the tangent vector field is

$$\left(-\frac{d\mathrm{Re}\left[I(\zeta_r + i\zeta_i)\right]}{d\zeta_i}, \frac{d\mathrm{Re}\left[I(\zeta_r + i\zeta_i)\right]}{d\zeta_r} \right).$$

(a) Subluminal: $c^2 < 1$ (b) Superluminal: $c^2 > 1$
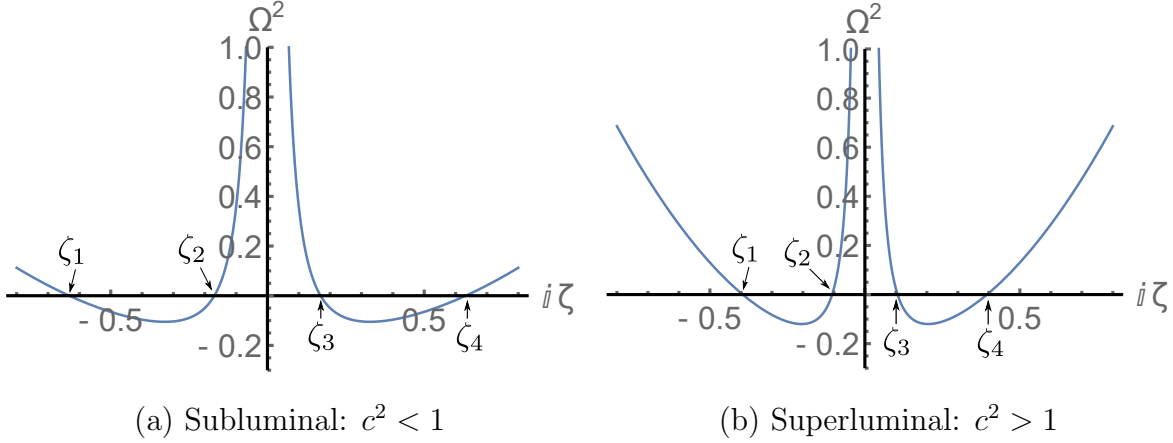
Figure 3.4: Ω^2 as a function of $i\zeta$, $\zeta \in \mathbb{R}$ for subluminal and superluminal rotational waves: (a) subluminal rotational: $c = 0.4$ and $E = -1$, and (b) superluminal rotational: $c = 1.4$ and $E = 3$.

By applying the chain rule and using $\mathrm{Re}[iz] = -\mathrm{Im}[z]$, we have that the tangent vector field to the level curves is

$$\left(\mathrm{Im}\left[\frac{\mathrm{d}I}{\mathrm{d}\zeta}\right], \mathrm{Re}\left[\frac{\mathrm{d}I}{\mathrm{d}\zeta}\right] \right). \tag{3.94}$$

Where $\frac{\mathrm{d}I}{\mathrm{d}\zeta}$ is given in (3.79). We note that the numerator of (3.79) is strictly real for $\zeta \in i\mathbb{R}$, thus

$$\mathrm{Im}\left[\frac{\mathrm{d}I}{\mathrm{d}\zeta}\right] = \left(3(c-1)\omega_1 - 48(c+1)\zeta^4\omega_1 - 8\zeta^2\left(3(c^2-1)\zeta_w(\omega_1) + (1-E)\omega_1\right)\right) \mathrm{Im}\left[\frac{1}{96\zeta^3\Omega(\zeta)}\right]. \tag{3.95}$$

Since $\Omega^2(\zeta) \leq 0$ for $\zeta \in [\zeta_1, \zeta_2] \subset i\mathbb{R}$ and for $\zeta \in [\zeta_3, \zeta_4] \subset i\mathbb{R}$ we have that

$$\mathrm{Im}\left[\frac{\mathrm{d}I}{\mathrm{d}\zeta}\right] = 0, \tag{3.96}$$

and thus $\mathrm{Re}\left[I(\zeta)\right] = C$ on these intervals. Since $\mathrm{Re}\left[I(\zeta)\right] = 0$ at the endpoints ζ_c, $C = 0$ and (3.73) is satisfied. $\qquad\square$

At this point we know that $[\zeta_1, \zeta_2] \cup [\zeta_3, \zeta_4] \subset \sigma_L$. We wish to see what this corresponds to for $\sigma_{\mathcal{L}}$. Representative plots of $\Omega^2(i\zeta)$, $\zeta \in \mathbb{R}$ are shown in Figure 3.4. The subset of S_Ω corresponding to $\zeta \in [\zeta_1, \zeta_2] \cup [\zeta_3, \zeta_4]$ consists of $[-i|\Omega_n|, 0]$, where Ω_n^2 is the minimum

value of Ω^2. The set S_Ω corresponding to $\zeta \in [\zeta_1, \zeta_2] \cup [\zeta_3, \zeta_4]$ is quadruple covered, except at the points $\pm\Omega_n$, where the set is double-covered. Ω_n can be found explicitly by finding the extrema of $\Omega^2(i\zeta)$. In the subluminal rotational case, $\Omega^2(\zeta)$ reaches its minima at

$$\zeta_n = \pm\sqrt{\frac{1-c}{4(c+1)}}i, \quad \Omega_n^2(\zeta) = \frac{1}{8}(1-c^2)E, \tag{3.97}$$

and in the superluminal rotational case, $\Omega^2(\zeta)$ reaches its minima at

$$\zeta_n = \pm\sqrt{\frac{c-1}{4(c+1)}}i, \quad \Omega_n^2(\zeta) = \frac{1}{8}(c^2-1)(E-2). \tag{3.98}$$

Applying (3.56) we have $[-\lambda_2, \lambda_2] \subset \sigma_{\mathcal{L}}$ where

$$\lambda_2 = \sqrt{\frac{(1-c^2)E}{2}}i, \tag{3.99}$$

in the subluminal rotational case, and

$$\lambda_2 = \sqrt{\frac{(c^2-1)(E-2)}{2}}i, \tag{3.100}$$

in the superluminal rotational case.

3.8 Qualitatively different parts of the spectrum

Up to this point we have discussed only the subset of $\sigma_{\mathcal{L}}$ that is on the imaginary axis. In this section we discuss the rest of the spectrum. Except in the subluminal, rotational case, a part of $\sigma_{\mathcal{L}}$ is in the right-half plane (corresponding to unstable modes). For each of the other three regions we split parameter space into two subregions where $\overline{\sigma_{\mathcal{L}} \setminus i\mathbb{R}}$ is qualitatively different. Here $\overline{\sigma_{\mathcal{L}} \setminus i\mathbb{R}}$ is the closure of $\sigma_{\mathcal{L}}$ not on the imaginary axis.

We refer to Figure 3.5, which shows (E, c) parameter space with curves that split it into subregions where $\overline{\sigma_{\mathcal{L}} \setminus i\mathbb{R}}$ is qualitatively different. The exact curves splitting up the regions, and their derivations, are given below. In Figure 3.6 we show representative plots of $\sigma_{\mathcal{L}}$ for all qualitatively different spectra, and in Figure 3.7 we show the corresponding σ_L spectrum.

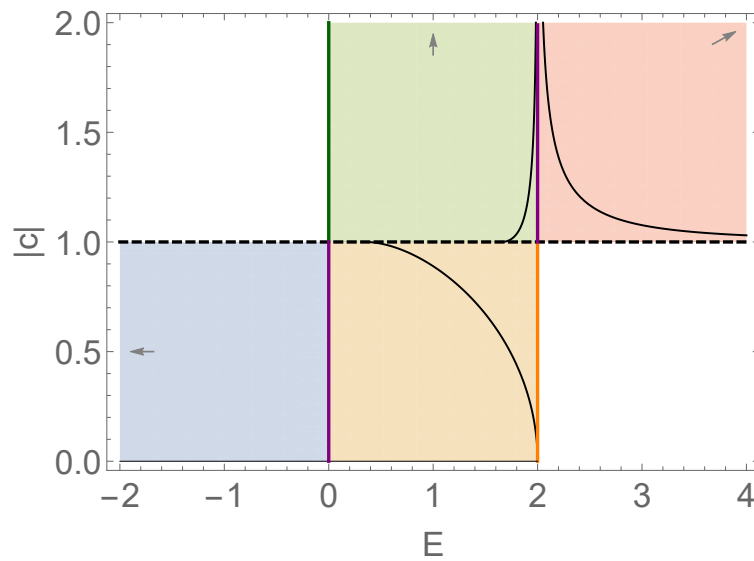Figure 3.5: Parameter space with regions corresponding to different qualitative behavior in the linear stability spectrum separated by black curves. Colors correspond to solutions in Figure 3.1. Blue: subluminal rotational ($0 \leq |c| < 1$, $E < 0$), orange: subluminal librational ($0 \leq |c| < 1$, $0 < E \leq 2$), green: superluminal librational ($|c| > 1$, $0 \leq E < 2$), red: superluminal rotational ($0 \leq |c| > 1$, $E > 2$).

- The spectral stability of subluminal rotational solutions is well known [45, 46] and $\sigma_{\mathcal{L}} \subset i\mathbb{R}$. A representative plot of $\sigma_{\mathcal{L}}$ is seen in Figure 3.6(e).

- For the subluminal librational solutions, $\overline{\sigma_{\mathcal{L}} \setminus i\mathbb{R}}$ consists of either a double-covered infinity symbol, see Figure 3.6(f), or a double-covered figure 8 inset inside a double-covered ellipse-like curve, see Figure 3.6(g). The boundary between these regions is given explicitly below and a representative plot of $\sigma_{\mathcal{L}}$ on this boundary is seen in Figure 3.8(3a).

- For the superluminal librational solutions, $\overline{\sigma_{\mathcal{L}} \setminus i\mathbb{R}}$ consists of either a double-covered figure 8, see Figure 3.6(a), or a double-covered infinity symbol inset inside a double-covered ellipse-like curve, see Figure 3.6(b). The boundary between these regions is given below and a representative plot of $\sigma_{\mathcal{L}}$ on this boundary is seen in Figure 3.8(1a).

- For the superluminal rotational solutions, $\overline{\sigma_{\mathcal{L}} \setminus i\mathbb{R}}$ consists of either a double-covered ellipse-like curve surrounding the origin, see Figure 3.6(c), or a double-covered ellipse-like curve in the upper- and lower-half plane, see Figure 3.6(d). The boundary between these regions is given explicitly below and a representative plot of $\sigma_{\mathcal{L}}$ on this boundary is seen in Figure 3.8(2a).

For all these cases, much can be proven and quantified explicitly, *i.e.*, not in terms of special functions. Specifically, we calculate explicit expressions for $\sigma_{\mathcal{L}} \cap i\mathbb{R}$ and in the librational case we find explicit expressions for the tangents to $\sigma_{\mathcal{L}}$ around the origin. In fact, we are able to approximate the spectrum at the origin and around all points $\sigma_{\mathcal{L}} \cap i\mathbb{R}$ using a Taylor series to arbitrary order. These series give good approximations to the greatest real part of $\sigma_{\mathcal{L}}$ using only a few terms. They are not given in this chapter, but follow from the same procedure as outlined in Chapter 2.

A method for determining σ_L is to take known points satisfying (3.73) and to follow the tangent vector field (3.94) from those points. We apply this technique from $\zeta \in \mathbb{R}$ which we know to satisfy (3.73) from Theorem 3.7.1 as well as from the points ζ satisfying $\Omega^2(\zeta) = 0$.

Figure 3.6: The stability spectrum for superluminal (a-d), subluminal (e-g), librational (a,b,f,g) and rotational (c,d,e) waves. (a) $c = 1.5$, $E = 1.5$; (b) $c = 1.02$, $E = 1.8$; (c) $c = 1.1$, $E = 2.2$; (d) $c = 1.4$, $E = 2.4$; (e) $c = 0.6$, $E = -0.75$; (f) $c = 0.6$, $E = 1.0$; (g) $c = 0.8$, $E = 1.5$; Colors correspond to Figure 3.2, thickness of lines corresponds to double or quadruple covering of spectrum.

3.8.1 Subluminal librational solutions

The roots of $\Omega^2(\zeta) = 0$ are given by

$$\zeta_c = \left\{ \frac{\sqrt{1-c^2}\sqrt{E}}{2\sqrt{2}(c+1)} \pm \frac{\sqrt{1-c^2}\sqrt{2-e}}{2\sqrt{2}(c+1)}i, -\frac{\sqrt{1-c^2}\sqrt{E}}{2\sqrt{2}(c+1)} \pm \frac{\sqrt{1-c^2}\sqrt{2-e}}{2\sqrt{2}(c+1)}i \right\}, \qquad (3.101)$$

seen as red crosses in Figure 3.7(f,g). For convenience, we label these four roots ζ_1, ζ_2, ζ_3, ζ_4, where the subscript corresponds to the quadrant on the real and imaginary plane the root is in. In this case, (3.79) is

$$\frac{dI(\zeta)}{d\zeta} = \sqrt{1-c^2}\frac{16\zeta^2\mathcal{E}(k) + (c - 1 - 8\zeta^2 - 16(c+1)\zeta^4)\,\mathcal{K}(k)}{32\zeta^3\Omega(z)}. \qquad (3.102)$$

Examining (3.94) for $\zeta \in \mathbb{R}$, for a vertical tangent in σ_L to occur, we need the numerator of (3.102) to be zero. Using the discriminant of $16\zeta^2\mathcal{E}(k) + (c - 1 - 8\zeta^2 - 16(c+1)\zeta^4)\,\mathcal{K}(k)$
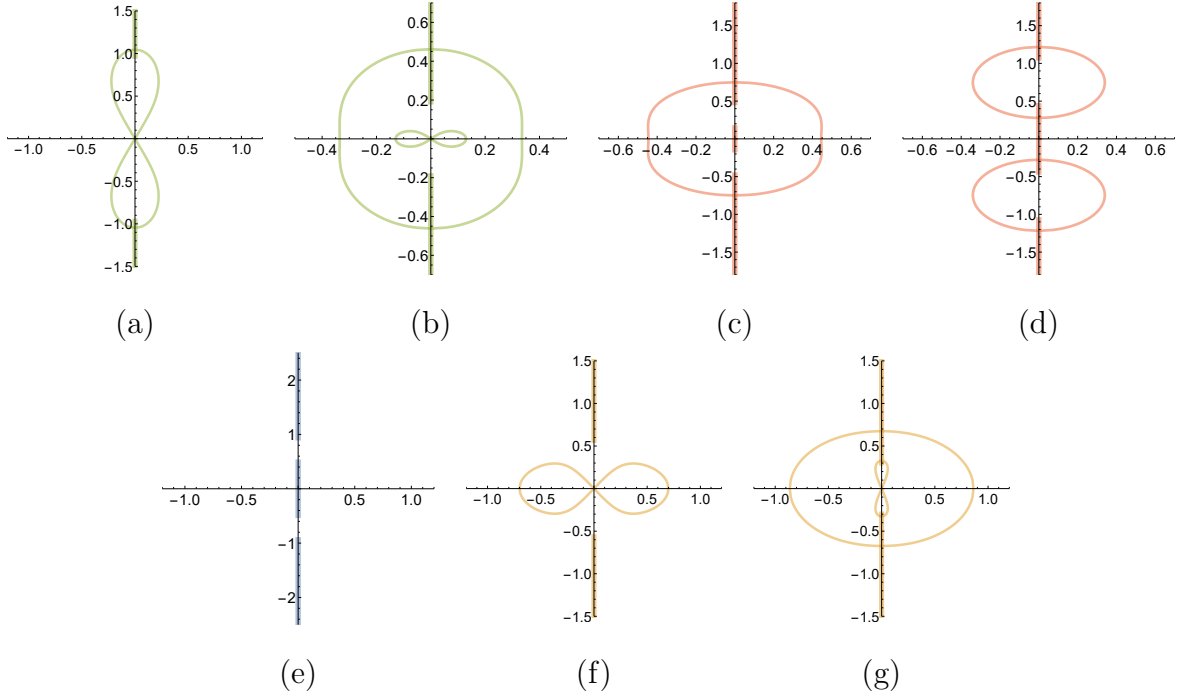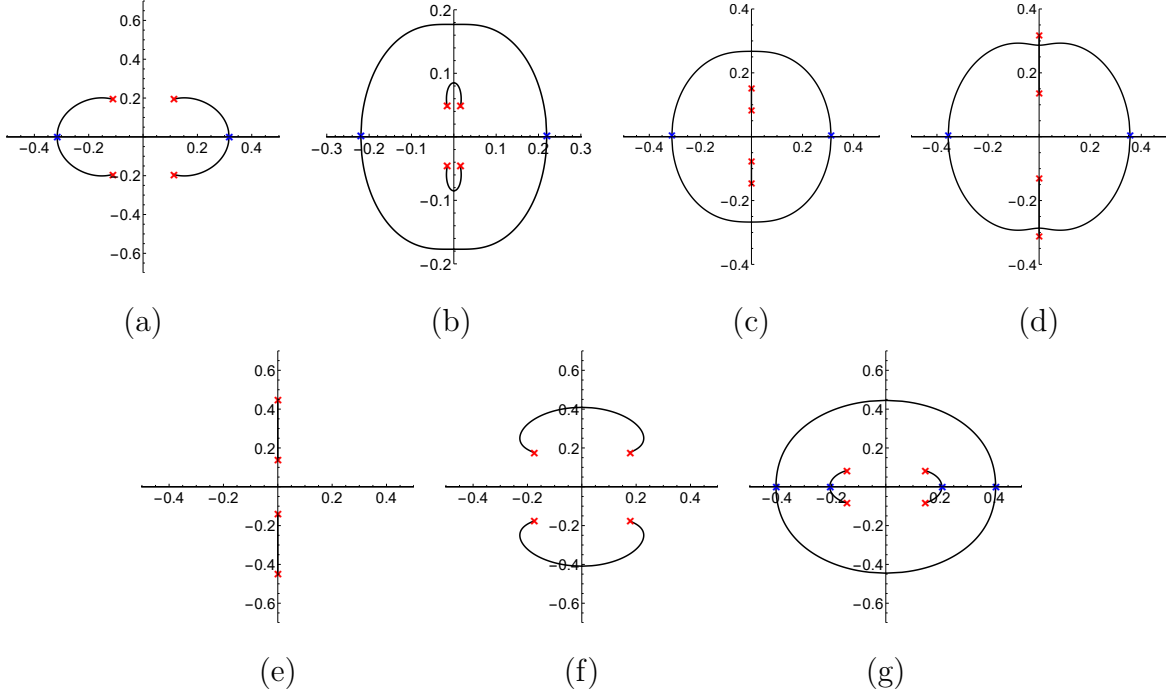
Figure 3.7: The Lax spectrum (black curves) for superluminal (a-d), subluminal (e-g), librational (a,b,f,g) and rotational (c,d,e) waves. (a) $c = 1.5$, $E = 1.5$; (b) $c = 1.02$, $E = 1.8$; (c) $c = 1.1$, $E = 2.2$; (d) $c = 1.4$, $E = 2.4$; (e) $c = 0.6$, $E = -0.75$; (f) $c = 0.6$, $E = 1.0$; (g) $c = 0.8$, $E = 1.5$. Red crosses signify values of ζ for which $\Omega^2(\zeta) = 0$. Blue crosses signify values of $\zeta \in \mathbb{R}$ for which σ_L has a vertical tangent.

as a function of ζ, we find the condition

$$c = \frac{2\sqrt{-\mathcal{E}^2(k) + \mathcal{E}(k)\mathcal{K}(k)}}{\mathcal{K}(k)}, \tag{3.103}$$

for a vertical tangent to occur on the real axis. This condition is plotted as the black curve in the subluminal rotational region of Figure 3.5, and defines the split between qualitatively different spectra. Representative spectral plots for E and c on this boundary are seen in Figure 3.8(3). For solutions satisfying (3.103) we have the following

$$\zeta_{t1} = \pm\frac{1}{2}\sqrt{\frac{1}{(1+c)\mathcal{K}(k)}\left(2\mathcal{E}(k) - \mathcal{K}(k) + \sqrt{4\mathcal{E}^2(k) - 4\mathcal{E}(k)\mathcal{K}(k) + c^2\mathcal{K}^2(k)}\right)}, \tag{3.104}$$

and

$$\zeta_{t2} = \pm\frac{1}{2}\sqrt{\frac{1}{(1+c)\mathcal{K}(k)}\left(2\mathcal{E}(k) - \mathcal{K}(k) - \sqrt{4\mathcal{E}^2(k) - 4\mathcal{E}(k)\mathcal{K}(k) + c^2\mathcal{K}^2(k)}\right)}, \qquad (3.105)$$

shown as blue crosses in Figure 3.7(g). Mapping these points back to $\sigma_\mathcal{L}$ these points correspond to the top (or bottom) of the inset figure 8 in Figure 3.6(g):

$$\lambda_{t1} = \pm\sqrt{\frac{E - c^2(E-1)}{2} + \frac{-2\mathcal{E}(k) + c\sqrt{4\mathcal{E}^2(k) - 4\mathcal{E}(k)\mathcal{K}(k) + c^2\mathcal{K}^2(k)}}{2\mathcal{K}(k)}}, \qquad (3.106)$$

and the ellipse-like curve in Figure 3.6(g):

$$\lambda_{t2} = \pm\sqrt{\frac{E - c^2(E-1)}{2} + \frac{-2\mathcal{E}(k) - c\sqrt{4\mathcal{E}^2(k) - 4\mathcal{E}(k)\mathcal{K}(k) + c^2\mathcal{K}^2(k)}}{2\mathcal{K}(k)}}. \qquad (3.107)$$

Next we examine the slopes of $\sigma_\mathcal{L}$ at the origin. Because $\sigma_\mathcal{L} = 2S_\Omega$ it suffices to examine the slopes for the set S_Ω. We let $\Omega = \Omega_r + i\Omega_i$, and we consider ζ_i as a function of ζ_r so that $\Omega\left(\zeta_r, \zeta_i(\zeta_r)\right)$. Applying the chain rule we have that the slope at any point in the set S_Ω is

$$\frac{d\Omega_i}{d\Omega_r} = \frac{d\Omega_i/d\zeta_r}{d\Omega_r/d\zeta_r} = \frac{\dfrac{d\Omega_i}{d\zeta_r} + \dfrac{d\Omega_i}{d\zeta_i}\dfrac{d\zeta_i}{d\zeta_r}}{\dfrac{d\Omega_r}{d\zeta_r} + \dfrac{d\Omega_r}{d\zeta_i}\dfrac{d\zeta_i}{d\zeta_r}}, \qquad (3.108)$$

where

$$\frac{d\zeta_i}{d\zeta_r} = -\frac{d\mathrm{Re}(I)/d\zeta_r}{d\mathrm{Re}(I)/d\zeta_i}. \qquad (3.109)$$

We examine (3.108) near where $\Omega = 0$ and $\zeta = \zeta_c$. The slopes at the origin are

$$\frac{d\Omega_i}{d\Omega_r} = \pm\frac{c\sqrt{E(2-E)}\mathcal{K}(k)}{-2\mathcal{E}(k) + E\mathcal{K}(k)}. \qquad (3.110)$$

Further application of the chain rule can yield expressions for derivatives around the origin of any order, and the same technique can be applied around (3.106) and (3.107). In doing this we can obtain Taylor series approximations of $\sigma_\mathcal{L}$ to any order.

3.8.2 Superluminal librational solutions

The roots of $\Omega^2(\zeta) = 0$ are given by

$$\zeta_c = \left\{\frac{\sqrt{c^2-1}\sqrt{2-E}}{2\sqrt{2}(c+1)} \pm \frac{\sqrt{c^2-1}\sqrt{E}}{2\sqrt{2}(c+1)}i, -\frac{\sqrt{c^2-1}\sqrt{2-E}}{2\sqrt{2}(c+1)} \pm \frac{\sqrt{c^2-1}\sqrt{E}}{2\sqrt{2}(c+1)}i\right\}, \qquad (3.111)$$
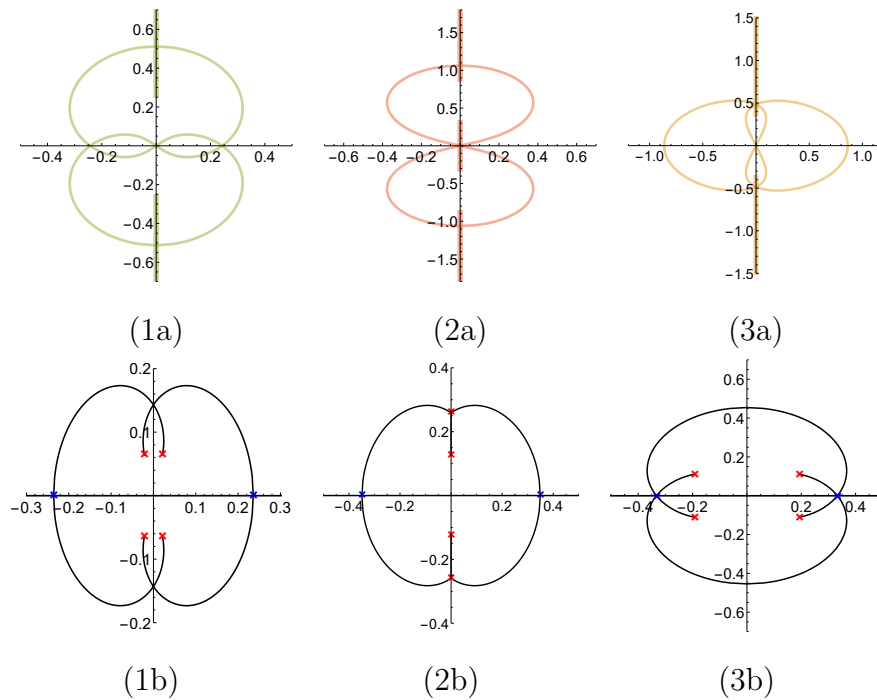
Figure 3.8: (1) The stability spectrum for the cases separating subregions and (2) the corresponding Lax spectrum (black curves). Red crosses signify values of ζ for which $\Omega^2(\zeta) = 0$. Blue crosses signify values of $\zeta \in \mathbb{R}$ for which σ_L has a vertical tangent. (a) Superluminal librational: $c = 1.03702$, $E = 1.8$, (b) superluminal rotational: $c = 1.3$, $E = 2.27060$ (c) subluminal librational: $c = 0.67148$, $E = 1.5$.

seen as red crosses in Figure 3.7(f,g). As in Section 3.8.1, we label these four roots ζ_1, ζ_2, ζ_3, ζ_4, where the subscript corresponds to the quadrant on the real and imaginary plane the root is in. In this case, (3.79) is

$$\frac{\mathrm{d}I(\zeta)}{\mathrm{d}\zeta} = \sqrt{c^2 - 1} \frac{-16\zeta^2 \mathcal{E}(k) + (c - 1 + 8\zeta^2 - 16(c + 1)\zeta^4)\mathcal{K}(k)}{32\zeta^3 \Omega(z)}. \tag{3.112}$$

Examining (3.94) for $\zeta \in \mathbb{R}$, for a vertical tangent in σ_L to occur, we need the numerator of (3.112) to be zero. In this case, there are always two real values of ζ for which vertical tangents in σ_L occur:

$$\zeta_t = \pm \frac{1}{2} \sqrt{\frac{1}{(1 + c)\mathcal{K}(k)} \left(-2\mathcal{E}(k) - \mathcal{K}(k) + \sqrt{4\mathcal{E}^2(k) - 4\mathcal{E}(k)\mathcal{K}(k) + c^2 \mathcal{K}^2(k)} \right)}, \tag{3.113}$$

shown as blue crosses in Figure 3.7(a,b). Mapping these points back to $\sigma_{\mathcal{L}}$ these points correspond to the top (or bottom) of the figure 8 in Figure 3.6(a) or the top (or bottom) of the ellipse-like curve in Figure 3.6(b):

$$\lambda_t = \pm \sqrt{\frac{E - 2 - c^2(e - 1)}{2} + \frac{2\mathcal{E}(k) - c\sqrt{4\mathcal{E}^2(k) - 4\mathcal{E}(k)\mathcal{K}(k) + c^2 \mathcal{K}^2(k)}}{2\mathcal{K}(k)}}. \tag{3.114}$$

In the subluminal librational case in Section 3.8.1, the qualitative change in the spectrum occurred when there was a bifurcation in the real values of ζ with vertical tangents. In this case, there is no such bifurcation. The qualitative change in the spectrum occurs when there is a bifurcation in imaginary values of ζ. The imaginary roots of the numerator of (3.112) are

$$\zeta_p = \pm \frac{1}{2}i \sqrt{\frac{1}{(1 + c)\mathcal{K}(k)} \left(2\mathcal{E}(k) + \mathcal{K}(k) + \sqrt{4\mathcal{E}^2(k) - 4\mathcal{E}(k)\mathcal{K}(k) + c^2 \mathcal{K}^2(k)} \right)}. \tag{3.115}$$

The qualitative change occurs for E and c such that ζ_p satisfies (3.73). This defines the curve seen in the superluminal librational region of Figure 3.5. Representative spectral plots for E and c on this boundary are seen in Figure 3.8(1). The slopes of $\sigma_{\mathcal{L}}$ at the origin are computed using the method described in Section 3.8.1. They are

$$\frac{\mathrm{d}\Omega_i}{\mathrm{d}\Omega_r} = \pm \frac{c\sqrt{E(2 - E)}\mathcal{K}(k)}{2\mathcal{E}(k) + (E - 2)\mathcal{K}(k)}. \tag{3.116}$$

As with the subluminal librational solutions, expressions for derivatives of any order around the origin and around (3.114) can be computed.

3.8.3 Superluminal rotational solutions

The roots of $\Omega^2(\zeta) = 0$ are given in (3.92), seen as red crosses in Figure 3.7(c,d). In this case, (3.79) is

$$\frac{\mathrm{d}I(\zeta)}{\mathrm{d}\zeta} = \sqrt{c^2 - 1} \frac{-8E\zeta^2\mathcal{E}(k) + (c - 1 + 8(E - 1)\zeta^2 - 16(c + 1)\zeta^4)\,\mathcal{K}(k)}{16\sqrt{2}\zeta^3\Omega(z)}. \tag{3.117}$$

Examining (3.94) for $\zeta \in \mathbb{R}$, for a vertical tangent in σ_L to occur, we need the numerator of (3.117) to be zero. In this case, again, there are always two real values of ζ for which vertical tangents in σ_L occur:

$$\zeta_t = \pm\frac{1}{2}\sqrt{\frac{1}{(1 + c)\mathcal{K}(k)}\left(-E\mathcal{E}(k) + (E - 1)\mathcal{K}(k) + \sqrt{E^2\mathcal{E}^2(k) - 2(E - 1)E\mathcal{E}(k)\mathcal{K}(k) + (c^2 + (E - 2)E)\mathcal{K}^2(k)}\right)}, \tag{3.118}$$

shown as blue crosses in Figure 3.7(a,b). Mapping these points back to $\sigma_{\mathcal{L}}$ these points correspond to the top (or bottom) of the ellipse-like curve in Figure 3.6(c) and the top of the ellipse-like curve in the upper-half plane and the bottom of the ellipse-like curve in the lower-half plane in Figure 3.6(d):

$$\lambda_t = \pm\sqrt{\frac{E\mathcal{E}(k) - c^2(E - 1)\mathcal{K}(k) - c\sqrt{E^2\mathcal{E}^2(k) - 2(E - 1)E\mathcal{E}(k)\mathcal{K}(k) + (c^2 + (E - 2)E)\mathcal{K}^2(k)}}{2\mathcal{K}(k)}}. \tag{3.119}$$

As in the superluminal librational case above, we do not have a bifurcation in the real values of ζ with vertical tangents. The qualitative change in the spectrum occurs when there is a bifurcation in imaginary values of ζ. The imaginary roots of the numerator of (3.117) are

$$\zeta_p = \pm\frac{1}{2}i\sqrt{\frac{1}{(1 + c)\mathcal{K}(k)}\left(E\mathcal{E}(k) + (1 - E)\mathcal{K}(k) + \sqrt{E^2\mathcal{E}^2(k) - 2(E - 1)E\mathcal{E}(k)\mathcal{K}(k) + (c^2 + (E - 2)E)\mathcal{K}^2(k)}\right)}. \tag{3.120}$$

The qualitative change occurs for E and c such that $|\zeta_p| = \zeta_4$ and $-|\zeta_p| = \zeta_1$ where ζ_1 and ζ_4 are the smallest and largest roots of $\Omega^2(\zeta) = 0$ respectively. This condition is seen in Figure 3.8(2b) and is

$$c = \frac{\mathcal{E}(k)}{\mathcal{K}(k)}\sqrt{\frac{E}{E - 2}}. \tag{3.121}$$

For $c > \sqrt{\frac{E}{E-2}}\frac{\mathcal{E}(k)}{\mathcal{K}(k)}$, we map ζ_p to $\sigma_{\mathcal{L}}$ and find these points corresponding to the bottom of the ellipse-like curve in the upper-half plane and the top of the ellipse-like curve in the lower-half plane in Figure 3.6(d):

$$\lambda = \pm\sqrt{\frac{E\mathcal{E}(k) - c^2(E-1)\mathcal{K}(k) + c\sqrt{E^2\mathcal{E}^2(k) - 2(E-1)E\mathcal{E}(k)\mathcal{K}(k) + (c^2 + (E-2)E)\mathcal{K}^2(k)}}{2\mathcal{K}(k)}}.$$

(3.122)

3.9 Floquet theory and subharmonic perturbations

We examine $\sigma_{\mathcal{L}}$ using a Floquet parameter description. We use this to prove spectral *stability* results with respect to perturbations of an integer multiple of the fundamental period of the solution, *i.e.*, subharmonic perturbations.

We write the eigenfunctions from (3.37) using a Floquet-Bloch decomposition

$$\begin{pmatrix} W_1(z) \\ W_2(z) \end{pmatrix} = e^{i\mu z}\begin{pmatrix} \hat{W}_1(z) \\ \hat{W}_2(z) \end{pmatrix}, \quad \hat{W}_1(z + T(k)) = \hat{W}_1(z), \quad \hat{W}_2(z + T(k)) = \hat{W}_2(z), \quad (3.123)$$

with $\mu \in [-\pi/T(k), \pi/T(k))$ [23, 27]. Here $T(k) = 2\mathcal{K}(k)$ for all solutions. From Floquet's Theorem [23], all bounded solutions of (3.37) are of this form, and our analysis includes perturbations of an arbitrary period. Specifically, $\mu = 2m\pi/T(k)$ for $m \in \mathbb{Z}$ corresponds to perturbations of the same period $T(k)$ of the solutions, and in general

$$\mu = \frac{2m\pi}{PT(k)}, \quad m, P \in \mathbb{Z}, \tag{3.124}$$

corresponds to perturbations of period $PT(K)$. The choice of the specific range of μ is arbitrary as long as it is of length $2\pi/T(k)$. For added clarity in this section, we plot figures using the larger ranges $[-2\pi/T(k), 2\pi/T(k))$, periodically extending μ beyond the basic region.

In the previous sections $\sigma_{\mathcal{L}}$ is parameterized in terms of ζ. We wish to re-parameterize $\sigma_{\mathcal{L}}$ in terms of μ. We examine the eigenfunction W_1 from (3.123). From the periodicity of $\hat{W}_1$ we have

$$e^{i\mu T(k)} = \frac{W_1(z + T(k))}{W_1(z)}. \tag{3.125}$$

Using (3.57), (3.51), and (3.52), we find

$$e^{i\mu T(k)} = \exp\left(-2\int_0^{T(k)} \frac{-BC + D(A-\Omega) + B_z}{B}\,dz\right),\tag{3.126}$$

where we have used the periodicity properties

$$A\left(z + T(k)\right) = A(z),\ \ B\left(z + T(k)\right) = B(z).\tag{3.127}$$

Using (3.73),

$$\mu(\zeta) = -\frac{2iI(\zeta)}{T(k)} + \frac{2\pi n}{T(k)},\tag{3.128}$$

where $I(\zeta)$ is given in (3.75) and $n \in \mathbb{Z}$.

In what follows we discuss the stability of solutions with respect to perturbations of integer multiples of their fundamental periods, so-called subharmonic perturbations [39]. The expression (3.128) gives an easy way to do this. Specifically, from (3.124) we know which values of μ correspond to perturbations of what type. For stability with respect to perturbations of period $2\pi m/\mu = PT(k)$, we need all spectral elements associated with a given μ value to have zero real part. In Figure 3.9 we plot the real part of $\sigma_{\mathcal{L}}$ as a function of $\mu T(k)$ using (3.50), (3.56), and (3.128). We rescale μ by $T(k)$ for consistency in our figures. Here

$$\mu T(k) = \frac{2\pi m}{P},\tag{3.129}$$

corresponds to perturbations of $PT(k)$ for any integer m.

The following results are obtained in each region of parameter space:

- For the subluminal rotational case, all solutions are spectrally stable [45, 46].

- For the subluminal librational case, all solutions are spectrally unstable with respect to all subharmonic perturbations. This is shown in Section 3.9.1.

- For the superluminal librational case, all solutions are spectrally unstable, but all solutions left of curve 2 in Figure 3.10 are stable with respect to perturbations of twice
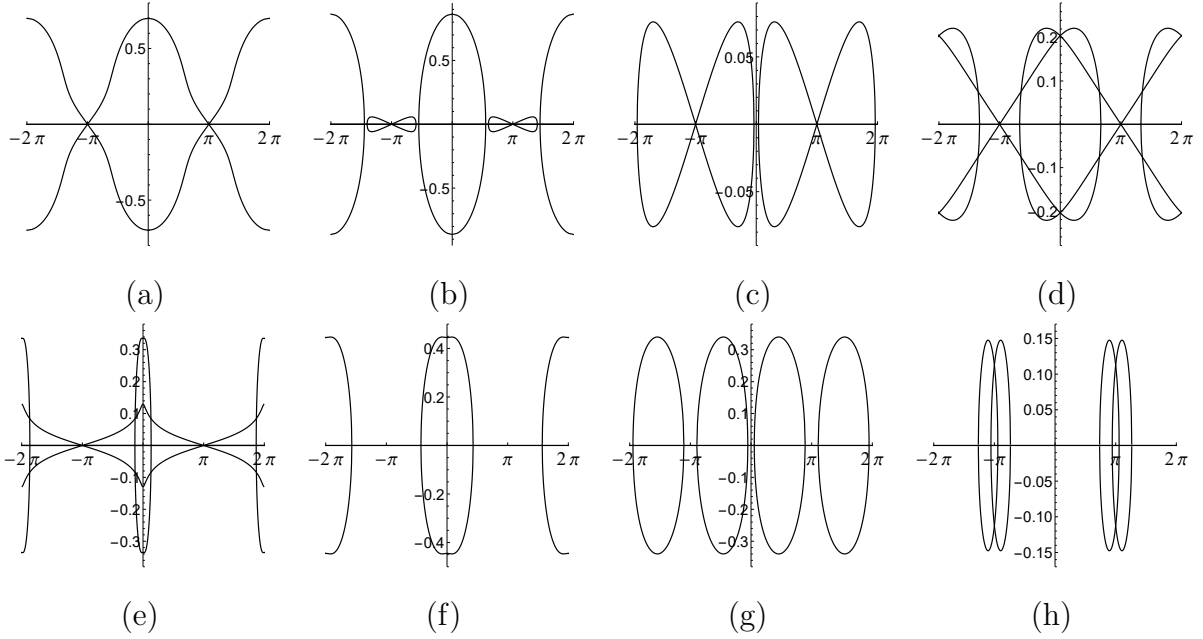
Figure 3.9: The real part of the spectrum $\mathrm{Re}(\lambda)$ (vertical axis) as a function of $\mu T(k)$ (horizontal axis): for subluminal librational (a-b), superluminal librational (c-e), and superluminal rotational (f-h) solutions. (a) $c = 0.6$, $E = 1.0$; (b) $c = 0.8$, $E = 1.5$; (c) $c = 1.5$, $E = 0.7$; (d) $c = 1.5$, $E = 1.5$; (e) $c = 1.02$, $E = 1.8$; (f) $c = 1.3$, $E = 2.9$; (g) $c = 1.4$, $E = 2.4$; (h) $c = 2.1$, $E = 6.8$.

the period and the same period, all solutions left of curve 4 are stable with respect to perturbations of four times the period, all solutions left of curve 6 are stable with respect to perturbations of six times the period, as well as three times the period, etc. This is shown in Section 3.9.2.

- For the superluminal rotational case, all solutions are spectrally unstable, but there are regions of stability with respect to subharmonic perturbations, see Figure 3.12 and Section 3.9.3 for details.

We provide the following useful lemma:

Lemma 3.9.1. *For any analytic function $f(z) = u(x,y) + iv(x,y)$, on a contour where $u(x,y) = constant$, $v(x,y)$ is strictly monotone, provided the contour does not traverse a*

saddle point. Similarly, on a contour where $v(x, y) = constant$, $u(x, y)$ is strictly monotone, provided the contour does not traverse a saddle point.

Proof. This is an immediate consequence of the Cauchy-Riemann relations [10]. $\square$

Thus along contours where $\text{Re}(I(\zeta)) = 0$, if there are no saddle points, then $\text{Im}(I(\zeta))$ is monotone. If we fix c and E, using (3.128) we see that $\mu(\zeta)T(k) = 2\pi n + 2\text{Im}(I(\zeta)) - 2i\text{Re}(I(\zeta))$ is also monotone along curves with $\text{Re}(I(\zeta)) = 0$. In what follows, we omit $\sigma_{\mathcal{L}} \cap i\mathbb{R}$.

3.9.1 Subluminal librational solutions

There are two cases to consider for subluminal librational solutions, corresponding to the two qualitatively different stability spectra seen in Figure 3.6(f,g), and their corresponding Lax spectra in Figure 3.7(f,g). Representative plots of $\mu T(k)$ *vs.* $\text{Re}(\lambda)$ for these cases are shown in Figure 3.9(a,b). We prove the following theorem:

Theorem 3.9.2. *The subluminal librational solutions to (3.1) are unstable with respect to all subharmonic perturbations.*

Proof. It suffices to show that for some $\zeta \in \sigma_L$, $\mu = 0$ and $\text{Re}(\lambda) > 0$. We split into cases with qualitatively different spectra:

1. In the case where the stability spectrum looks qualitatively like an infinity symbol, we examine $\zeta \in \sigma_L$, see Figure 3.7(f). The infinity symbol spectrum is double covered, so without loss of generality, we consider only values of ζ in the upper-half plane. Specifically, we consider values of ζ ranging from ζ_2 to ζ_1, moving from the red cross in the second quadrant to the red cross in the first quadrant of Figure 3.7(f). At ζ_2, $\mu T(k) = -\pi$ and $\text{Re}(\lambda) = 0$. As ζ moves from ζ_2 to ζ_1, $\mu T(k)$ monotonically increases (Lemma 3.9.1) until it reaches $\mu T(k) = \pi$ at $\zeta = \zeta_1$, where $\text{Re}(\lambda) = 0$, see Figure 3.9(a). Along this curve $\text{Re}(\lambda) \neq 0$ so by the intermediate value theorem at some point between ζ_2 and ζ_2, $\mu T(k) = 0$ with $\text{Re}(\lambda) > 0$.

2. In the case where the stability spectrum looks qualitatively like a figure 8 inset in an ellipse-like curve, examine $\zeta \in \sigma_L$, see Figure 3.7(g). The ζ spectrum has two components, ζ corresponding to the figure 8, and ζ corresponding to the ellipse-like curve. For instability, we only need to examine ζ corresponding to the ellipse-like curve. Again, we consider only values of ζ in the upper-half plane. Specifically, we consider values of ζ ranging from $-|\zeta_{t2}|$ to $|\zeta_{t2}|$, moving from the blue cross in the second quadrant to the blue cross in the first quadrant of Figure 3.7(g). At $-|\zeta_{t2}|$, $\mu T(k) = -2iI(-|\zeta_{t2}|)$, and $\text{Re}(\lambda) = 0$. As ζ moves from $-|\zeta_{t2}|$ to $|\zeta_{t2}|$, $\mu T(k)$ monotonically increases (Lemma 3.9.1) until it reaches $\mu T(k) = -2iI(|\zeta_{t2}|)$ at $\zeta = |\zeta_{t2}|$, with $\text{Re}(\lambda) = 0$, see the ellipse-like curve in Figure 3.9(b). Because of the symmetries of $I(\zeta)$ for $\zeta \in \mathbb{R}$ we have that $\mu T(k) = -2iI(|\zeta_{t2}|) = 2iI(-|\zeta_{t2}|)$. Along this curve $\text{Re}(\lambda) \neq 0$ so again by the intermediate value theorem at some point between $-|\zeta_{t2}|$ and $|\zeta_{t2}|$, $\mu T(k) = 0$ with $\text{Re}(\lambda) > 0$.

$\square$

3.9.2 Superluminal librational solutions

Theorem 3.9.3. *The superluminal librational solutions to (3.1) are stable with respect to subharmonic perturbations of period $PT(k)$ if they satisfy the condition*

$$-2iI(-|\zeta_t|) \geq \frac{(P-1)\pi}{P}, \tag{3.130}$$

for P odd, and

$$-2iI(-|\zeta_t|) \geq \frac{(P-2)\pi}{P}, \tag{3.131}$$

for P even.

Proof. For stability with respect to perturbations of period $PT(k)$ we need that for $\mu T(k) = 2\pi m/P$, the spectral elements $\lambda \in \sigma_{\mathcal{L}}$ have zero real part, *i.e.*, for $\mu T(k) = 0, \frac{2\pi}{P}, \ldots, \frac{2\pi(P-1)}{P}$, $\text{Re}(\lambda) = 0$.
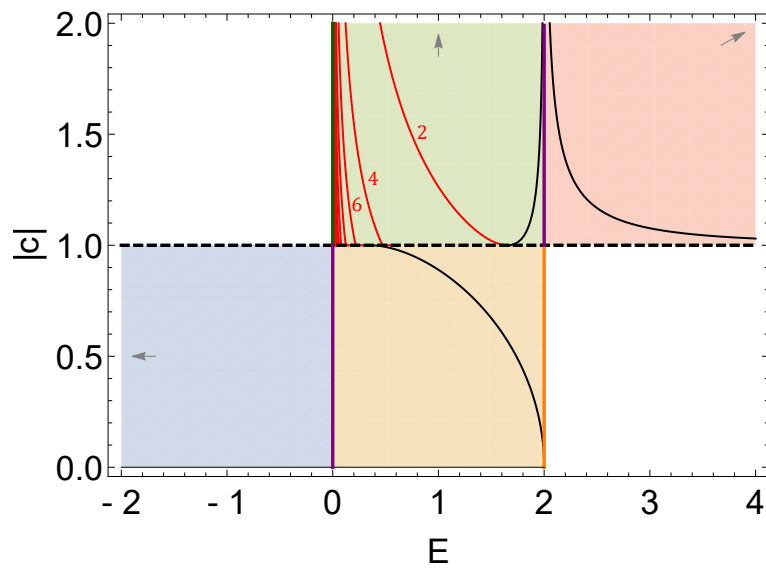
Figure 3.10: A plot of parameter space showing the spectral stability of superluminal libra-tional solutions with respect to various subharmonic perturbations. Within the superluminal librational region, all solutions left of curve 2 are stable with respect to perturbations of twice the period as well as perturbations of the same period, all solutions left of curve 4 are stable with respect to perturbations of four times the period, all solutions left of curve 6 are stable with respect to perturbations of six times the period as well as perturbations of three times the period, etc.

We examine $\zeta \in \sigma_L$, in the figure 8 case, see Figure 3.7(a). The figure 8 spectrum is double covered, so, without loss of generality, we consider only values of ζ in the left-half plane. Specifically we consider values of ζ ranging from ζ_3 to ζ_2 passing along the level curve through $\zeta = -|\zeta_t|$. At ζ_3, $\mu T(k) = \pi$ and $\mathrm{Re}(\lambda) = 0$. As ζ moves from ζ_3 to $-|\zeta_t|$, $\mu T(k)$ monotonically decreases (Lemma 3.9.1) until it reaches $\mu_t T(k) = -2iI(-|\zeta_t|)$ at $\zeta = -|\zeta_t|$. At $-|\zeta_t|$, $\mathrm{Re}(\lambda) = 0$. Note that we are only considering the lower-left quarter plane. The analysis for ζ ranging from ζ_1 to $|\zeta_t|$ is symmetric in $\mu T(k)$.

Qualitatively, we have figure 8s centered at $\mu T(k) = \pi + 2\pi n$ and extending over $[\mu_t T(k) + 2\pi n, \pi + (\pi - \mu_t T(k)) + 2\pi n]$, see Figure 3.9(c,d). Since we are considering $\mu \in [0, 2\pi)$ it suffices to examine the figure 8 centered at π with $n = 0$.. For stability, we need the left-most edge of the figure 8 to be to the right of $\frac{(P-1)\pi}{P}$ for P odd and to the right of $\frac{(P-2)\pi}{P}$ for P even. Similarly, we need the right-most edge of the figure 8 to be to the left of $\frac{(P+1)\pi}{P}$ for P odd and to the left of $\frac{(P+2)\pi}{P}$ for P even. These conditions are for P odd:

$$\mu_t T(k) \geq \frac{(P-1)\pi}{P} \text{ and } \pi + (\pi - \mu_t T(k)) \leq \frac{(P+1)\pi}{P}, \tag{3.132}$$

and for P even:

$$\mu_t T(k) \geq \frac{(P-2)\pi}{P} \text{ and } \pi + (\pi - \mu_t T(k)) \leq \frac{(P+2)\pi}{P}. \tag{3.133}$$

These conditions simplify to give (3.130) and (3.131) respectively. $\qquad \square$

We remark that for a given odd P the condition (3.130) is the same as the condition (3.131) for $2P$. Thus, for superluminal librational waves if we have stability with respect to perturbations of some odd multiple P of the period $T(k)$ we also have stability with respect to perturbations of $2PT(k)$. This is shown in the case when $P = 3$ in Figure 3.11(a). These results are summarized in Figure 3.10 where we plot only the condition (3.131). We remark that it is possible for solutions to be stable with respect to perturbations of four times the period but not with respect to three times the period. Solutions of this type would lie to the left of curve 4 but to the right of curve 6 in Figure 3.10. More generally it is possible to

(a) Superluminal librational

(b) Superluminal rotational
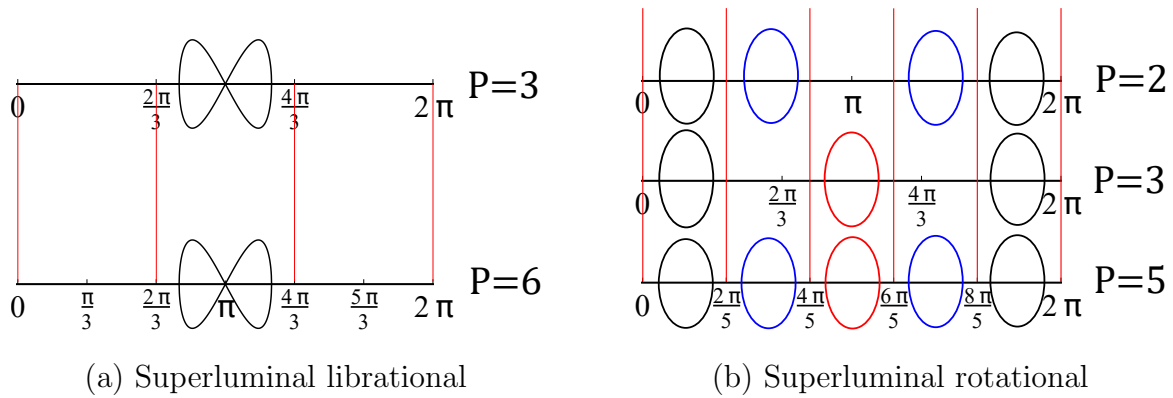
Figure 3.11: The real part of the spectrum $\text{Re}(\lambda)$ (vertical axes) as a function of $\mu T(k)$ (horizontal axes): $\mu T(k) = 2m\pi/P$ for integers m and P corresponds to perturbations of period P times the period of the underlying solution. (a) The superluminal solution is stable with respect to perturbations of three times its period is necessarily stable with respect to perturbations of six times its period. (b) If a superluminal rotational solution is stable with respect to perturbations of five times its period, it is stable with respect to perturbations of three times its period or perturbations of two times its period. (i) If the ellipse-like curves are in $(4\pi/5, 6\pi/5)$ they are necessarily in $(2\pi/3, 4\pi/3)$ (red), (ii) if the ellipse-like curves are in $(2\pi/5, 4\pi/5)$ and $(6\pi/5, 8\pi/5)$ they are necessarily in $(0, \pi)$ and $(\pi, 2\pi)$ respectively (blue), (iii) if the ellipse-like curves are in $(0, 2\pi/5)$ and $(8\pi/5, 2\pi)$ they are necessarily in both $(0, \pi)$ and $(\pi, 2\pi)$ respectively as well as $(0, 2\pi/3)$ and $(2\pi/3, 4\pi/3)$ respectively (black).

have solutions which are stable with respect to p times the period but not with respect to q times the period where p is even and less than $q < p < 2q$.

3.9.3 Superluminal rotational solutions

Theorem 3.9.4. *The superluminal rotational solutions to (3.1) are stable with respect to subharmonic perturbations of period $PT(k)$ if they simultaneously satisfy the conditions*

$$2\pi n - 2iI(-|\zeta_t|) \leq \frac{2\pi(m+1)}{P}, \tag{3.134}$$

$$2\pi n - 2iI(|\zeta_p|i) \geq \frac{2\pi m}{P}, \tag{3.135}$$

for some $n \in \mathbb{Z}$ and some $m \in \{0, 1, \ldots, P-1\}$. Note that $Re\left(I(-|\zeta_t|)\right) = 0$ and $Re\left(I(|\zeta_p|i)\right) = 0$.

Proof. For stability with respect to perturbations of period $PT(k)$ we need that for $\mu T(k) = 2\pi m/P$, the spectral elements $\lambda \in \sigma_{\mathcal{L}}$ have zero real part for all $m \in \{0, 1, \ldots, P-1\}$.

We examine $\zeta \in \sigma_L$, in the case where we have ellipse-like curves in the upper- and lower-half planes, see Figure 3.7(d). As in Theorem 3.9.3, using symmetries we restrict ourselves to ζ in the upper-left quarter plane. Specifically we consider values of ζ ranging from $-|\zeta_t|$ to $|\zeta_p|i$. At $-|\zeta_t|$, $\mu T(k) = -2iI(-|\zeta_t|)$ and $\mathrm{Re}(\lambda) = 0$. As ζ moves from $-|\zeta_t|$ to $|\zeta_p|i$, $\mu T(k)$ monotonically decreases (Lemma 3.9.1) until it reaches $\mu_t T(k) = -2iI(|\zeta_p|i)$ at $\zeta = |\zeta_p|i$. At $|\zeta_p|i$, $\mathrm{Re}(\lambda) = 0$.

Qualitatively, we have an ellipse-like curve beginning at $-2iI(-|\zeta_t|)+2\pi n$ and extending to $-2iI(|\zeta_p|i)+2\pi n$, see Figure 3.9(g,h). The only values of $\mu T(k)$ with $\mathrm{Re}(\lambda) > 0$ lie within the range $(2iI(|\zeta_p|i) + 2\pi n, 2iI(-|\zeta_t|) + 2\pi n)$. So if $(2iI(|\zeta_p|i) + 2\pi n, 2iI(-|\zeta_t|) + 2\pi n) \subset (\frac{2\pi m}{P}, \frac{2\pi(m+1)}{P})$, for some $m \in \{0, 1, \ldots, P-1\}$, then $\mathrm{Re}(\lambda) = 0$ for $\mu T(k) = 2\pi m/P$ for all $m \in \{0, 1, \ldots, P-1\}$.

Thus for stability we need the right-most edge of each of these ellipse-like curves to be to the left of $2\pi(m+1)/P$, and the left-most edge of each of these ellipse-like curves to be
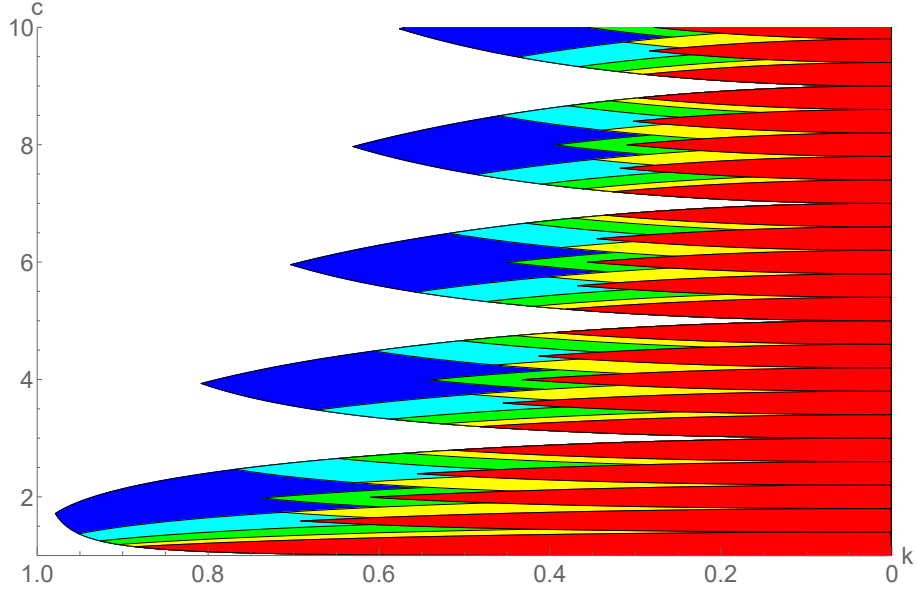
Figure 3.12: A plot of the superluminal rotational region of parameter space showing the spectral stability with respect to various subharmonic perturbations. Parameter space is rescaled using the elliptic modulus $k = \sqrt{2/E}$, to show the extent of the curves as $E \to \infty$. Solutions within the blue (light blue, green, yellow, red) region are stable with respect to perturbations of one (two, three, four, five) times the period respectively.

to the right of $2\pi m/P$ for some $m \in \{0, 1, \ldots, P-1\}$. This gives us conditions (3.134) and (3.135). $\qquad\qquad\qquad\qquad\qquad\qquad\qquad\qquad\qquad\qquad\qquad\qquad\qquad\qquad\quad\square$

These results are summarized in Figure 3.12. We choose to rescale parameter space using the elliptic modulus $k = \sqrt{2/E}$, to show the extent of the subharmonic stability regions as $E \to \infty$. We only show regions for $P = 1, 2, 3, 4, 5$ for the sake of clarity.

We see that there are many disjoint regions of subharmonic stability for each value of P corresponding to the various choices for m. Within each disjoint region of stability for same period perturbations (blue) there are P disjoint regions of stability with respect to perturbations of P times the period. This follows directly from the conditions (3.134) and (3.135). We note the possibility of solutions which are stable with respect to three times the period of the solution but not with respect to two times the period of the solution. An

example of what $\mu T(k)$ looks like in this case is shown in Figure 3.9(h) with $c = 2.1$, $E = 6.8$, $k = 0.542326$. Indeed it is possible to have solutions which are stable with respect to p times the period of the solution but not with respect to q times the period of the solution for any $p > q$ where $q \nmid p$. From Figure 3.12 we notice that if a solution is stable with respect to perturbations of five times the period (red) it is stable with respect to either perturbations of two times the period (light blue) or three times the period (green). This is proved by a simple topological argument shown in Figure 3.11(b) and explained in the caption.

3.10   Conclusion

In this chapter, the methods of [27] are used to examine and explicitly determine the stability spectrum of the stationary solutions of the sine-Gordon equation. As in [27], we demonstrate that the parameter space for the stationary solution separates in different regions where the topology of the spectrum is different. An additional subdivision of this parameter space is found for superluminal waves when considering the stability of the solutions with respect to subharmonic perturbations of a specific period. We find solutions which are stable with respect to perturbations of p times the period but unstable with respect to q times the period, where $p < q$.

Chapter 4

CONCLUSION AND FUTURE WORK

In this thesis, I have taken the next step in an ongoing research program of analyzing the stability of periodic solutions of integrable equations. Our methods rely on the squared eigenfunction connection [1] and the existence of an infinite sequence of conserved quantities, as described below. Thus far, the following results have been obtained:

- **The KdV equation.** In [11], the squared eigenfunction connection was used to establish the spectral stability of the periodic traveling waves of the KdV equation with respect to perturbations that are bounded on the whole line (periodic, quasi-periodic, or linear superpositions of such). This result was built on in [23] to establish the orbital stability of these solutions with respect to subharmonic perturbations of any period, using an extra conserved quantity as an appropriate Lyapunov function. This method, employing all conserved quantities, was extended to establish the orbital stability of the periodic finite-gap solutions of the equation in [26], again with respect to subharmonic perturbations.

- **The defocusing mKdV equation.** In [26], the method of [11] was adapted to the defocusing modified KdV equation to prove the spectral stability of the periodic traveling waves with respect to bounded perturbations.

- **The defocusing NLS equation.** In [12], the squared eigenfunction connection was employed to show the spectral stability of the stationary solutions of the defocusing NLS equation. Orbital stability with respect to subharmonic perturbations is also demonstrated in [12], again requires the use of an additional conserved quantity.

- **The focusing NLS equation.** In Chapter 2 and in [27], the method of [11] and [12] is used to examine the stability spectrum of the stationary solutions of the focusing NLS equation. Because the underlying Lax pair is not self adjoint, the application of the method does not simplify as it does for the above equations. Unbridled use of elliptic function identities allows for the explicit determination of the spectrum, demonstrating spectral instability for all stationary (non-soliton) solutions. We demonstrate that the parameter space for the stationary solution separates in different regions where the topology of the spectrum is different. An additional subdivision of this parameter space is found when considering the stability of the solutions with respect to subharmonic perturbations of a specific period, leading to the conclusion of spectral stability of some solutions with respect to some smaller classes of physically relevant perturbations.

- **The sine-Gordon equation.** In Chapter 3 and in [25], the methods of [27] are used to examine and explicitly determine the stability spectrum of the stationary solutions of the sine-Gordon equation. As in [27], we demonstrate that the parameter space for the stationary solution separates in different regions where the topology of the spectrum is different. An additional subdivision of this parameter space is found for superluminal waves when considering the stability of the solutions with respect to subharmonic perturbations of a specific period. We find solutions which are stable with respect to perturbations of p times the period but unstable with respect to q times the period, where $p < q$.

Many directions for future research remain. Building on the work in Chapters 2 and 3, I hope to extend these results to study the transverse spectral stability of periodic traveling waves in the Kadomtsev-Petviashvili equation [5, 40, 43]. Future work could also consider the modified Korteweg-de Vries equation (mKdV) [69] the Benjamin-Ono equation [31], and the Boussinesq equation [21] as well. Each of these equations come with different challenges, and deriving a condition for the stability spectrum for elliptic solutions may not be as simple as shown here. That said, the mKdV equation has Lax pairs in the AKNS form [1]

similar to NLS and SG and the techniques used in this thesis should extend easily. For the Benjamin-Ono equation, the Lax pair is defined in a piecewise manner, and for the Boussinesq equation, the Lax pair is consists of three by three matrices instead of two by two matrices. Using techniques of [12, 26], another avenue of research is extending the spectral stability results of Sections 2.9 and 3.9 to orbital stability [28].

BIBLIOGRAPHY

[1] M. J. Ablowitz, D. J. Kaup, and A. C. Newell. The inverse scattering transform-Fourier analysis for nonlinear problems. *Studies in Applied Mathematics*, 53:249–315, 1974.

[2] M. J. Ablowitz, D. J. Kaup, A. C. Newell, and H. Segur. Method for solving the sine-Gordon equation. *Phys. Rev. Lett.*, 30:1262–1264, 1973.

[3] M. J. Ablowitz, D. J. Kaup, A. C Newell, and H. Segur. Method for solving the sine-Gordon equation. *Physical Review Letters*, 30, 1973.

[4] M. J. Ablowitz and H. Segur. *Solitons and the inverse scattering transform*, volume 4. Society for Industrial and Applied Mathematics (SIAM), Philadelphia, 1981.

[5] M. J. Ablowitz, D B. Yaacov, and A. S. Fokas. On the inverse scattering transform for the Kadomtsev-Petviashvili equation. *Studies in Applied Mathematics*, 69:135–143, 1983.

[6] J. M. Arnold. Stability theory for periodic pulse train solutions of the nonlinear schrödinger equation. *IMA Journal of Applied Mathematics*, 52:123–140, 1994.

[7] A. Barone, F. Esposito, C. J. Magee, and A. C. Scott. Theory and applications of the sine-Gordon equation. *La Rivista del Nuovo Cimento*, 1(2):227–267, 1971.

[8] E. D. Belokolos, A. I. Bobenko, V. Z. Enol'skii, A. R. Its, and V. B. Matveev. *Algebro-geometric approach to nonlinear integrable problems*. Springer Series in Nonlinear Dynamics. Springer-Verlag, Berlin, 1994.

[9] T. B. Benjamin. The stability of solitary waves. *Proc. Roy. Soc. (London) Ser. A*, 328:153–183, 1972.

[10] M. Born and E. Wolf. *Principles of optics: Electromagnetic theory of propagation, interference and diffraction of light*. Pergamon Press, New York, 1959.

[11] N. Bottman and B. Deconinck. KdV cnoidal waves are spectrally stable. *Discrete and Continuous Dynamical Systems-Series A (DCDS-A)*, 25:11631180, 2009.

[12] N.l Bottman, B. Deconinck, and M. Nivala. Elliptic solutions of the defocusing NLS equation are stable. *Journal of Physics A: Mathematical and Theoretical*, 44:285201, 2011.

[13] E. M. Bour. Théorie de la déformation des surfaces. *Journal de L'école Impériale Polytechnique*, 22:1–148, 1862.

[14] W. E. Boyce and R. C. DiPrima. *Elementary differential equations and boundary value problems.* John Wiley & Sons, Inc., New York, 1965.

[15] R. J. Buckingham and P. D. Miller. Exact solutions of semiclassical non-characteristic Cauchy problems for the sine-Gordon equation. *Phys. D*, 237(18):2296–2341, 2008.

[16] R. J. Buckingham and P. D. Miller. The sine-Gordon equation in the semiclassical limit: dynamics of fluxon condensates. *Mem. Amer. Math. Soc.*, 225(1059):vi+136, 2013.

[17] P. F. Byrd and M. D. Friedman. *Handbook of elliptic integrals for engineers and physicists.* Springer-Verlag, Berlin, 1954.

[18] L. D. Carr, C. W. Clark, and W. P. Reinhardt. Stationary solutions of the one-dimensional nonlinear Schrödinger equation. ii. Case of attractive nonlinearity. *Physical Review A*, 62:063611, 2000.

[19] F. F. Chen. *Introduction to Plasma Physics and Controlled Fusion.* Plenum Press, New York, 1984.

[20] S. Coleman. Quantum sine-gordon equation as the massive Thirring model. *Phys. Rev. D*, 11:2088–2097, 1975.

[21] R. Conte and M. Musette. *The Painlevé handbook.* Springer, Dordrecht, 2008.

[22] T. Dauxois and M. Peyrard. *Physics of solitons.* Cambridge University Press, Cambridge, 2006.

[23] B. Deconinck and T. Kapitula. The orbital stability of the cnoidal waves of the Korteweg–de Vries equation. *Physics Letters A*, 374:4018–4022, 2010.

[24] B. Deconinck and J. N. Kutz. Computing spectra of linear operators using the Floquet–Fourier–Hill method. *Journal of Computational Physics*, 219:296–321, 2006.

[25] B. Deconinck, P. McGill, and B. L. Segal. The stability spectrum for elliptic solutions to the sine-Gordon equation. *Submitted for publication*, 2017.

[26] B. Deconinck and M. Nivala. The stability analysis of the periodic traveling wave solutions of the mKdV equation. *Stud. Appl. Math.*, 126(1):17–48, 2011.

[27] B. Deconinck and B. L. Segal. The stability spectrum for elliptic solutions to the focusing NLS equation. *Physica D: Nonlinear Phenomena*, 346:1–19, 2017.

[28] B. Deconinck, B. L. Segal, and J. Upsal. The stability of stationary solutions of the focusing NLS equation with respect to subharmonic perturbations. *In progress*, 2017.

[29] G. Derks, A. Doelman, S. A. van Gils, and T. Visser. Travelling waves in a singularly perturbed sine-Gordon equation. *Phys. D*, 180(1-2):40–70, 2003.

[30] D. Duval. Rational puiseux expansions. *Compositio mathematica*, 70:119–154, 1989.

[31] A. S. Fokas and M. J. Ablowitz. The inverse scattering transform for the Benjamin-Ono equation – a pivot to multidimensional problems. *Studies in Applied Mathematics*, 68:1–10, 1983.

[32] J. Frenkel and T. Kontorova. On the theory of plastic deformation and twinning. *Acad. Sci. U.S.S.R. J. Phys.*, 1:137–149, 1939.

[33] T. Gallay and M. Hărăguş. Orbital stability of periodic waves for the nonlinear Schrödinger equation. *Journal of Dynamics and Differential Equations*, 19:825–865, 2007.

[34] T. Gallay and M. Hărăguş. Stability of small periodic waves for the nonlinear Schrödinger equation. *Journal of Differential Equations*, 234:544–581, 2007.

[35] I. S. Gradshteyn and I. M. Ryzhik. *Table of integrals, series, and products*. Elsevier/Academic Press, Amsterdam, eighth edition, 2015.

[36] M. Grillakis, J. Shatah, and W. Strauss. Stability theory of solitary waves in the presence of symmetry, i. *Journal of Functional Analysis*, 74:160–197, 1987.

[37] M. Grillakis, J. Shatah, and W. Strauss. Stability theory of solitary waves in the presence of symmetry, ii. *Journal of Functional Analysis*, 94:308–348, 1990.

[38] E. P. Gross. Structure of a quantized vortex in boson systems. *Il Nuovo Cimento (1955-1965)*, 20:454–477, 1961.

[39] S. Gustafson, S. Le Coz, and T.-P. Tsai. Stability of periodic waves of 1D cubic nonlinear Schrödinger equations. *arXiv:1606.04215*.

[40] M. Hărăguş. Transverse spectral stability of small periodic traveling waves for the KP equation. *Stud. Appl. Math.*, 126(2):157–185, 2011.

[41] M. Hărăguş and T. Kapitula. On the spectra of periodic waves for infinite-dimensional Hamiltonian systems. *Physica D: Nonlinear Phenomena*, 237:2649–2671, 2008.

[42] T. Ivey and S. Lafortune. Spectral stability analysis for periodic traveling wave solutions of NLS and CGL perturbations. *Physica D: Nonlinear Phenomena*, 237:1750–1772, 2008.

[43] M. A. Johnson and K. Zumbrun. Transverse instability of periodic traveling waves in the generalized Kadomtsev-Petviashvili equation. *SIAM J. Math. Anal.*, 42(6):2681–2702, 2010.

[44] M. A. Johnson and K. Zumbrun. Convergence of Hill's method for nonselfadjoint operators. *SIAM Journal on Numerical Analysis*, 50:64–78, 2012.

[45] C. K. R. T. Jones, R. Marangell, P. D. Miller, and R. G. Plaza. On the stability analysis of periodic sine–Gordon traveling waves. *Physica D: Nonlinear Phenomena*, 251:63–74, 2013.

[46] C. K. R. T. Jones, R. Marangell, P. D. Miller, and R. G. Plaza. Spectral and modulational stability of periodic wavetrains for the nonlinear Klein-Gordon equation. *J. Differential Equations*, 257(12):4632–4703, 2014.

[47] T. Kapitula and K. Promislow. *Spectral and dynamical stability of nonlinear waves*, volume 185. Springer, New York, 2013.

[48] Y. V. Kartashov, V. A. Aleshkevich, V. A. Vysloukh, A. A. Egorov, and A. S. Zelenina. Stability analysis of (1+1)-dimensional cnoidal waves in media with cubic nonlinearity. *Physical Review E*, 67:036613.

[49] T. Kato. *Perturbation theory for linear operators*. Springer-Verlag, Berlin, 1995.

[50] D. J. Kaup. Method for solving the sine-Gordon equation in laboratory coordinates. *Studies in Appl. Math.*, 54(2):165–179, 1975.

[51] Y. S. Kivshar and G. Agrawal. *Optical solitons: from fibers to photonic crystals*. Academic press, San Diego, 2003.

[52] D. F. Lawden. *Elliptic functions and applications*, volume 80. Springer-Verlag, New York, 1989.

[53] E. P. T. Liang. Nonlinear periodic waves in a self-gravitating fluid and galaxy formation. *The Astrophysical Journal*, 230:325–329, 1979.

[54] A. C. Newell. *Solitons in mathematics and physics*, volume 48 of *CBMS-NSF Regional Conference Series in Applied Mathematics*. Society for Industrial and Applied Mathematics (SIAM), Philadelphia, PA, 1985.

[55] F. W. J. Olver, editor. *NIST handbook of mathematical functions*. Cambridge University Press, New York, 2010.

[56] P. J. Olver. *Applications of Lie groups to differential equations*, volume 107. Springer-Verlag, New York, second edition, 1993.

[57] J. A. Pava and R. G. Plaza. Transverse orbital stability of periodic traveling waves for nonlinear Klein-Gordon equations. *Stud. Appl. Math.*, 137(4):473–501, 2016.

[58] L. P. Pitaevskii. Vortex lines in an imperfect bose gas. *Sov. Phys. JETP*, 13:451–454, 1961.

[59] M. Remoissenet. *Waves called solitons: concepts and experiments*. Springer-Verlag, Berlin, 1994.

[60] G. Rowlands. On the stability of solutions of the non-linear Schrödinger equation. *IMA Journal of Applied Mathematics*, 13:367–377, 1974.

[61] A. C. Scott. A nonlinear Klein-Gordon equation. *American Journal of Physics*, 37(1):52–61, 1969.

[62] A. C. Scott. Waveform stability on a nonlinear Klein-Gordon equation. *Proceedings of the IEEE*, 57(7):1338–1339, 1969.

[63] A. C. Scott. Propagation of magnetic flux on a long Josephson tunnel junction. *Il Nuovo Cimento B*, 69(2):241–261, 1970.

[64] J. Stewart. *Single variable calculus: Early transcendentals*. Brooks/Cole Publishing Company, Boston, 2015.

[65] C. Sulem and P.-L. Sulem. *The nonlinear Schrödinger equation: Self-focusing and wave collapse*, volume 139. Springer-Verlag, New York, 1999.

[66] N. Voglis. Solitons and breathers from the third integral of motion in galaxies. *Monthly Notices of the Royal Astronomical Society*, 344(2):575–582, 2003.

[67] N. Voglis, P. Tsoutsis, and C. Efthymiopoulos. Invariant manifolds, phase correlations of chaotic orbits and the spiral structure of galaxies. *Monthly Notices of the Royal Astronomical Society*, 373(1):280–294, 2006.

[68] J.R. Waldram, A.B. Pippard, and J. Clarke. Theory of the current–voltage characteristics of SNS junctions and other superconducting weak links. *Phil. Trans. Roy. Soc. London, Ser. A 268: 265-87*, 1970.

[69] H. Wang and C. Xiang. Jacobi elliptic function solutions for the modified Korteweg–de Vries equation. *Journal of King Saud University-Science*, 25:271–274, 2013.

[70] E. T. Whittaker and G. N. Watson. *A course of modern analysis. An introduction to the general theory of infinite processes and of analytic functions: with an account of the principal transcendental functions*. Cambridge University Press, New York, 1962.

[71] S. Wiggins. *Introduction to applied nonlinear dynamical systems and chaos*, volume 2. Springer-Verlag, New York, second edition, 2003.

[72] L. V. Yakushevich. *Nonlinear physics of DNA*. John Wiley & Sons, Weinheim, 2006.

[73] V. E. Zakharov. Stability of periodic waves of finite amplitude on the surface of a deep fluid. *Journal of Applied Mechanics and Technical Physics*, 9:190–194, 1968.

[74] V. E. Zakharov and A. B. Shabat. Exact theory of two-dimensional self-focussing and one-dimensional self-modulating waves in nonlinear media. *Sov. Phys.-JETP (Engl. Transl.)*, 34:62–65, 1972.

VITA

Benjamin L. Segal received his Bachelor of Science degree in Applied Mathematics with Department Honors and Summa cum Laude distinction from the McCormick School of Engineering and Applied Sciences at Northwestern University with a Mathematics double major in 2012. Concurrently, in 2012, he received a Master of Science degree in Applied Mathematics from The Graduate School at Northwestern University. Subsequently, Ben joined the Department of Applied Mathematics at the University of Washington and obtained a second Masters of Science for Applied Mathematics in 2013.